9-2011

Controlled Oxygen Activation in Human Oxygen Sensor FIH

Evren Saban
University of Massachusetts Amherst

CONTROLLED OXYGEN ACTIVATION IN HUMAN OXYGEN SENSOR FIH

A Dissertation Presented

by

EVREN SABAN

Submitted to the Graduate School of the
University of Massachusetts Amherst in partial fulfillment
of the requirements for the degree of

DOCTOR OF PHILOSOPHY

September 2011

Department of Chemistry

CONTROLLED OXYGEN ACTIVATION IN HUMAN OXYGEN SENSOR FIH

A Dissertation Presented

by

EVREN SABAN

Approved as to style and content by:

_____
Michael J. Knapp, Chair

_____
Michael J. Maroney, Member

_____
Robert M. Weis, Member

_____
Stephen J. Eyles, Member

_____
Craig T. Martin, Department Head
Department of Chemistry

DEDICATION

This thesis is dedicated to my parents who have raised me and supported me. If I am here at this point that is because of my parents.

This thesis is also dedicated to Sinem who motivated me and showed her support by being with me.

ACKNOWLEDGMENTS

I would like to give my special thanks to my advisor Professor Knapp. I am grateful for all his contributions of ideas and knowledge to this research.

Thanks to Committee members

Prof. Eyles, thank you for helping me on mass spectroscopy.

Prof. Weis thank you for your support in DSC analysis.

Prof. Maroney, thank you for your collaboration and guidance.

I want to thank Yuan-Han Chen, the first member of Knapp group, for teaching and showing me new laboratory skills.

Shannon, it was a pleasure to work with you from the day we joined Knapp group and thanks to you for helping me on ROS work.

John and Cornelius, thank you for contributions of your time and effort on this thesis.

ABSTRACT

CONTROLLED OXYGEN ACTIVATION IN HUMAN OXYGEN SENSOR FIH

SEPTEMBER 2011

EVREN SABAN, B.S., BILKENT UNIVERSITY

Ph.D., UNIVERSITY OF MASSACHUSETTS AMHERST

Directed by: Professor Michael J. Knapp

One of the primary oxygen sensors in human cells, which controls gene expression by hydroxylating the hypoxia inducible transcription factor (HIFα) is the factor inhibiting HIF (FIH). As FIH is an alpha-ketoglutarate dependent non-heme iron dioxygenase, oxygen activation is thought to precede substrate hydroxylation. The coupling between oxygen activation and substrate hydroxylation was hypothesized to be very tight, in order for FIH to fulfill its function as a regulatory enzyme. Coupling was investigated by looking for reactive oxygen species production during turnover. Alkylsulfatase (AtsK), a metabolic bacterial enzyme with a related mechanism and similar turnover frequency, was used for comparison, and both FIH and AtsK were tested for H_2O_2, O_2^- and $OH^\bullet$ formation under steady and substrate-depleted conditions. Coupling ratios were determined by comparing the ratio of substrate consumed to product formed. AtsK reacted with O_2 on the seconds timescale in the absence of prime substrate, and uncoupled during turnover to produce H_2O_2; neither O_2^- nor $OH^\bullet$ were detected. In contrast, FIH was unreactive toward O_2 on the minutes timescale in the absence of prime substrate, and tightly coupled during steady-state turnover; any reactive oxygen species produced by FIH was not available for detection. Inactivation mechanisms of these enzymes were also investigated. AtsK likely inactivated due to deoligomerization,

whereas FIH inactivated by slow autohydroxylation. Autohydroxylated FIH could not be reactivated by dithiothreitol (DTT) nor is ascorbate, suggesting that autohydroxylation likely to be irreversible under physiological conditions.

Iron in the FIH active site is coordinated by a (His_2Asp) facial triad, αKG, and H_2O. Hydrogen bonding between the facial triad, the HIF-Asn^{803} sidechain, and various second-sphere residues suggests a functional role for the second coordination sphere in tuning the chemistry of the Fe(II) center. Point mutants of FIH were prepared to test the functional role of the αKG-centered (Asn^{205}, Asn^{294}) or HIF-Asn^{803} centered (Arg^{238}, Gln^{239}) second-sphere residues. The second sphere was tested for local effects on priming Fe(II) to react with O_2, oxidative decarboxylation, and substrate positioning. Steady-state kinetics were used to test for overall catalytic effects, autohydroxylation rates were used to test for priming and positioning, and electronic spectroscopy was used to assess the primary coordination sphere and the electrophilicity of αKG. Asn^{205}→Ala and Asn^{294}→Ala exhibited diminished rates of steady-state turnover, while minimally affecting autohydroxylation, consistent with impaired oxidative decarboxylation. Blue shifted MLCT transitions for (Fe+αKG)FIH indicated that these point mutations destabilized the π* orbitals of αKG, further supporting a slowed rate of oxidative decarboxylation. The Arg^{238}→Met mutant exhibited steady-state rates too low to measure and diminished product yields, suggesting impaired substrate positioning or priming; Arg^{238}→Met was capable of O_2-activation for the autohydroxylation reaction. The Gln^{239}→Asn mutant exhibited significantly slowed steady-state kinetics and diminished product yields, suggesting impaired substrate positioning or priming. As HIF binding to

Gln^{239}→Asn stimulated autohydroxylation, it is more likely that this point mutant simply mis-positions the HIF-Asn^{803} sidechain. By combining kinetics and spectroscopy, it was shown that these second sphere hydrogen bonds play roles in promoting oxidative decarboxylation, priming Fe(II) to bind O_2, and positioning HIF-Asn^{803}.

TABLE OF CONTENTS

Page

LIST OF TABLES

Table Page

LIST OF FIGURES

Figure Page

LIST OF SCHEMES

CHAPTER 1

KEY PLAYERS OF OXYGEN SENSING

1.1 Introduction

Molecular oxygen has a prime function in aerobes. It is the final electron acceptor in cellular aerobic respiration system to produce energy in the form of ATP. Energy production starts with glycolysis in cytoplasm and continues with oxidative decarboxylation of pyruvate, citric acid cycle and oxidative phosphorylation steps in mitochondria. Most of the ATP synthesis occurs in the last step in which oxygen is the terminal electron acceptor in electron transport chain. During glycolysis 2 ATP molecules are produced whereas 36 ATP molecules are formed with the help of molecular oxygen (*1*). Due to its high energy potential, oxygen is crucial for our life. Oxygen does not only play a key role in energy metabolism, it is also used as a substrate for the production of key cellular components in signaling. So this makes molecular oxygen even more important in our life.

A Constant source of energy is necessary to maintain our lives, but oxygen concentrations may vary due to environmental conditions or due to the type of tissues in which O_2 is distributed throughout the human body (*2*, *3*). Lack of oxygen for brief periods of time can be tolerated, but a continuous lack of oxygen requires more complicated responses (*4*). An adaptive response to the lack of oxygen in an effort to maintain energy requirements is called oxygen homeostasis (*2*). At high altitudes oxygen levels can decrease up to 30% due to air density and our bodies respond to this new

environment by triggering more red blood cell production so that more oxygen can be delivered to the cells. Low oxygen concentrations might also occur locally in our body as in the case of tumorous cells. They need oxygen to grow, so the adaptive response to lack of oxygen is to trigger angiogenesis.

1.2 Hypoxia Inducible Factor

When dioxygen levels change in a cellular environment, adaptation to a new environment is achieved by the transcriptional factor HIF. Under hypoxia (when dioxygen levels are low), HIF-1 induces the expression of over 100 genes associated with angiogenesis in cancer, immune response, erythropoiesis, energy metabolism, nutrient transport and cell migration (*5-12*). HIF is a heterodimeric transcription factor consisting of a constitutively expressed HIF-β subunit and oxygen regulated HIF-α subunit (*13-15*). There are three isoforms of HIF which are HIF-1, HIF-2 and HIF-3 in which HIF-1 is the most important and abundant and they are accepted as the master regulators in oxygen homeostasis (*16-19*). HIF-1α/β proteins contain basic-helix-loop-helix and Per-ARNT-SIM (bHLH-PAS) domains for DNA binding and heterodimerization (*9*). Studies showed that both bHLH and PAS domains are required for complex formation and DNA binding. Truncation of one of the domains revealed that bHLH can dimerize alone but the PAS domain is also required for DNA binding (*20*). HIF-1α also has oxygen dependent degradation (ODDD) and transcriptional activation domains (NTAD and CTAD). These domains are required for the regulation of HIF activity in the presence of normal oxygen levels (Figure 1.1) (*14, 21, 22*).

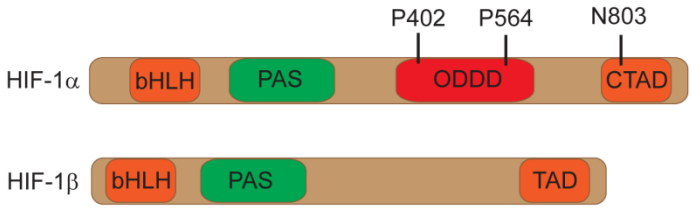

Figure 1.1: HIF-1α/β domains

Under hypoxic conditions HIF-1α levels rise and HIF-1α dimerizes with HIF-1β and initiates transcriptional activation. To activate gene transcription, the heterodimeric HIF-1α/β complex requires coactivators including p300, CBP, SRC-1 and TIF2. Once the active transcription complex forms, it binds to a core DNA motif (G/ACGTG) in hypoxia response elements (HREs) that are associated by HIF target genes. This results the induction of over 100 genes including angiogenesis, erythropoiesis, vascular remodeling, inflammation and other processes to achieve oxygen homeostasis (*23*).

1.3 HIF Hydroxylases

At normal oxygen levels HIF activity is regulated either by proteasomal degradation or prevention of coactivator binding. The key players in hypoxic response are the HIF hydroxylases, which regulate the activity level of HIF by dioxygen dependent modification under conditions of normal or elevated oxygen (*7, 24-26*). The regulation of HIF is shown in Figure 1.2.

1.3.1 Prolyl Hydroxylase

Two types of modification have been identified both of which inhibit HIF. In the first type of modification, the ODD domain of HIF-1α is hydroxylated at proline residues

(Pro-402 and Pro-564 in HIF-1α), which are mediated by PHD (Prolyl hydroxylase). The ODD domain possesses two sub-domains, NODD and CODD (N- and C- terminal ODD) each of which can be independently hydroxylated. This hydroxylation enables the recognition of modified HIF-1α ODD domain by von Hippel-Lindau tumor suppressor protein (pVHL) by increasing the affinity between these proteins. The hydroxylated proline residue excludes a water molecule and forms two hydrogen bonds with Ser-111 and His-115 residues of pVHL which makes this complex more stable. Ubiquitin ligase binds this complex and ubiquitinylates and targets HIF-1α for hydrolysis via ubiquitin-proteasome pathway (*27, 28*).

1.3.2 Factor Inhibiting HIF

In the second type of modification, the C-terminal transactivation domain (CTAD) of HIF-1α is hydroxylated at the β-Carbon of asparagine residue (Asn-803) by FIH (factor inhibiting HIF) in a process which is independent of ODD modification (*29-32*). Hydroxylation at this asparagine residue prevents interaction of HIF-1α with the CH-1 (Cysteine/Histidine rich) domain of the transcriptional co-activator p300. NMR structures of unhydroxylated CTAD bound to CH-1 of p300 showed that Asn-803 residue is buried at the complex interface, and this suggests that hydroxylation of β-Carbon of Asn-803 may decrease binding affinity either by disrupting the interaction between pVHL and HIF-1α and/or disrupting the α-helix structure of CTAD formed at the binding interface (*30, 33, 34*).

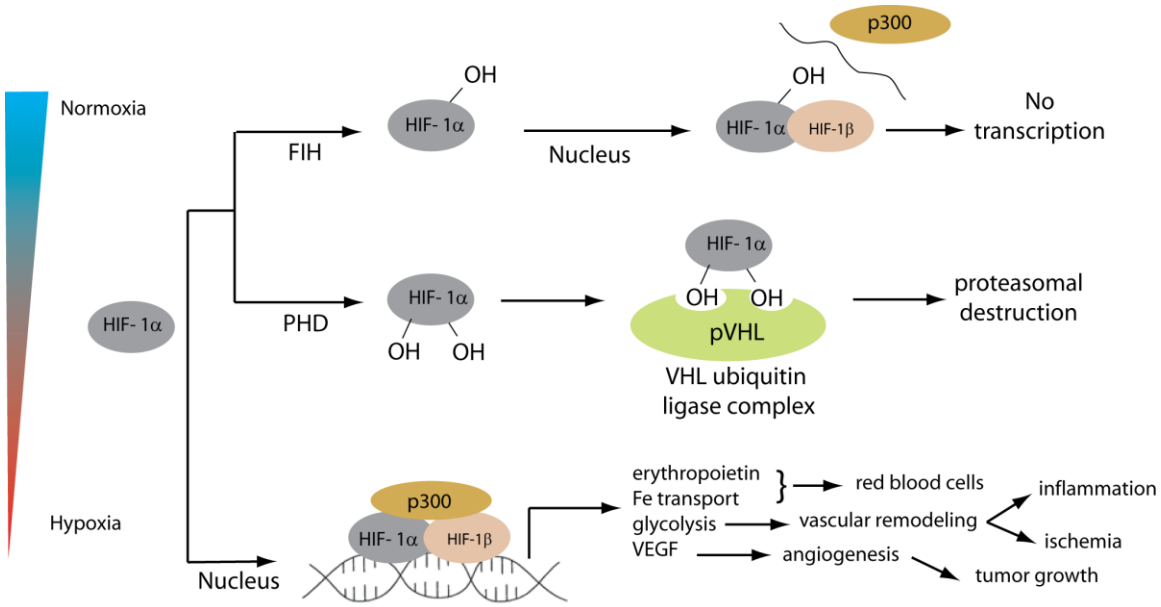

Figure 1.2 HIF pathway

Subtle changes in the oxygen concentrations in our body are sensed by these HIF hydroxylases. There are three isoforms of PHD enzyme (PHD1, PHD2 & PHD3) and with FIH; all four enzymes exist at different concentrations and in different compartments of cells. The activity of these enzymes depends on the available oxygen concentration and they are accepted as the primary oxygen sensors in our body. Generally K_m of oxygen for these enzymes are higher than the ambient oxygen levels, so small changes in the oxygen concentration have large impacts on the activity of these enzymes. $K_m(O_2)$ of FIH was determined to be less than for PHD enzymes. This suggests that HIF-1α which survived from the degradation pathway can continue to be regulated by FIH when PHD activity has already been suppressed by lowered O_2 levels (*35-37*).The HIF hydroxylases have different tissue distributions in our body at RNA level. PHD1 is abundant in testis, PHD2 and FIH are ubiquitous and PHD3 exist mostly in heart and

smooth muscles. Within the cell, PHD1 is nuclear, PHD2 and FIH are mainly in cytoplasm, and PHD3 is present both in nucleus and cytoplasm (*38-42*). Our body has a different number of copies of these enzymes, PHD2 is the most abundant and active among PHDs; together with FIH, they keep the system under check at all times by sensing small changes in available oxygen levels (*4, 43*).

1.3.3 Proposed Reaction Mechanism of FIH

The HIF-hydroxylases (FIH and PHD) belong to the Fe(II) and α-ketoglutarate (αKG) dependent dioxygenase superfamily. These enzymes are characterized by their jelly-roll motif in which eight anti-parallel β-strands form two β-sheets and Fe(II) is coordinated by the His_2(Asp/Glu) residues between β-sheets. Unlike heme-containing enzymes, Fe(II) forms a facial triad with His_2(Asp/Glu); leaving the other three coordination sites for reaction chemistry. They consume molecular oxygen and α-ketoglutarate to produce CO_2 and succinate while hydroxylating the primary substrate (R-H) to give product (R-OH) with a simplified reaction shown below (*32, 44-53*).

$$\alpha KG + O_2 + RH \rightarrow \text{succinate} + CO_2 + ROH$$

A consensus mechanism, which is shown in Scheme 1.1, has been proposed for FIH based on other αKG dependent enzymes. In the resting enzyme, Fe(II) is six coordinate which has 2-His-1-carboxylate facial triad and three water molecules bound. Initially the substrate α-ketoglutarate binds to the iron, releasing the two water molecules. Upon

primary substrate binding, the last water molecule leaves, making Fe(II) five-coordinated and creating an open coordination site for molecular oxygen.

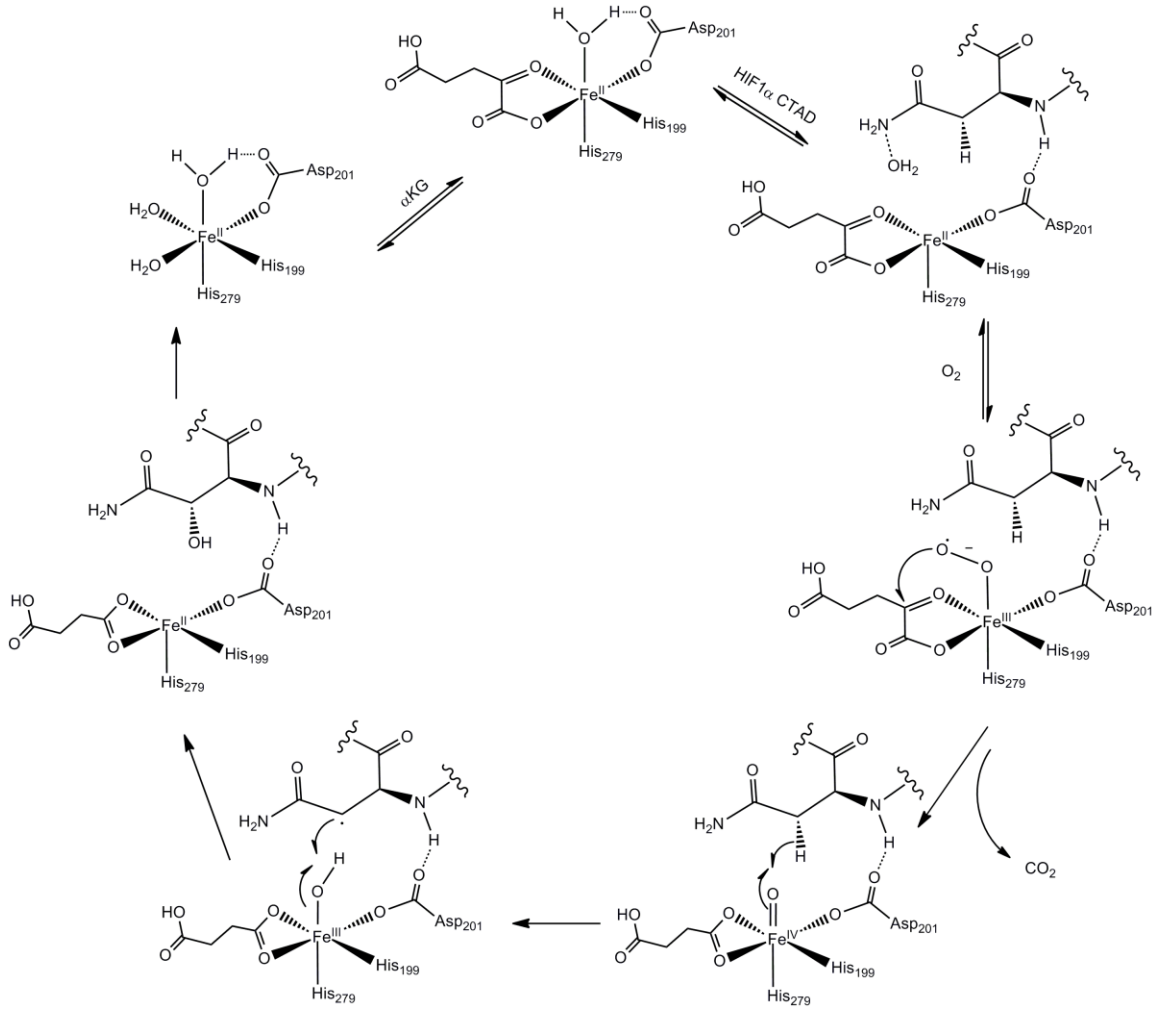

Scheme 1.1 Consensus reaction mechanism of FIH

Fe(II) is relatively unreactive toward molecular oxygen unless the coordination of metal center changes from six- to five-coordinate and when this happens the quaternary complex composed of Fe(II), α-ketoglutarate and substrate bound to the enzyme active site reacts with dioxygen. Because six coordinate Fe(II) is not reactive towards O_2,

substrate binding is accepted as the switch which activates Fe(II) for oxygen activation. First, Fe(II) activates oxygen by one-electron reduction to form a superoxide radical, which attacks C2 of α-ketoglutarate. The decarboxylation of α-ketoglutarate yields succinate and CO_2 with the concomitant formation of a highly reactive Fe(IV)=O intermediate (*54-58*). This reactive intermediate then abstracts a hydrogen atom from the primary substrate forming a substrate-centered radical. Finally, this radical binds the oxygen on the iron center and generates the final hydroxylated product and the enzyme returns to its Fe(II) active state. This final step is called a hydrogen abstraction - rebound mechanism (*59-64*).

1.4 α-Ketoglutarate Dependent Enzymes

The members of the α-ketoglutarate dependent dioxygenase family exist both in prokaryotes and eukaryotes and catalyze a wide range of reactions in which hydroxylation chemistry is the main reaction. These enzymes are accepted as dioxygenases but individual atoms of dioxygen are distributed to different products; one oxygen atom is incorporated into product while the other oxygen atom is incorporated into succinate that is derived from α-ketoglutarate. While the typical reaction is the hydroxylation, other oxidative processes like ring closure, ring opening, desaturation, elimination and epoxidation reactions are also common in this class of enzymes. In some of these reactions it is possible that one atom of dioxygen is incorporated into succinate, and the other oxygen atom is liberated as a water molecule. These enzymes are a part of important biological processes including post-translational modification of proteins, DNA repair, antibiotic biosynthesis and fatty acid metabolism, and they all posses α-

ketoglutarate dependent non-heme Fe(II) active site with His_2Asp/Glu facial triad (*44*, *47*, *65*, *66*).

α-Ketoglutarate dependent enzymes are only a subfamily of the non-heme iron enzyme superfamily, which possesses His_2Asp/Glu facial triad and catalyzes many diverse reactions. The diversity of these catalyzed reactions is broader than the reactions associated with heme-containing enzymes. The porphyrin of heme occupies four coordination sites of Fe and one proximal residue binds the fifth coordination site; leaving only one available site for binding which is for molecular oxygen. However in non-heme enzymes Fe is coordinated by three endogenous protein ligands forming a facial triad, and leaving the other three coordination sites for exogenous ligands such as oxygen, substrate and/or cofactor. This facial triad combined with the protein flexibility tunes the reactivity of active center and makes these enzymes versatile (*67*). This superfamily can be categorized into five families based on the reaction they catalyze and/or cofactors they use. These families are the extradiol cleaving catechol dioxygenases, Rieske dioxygenases, α-ketoglutarate dependent dioxygenases, tetrahydropterin dependent hydroxylases and biosynthetic oxidases (*45*, *46*, *61*, *62*, *68*).

1.5 Extradiol Cleaving Catechol Dioxygenases

Extradiol cleaving catechol dioxygenases catalyze the ring cleavage reactions of aromatic compounds (*48-50*). Aromatic ring cleavage of catechols occurs at C-C bond adjacent to enediol group and both atoms of molecular oxygen are incorporated into the product via four-electron oxidation. The best characterized enzyme in this class is

homoprotocatechuate 2,3-dioxygenase (HPCD). To better characterize this enzyme 4-nitrocatechol was used as an alternative substrate instead of homoprotocatechnic acid (HPCA). Crystal structure studies revealed three different intermediates during the catalytic cycle. The first one is Fe(II)-O_2 complex which showed that Fe-O bond length is long (2.4 Å) and the 4-nitrocatechol ring is not planar. This suggests that iron remains in the Fe(II) state and substrate gives an electron to activate oxygen. The second intermediate is an Fe(II)-peroxo-substrate complex in which oxygen attacks to C2 of 4-nitrocatechol forming a peroxo bridge. The third and final intermediate is the Fe(II)-product complex (Scheme 1.2). During the catalytic turnover, the reaction is driven by not only close coupling of the iron center and the substrate, but also the second sphere residues.

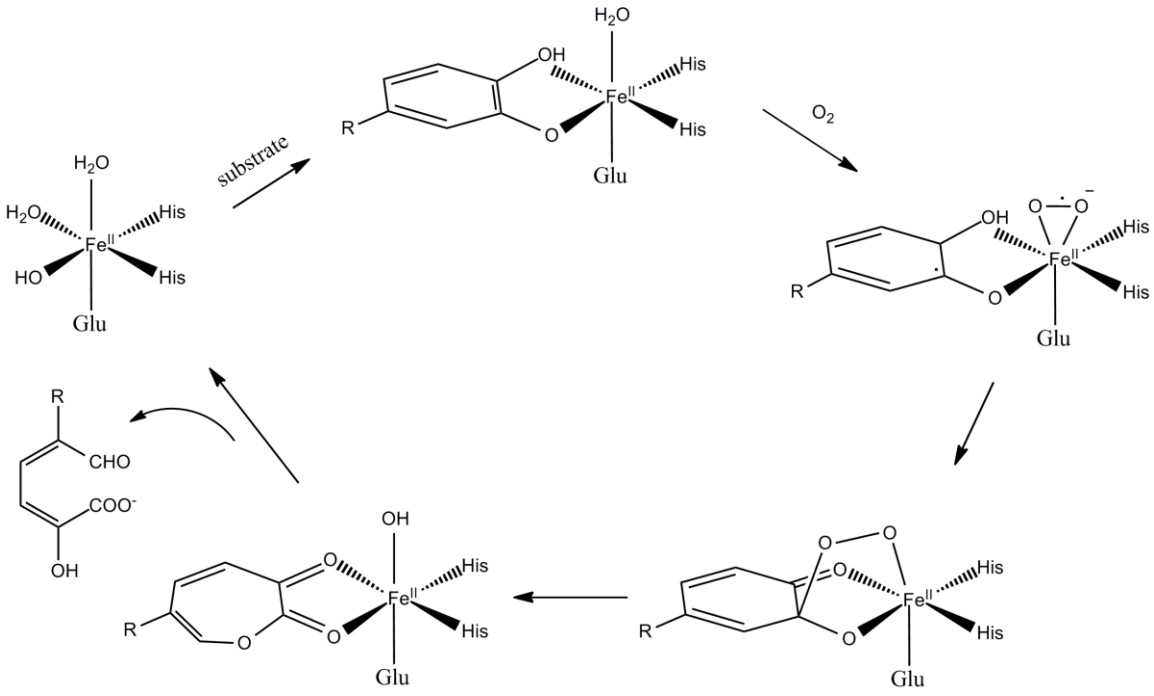

Scheme 1.2 Extradiol catechol dioxygenase catalytic cycle

There are two important second sphere residues (Tyr257 and His200), which form hydrogen bonds to stabilize the deprotonated substrate and promote heterolytic dioxygen bond cleavage, respectively (*69-75*).

1.6 Rieske Dioxygenases

Rieske dioxygenases catalyze the cis-dihydroxylation of aromatic compounds, which in turn become catechols during the downstream processes (*76*). The active site of these enzymes differs slightly from other non-heme enzymes in a way that Asp in the facial triad binds in a bidentate manner. The two other coordination sites are generally occupied with solvent molecules (*77, 78*). Near the active site, there is a Rieske type cluster (Fe2-S2), which acts as an external electron source. For the cis-dihydroxylation reaction two external electrons are needed, and these are supplied by NADH. A good example for this class of enzymes is naphthalene dioxygenase (NDO). Single turnover and crystallographic studies of NDO showed that at the end of one turnover both metal centers are fully oxidized. For another turnover these centers must be reduced by NADH (*79, 80*). The activated oxygen is proposed to be Fe(III)-hydroperoxo, in which O-O bond cleavage occurs and the hydroxylating reagent Fe(V)-oxo-hydroxo is formed, or it can directly react with the aryl substrate via a radical mechanism. The proposed reaction mechanism is shown Scheme 1.3. The yield of NDO catalytic cycle in the presence of alternate substrate benzene is about 50%. Oxygen consumption and benzene hydroxylation are not tightly coupled, and hydrogen peroxide is released during the turnover. Studies showed that hydrogen peroxide released acts as an inactivator, and it is

proposed that this occurs via a Fenton-type reaction forming strong reactive oxygen species like hydroxyl radicals (OH˙) (*81-84*).

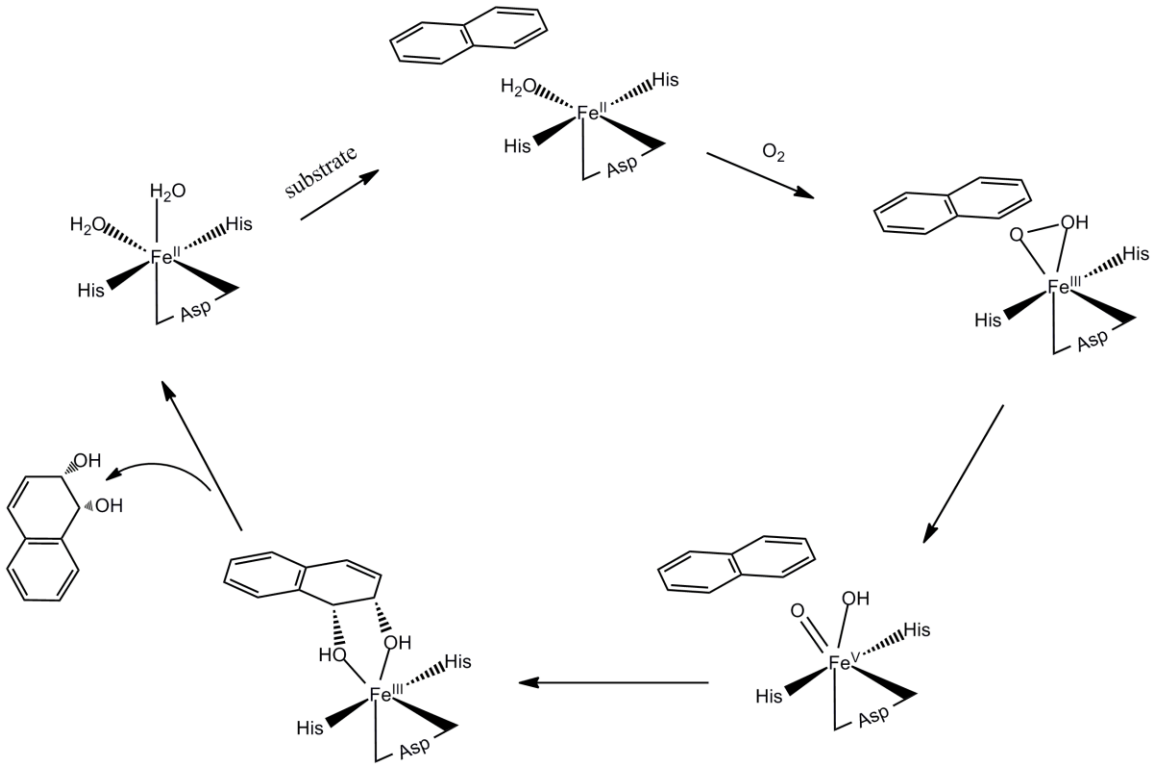

Scheme 1.3 Proposed Reaction mechanism of Naphthalene 1,2-dioxygenase

1.7 Tetrahydropterin Dependent Hydroxylases

Tetrahydropterin dependent hydroxylases catalyze the hydroxylation of aromatic amino acid residues using tetrahydropterin as a two-electron donor cofactor like α-ketoglutarate dependent enzymes. Tryptophan (TrpH), tyrosine (TryH) and phenylalanine (PheH) hydroxylases are responsible for the formation of the neurotransmitters serotonin and 3,4-dihydroxyphenylalanine, and the amino acid tyrosine, respectively (*85*, *86*). Binding of substrate and cofactor near the iron active site leaves an open coordination site for oxygen (Scheme 1.4). Once dioxygen binds, it forms a peroxo bridge between Fe(II) center and the cofactor. Heterolytic O-O bond cleavage of this peroxo bridge yields 4a-

hydroxypterin and an Fe(IV)=O species (*87, 88*). So two electrons come from cofactor and the other two electrons are supplied by Fe(II). Once the Fe(IV)=O intermediate forms, it can abstract a hydrogen from the near substrate. The active hydroxyl group then rebounds to the radical substrate like in the α-ketoglutarate dependent enzymes (*89*). When the substrate is not present near the active site, the enzyme chooses another pathway to protect itself from reactive oxygen species. In the absence of a hydroxylation reaction, two tetrahydropterin molecules are oxidized to dihydropterins per molecule of dioxygen consumed. The four-electron reduction of dioxygen to water prevents reactive oxygen species formation like hydrogen peroxide (*90, 91*).

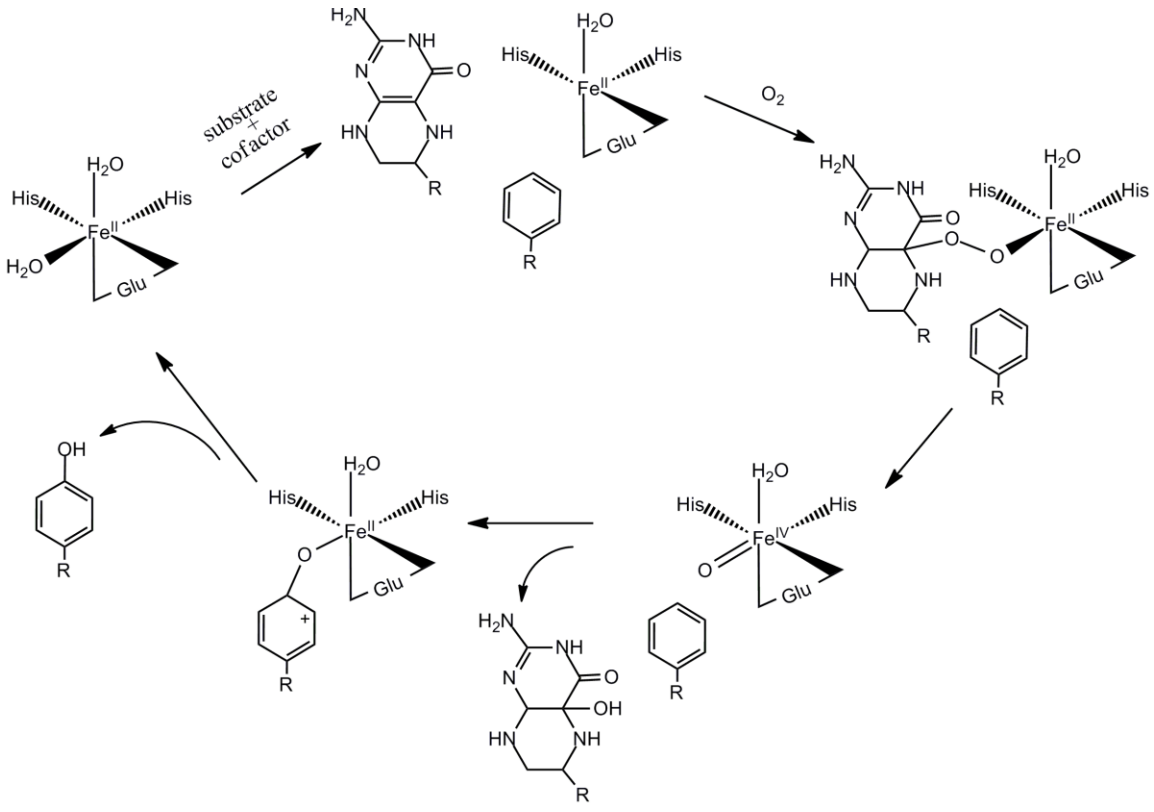

Scheme 1.4 Reaction mechanism of Aromatic aminoacid hydroxylases

1.8 Biosynthetic Oxidases

Biosynthetic oxidases are a family of enzymes that play key roles in the synthesis of biologically important molecules. In this family, substrates bind to the iron center like in extradiol dioxygenases, and using electrons from the substrate and/or a cofactor, oxygen is reduced to two water molecules in a four-electron reduction with the concomitant substrate catalysis. The best known example of this family is isopenicillin-N synthase (IPNS). IPNS catalyzes the synthesis of isopenicillin-N from δ-(L-α-aminoadipoyl)-L-cysteinyl-D-valine (ACV), which is a key step in biosynthesis of penicillin and cephalosporin antibiotics (*92*).

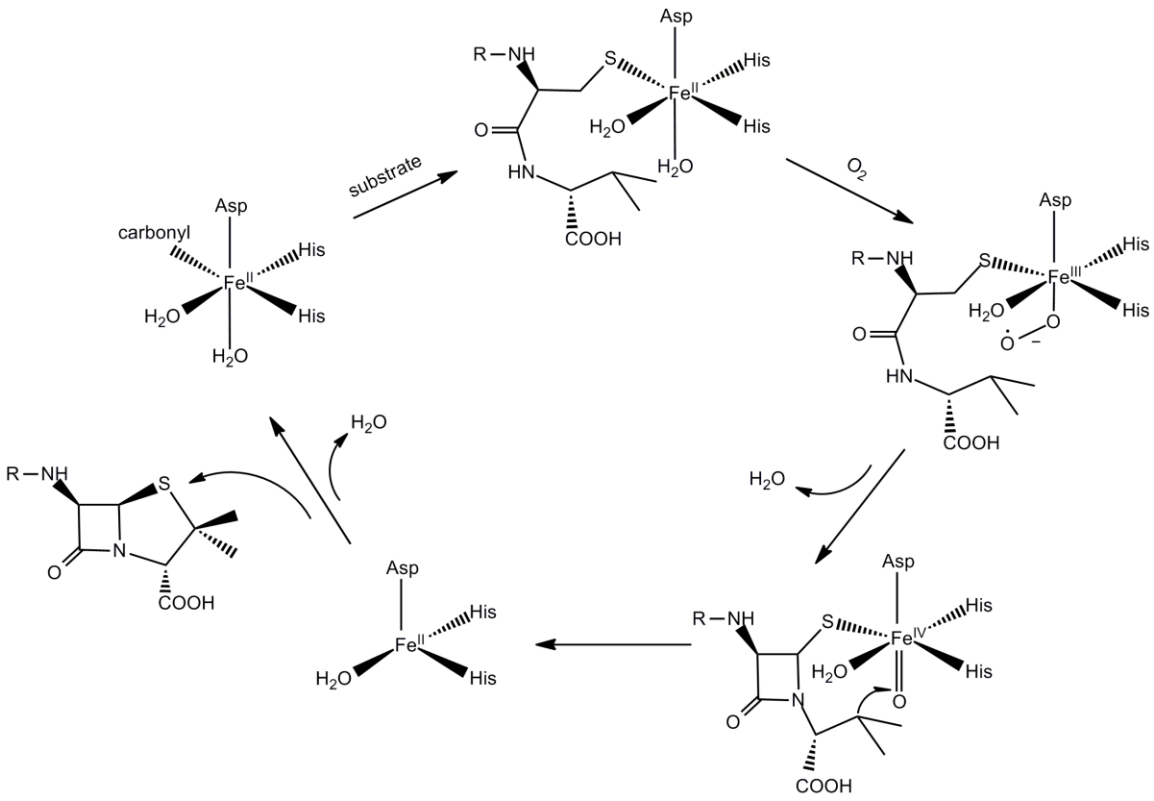

Scheme 1.5 Catalytic cycle of IPNS

When substrate (ACV) and oxygen bind to iron active site, it is proposed that Fe(III)-superoxo forms and electron transfer from substrate is promoted which causes the β-lactam ring closure, formation of the first water molecule and the Fe(IV)=O reactive intermediate. The Fe(IV)=O then causes the second ring closure and formation of the second water molecule (Scheme 1.5).

Kinetic studies showed that IPNS has no detectable uncoupling between oxygen depletion and ACV consumption, but the enzyme inactivates itself slowly with time. It is proposed that IPNS is vulnerable to oxidative damage, which is irreversible and cannot be rescued by reducing agents. Catalase protects IPNS from damage and reduces the inactivation to some extent, which suggests H_2O_2 formation. Since catalase does not rescue the enzyme at 100%, it is concluded that internal ROS formation also gives rise to oxidative damage near active site (*93, 94*).

Other examples of biosynthetic oxidases family are aminocyclopropane carboxylate oxidase (ACCO) and fosfomycin oxidase (FOS), which catalyze synthesis of the plant hormone ethylene and the fosfomycin antibiotic respectively. Unlike IPNS, these enzymes use two electrons from from substrate and two electrons from cofactors (ACCO uses ascorbic acid and FOS uses NADH) (*67*).

1.9 Activated Oxygen

As seen from the previously mentioned examples, mononuclear non-heme iron enzymes all possess His_2Asp/Glu facial triad and catalyze very diverse reactions by utilizing O_2.

Compared to heme proteins, the non-heme iron active site can accommodate more than one ligand. The facial triad occupies generally three coordination sites in these enzymes leaving the other three coordination sites for binding of O_2 and, in some cases, substrate or cofactor. All these enzymes activate dioxygen in different ways. The observed and proposed iron-oxo species are as the following: Fe(II)-superoxo, Fe(III)-hydroperoxo, Fe(III)-superperoxo and Fe(II)-alkylperoxo intermediates are converted to high valent Fe(IV)=O and Fe(V)=O-OH after O-O bond cleavage (*67*). Activated oxygen and reactive intermediates are summarized in Figure 1.3 and Figure 1.4.

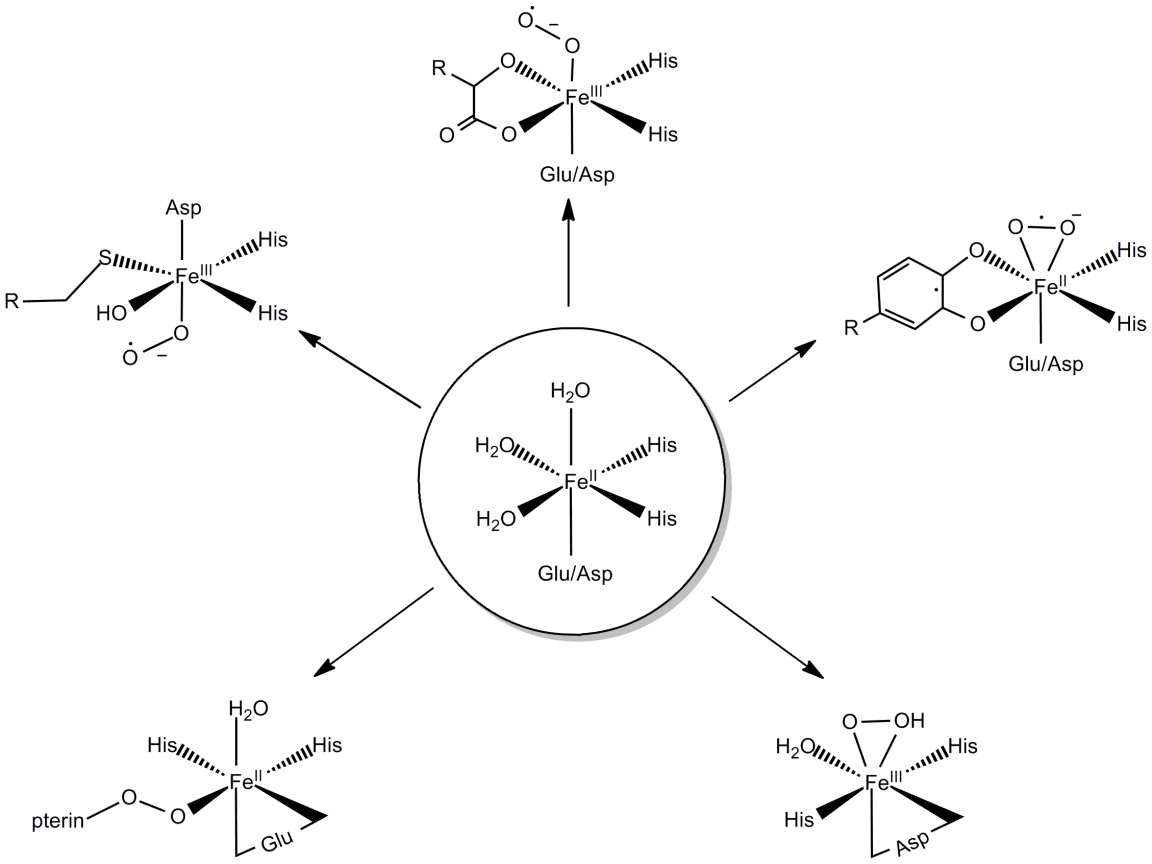

Figure 1.3 activated dioxygen in nonheme iron enzymes

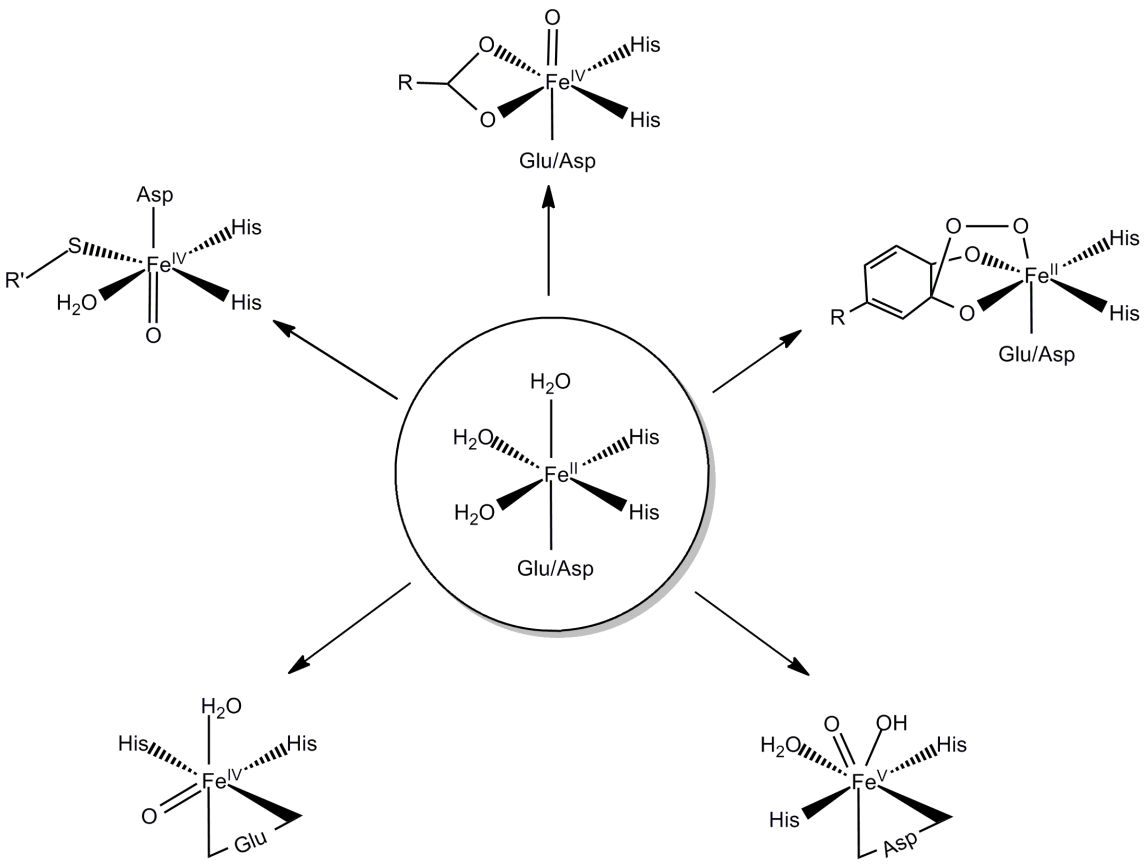

Figure 1.4 Reactive iron-oxo intermediates in nonheme iron enzymes

It would be interesting to understand how these enzymes control reactive iron-oxo intermediates when dioxygen is activated. If the oxygen activation is not coupled with the substrate catalysis, side reactions can occur. Reactive iron-oxo intermediates can attack internal amino acid residues causing self-hydroxylation and self-inhibition or they can produce reactive oxygen species (ROS) like H_2O_2, O_2^-, and $^{\cdot}OH$ and give oxidative damage to their environment.

In α-ketoglutarate dependent enzymes the proposed and, in some cases, observed intermediates are Fe(III)-peroxo and Fe(IV)=O intermediates. If the catalytic cycle is not

tightly coupled, H_2O_2 and O_2^- can be formed, likely from an Fe(III)-peroxo intermediate. As the catalytic turnover proceeds, ˙OH can also be formed after Fe(IV)=O step.

1.10 Coupling of Turnover

The active site structure including the second coordination sphere plays a key role in the reaction turnover. The protein flexibility, substrate binding, electron donating cofactor, second sphere residues and facial triad are all important players during the catalytic cycle. Any oxygen leakage can be avoided by coupling the dioxygen activation to the hydroxylation step so that the reaction is driven to the product without byproducts. However, uncoupling of oxygen activation to substrate hydroxylation can occur. The ideal stoichiometric ratio between oxygen consumption and product catalysis would be 1:1. Any oxygen leakage would cause more oxygen consumption and the stoichiometry would be higher than 1 in which reactive oxygen species can be generated or the enzyme can hydroxylate itself. Self hydroxylation generally occurs when the substrate is not present or not in the close proximity of iron active site. In the case of FIH, the rate of self-hydroxylation is diminished when the substrate CTAD is present. If the regulatory role of FIH in oxygen sensing is considered, uncoupling between oxygen activation and product catalysis must be low such that no excess reactive oxygen should give oxidative damage. The release of reactive oxygen species should also be minimal in order to prevent oxidative stress in the cells. Determining the extent of uncoupling and the propensity to produce ROS in FIH will help us to understand the link between oxygen activation and product hydroxylation.

1.11 Second Coordination Sphere

In order to determine how FIH controls activated oxygen, second coordination sphere residues should also be investigated. These residues play important roles in hydroxylation chemistry in which they tune the active site by making hydrogen bonds. The hydrogen bonding network with the second coordination sphere can also be found in other enzymes. In the case of FIH, there are four residues present in the second sphere which control the hydroxylation by either facilitating the decarboxylation of α-ketoglutarate or positioning the primary substrate. When activated oxygen attacks αKG, a buildup of negative charge can be pulled away by hydrogen bond donors in the second sphere so that decarboxylation can be facilitated. Subsequent to decarboxylation, hydroxylation of the primary substrate occurs via the hydrogen abstraction/rebound mechanism involving a putative Fe(IV)=O intermediate. It is crucial that the substrate is oriented in the correct position for hydroxylation. Hydrogen bonding networks in the second sphere provide stabilization for optimal orientation of the substrate.

Because of the simpler substrate requirements of AtsK, this enzyme will also be studied and compared with FIH. AtsK is a metabolic αKG-dependent dioxygenase involved in bacterial sulfur metabolism. Under sulfur starvation conditions, AtsK catalyzes the hydroxylation of alkylsulfate and releases inorganic sulfate to the medium. Hexylsulfate is hydroxylated to form 1-hydroxylhexylsulfate which decomposes spontaneously to hexanal and inorganic sulfate (*95*).

How FIH controls activated O_2, and the role of the second sphere residues on hydroxylation, will be the focus of this research. The steps between O_2 binding and decarboxylation are very important because the enzyme turnover rate is determined by these steps and it is related to the O_2 sensing function of FIH. So it is crucial to understand how oxygen activation is controlled by FIH, which performs its unique oxygen sensing role in our body.

1.12 Appendix

1.12.1 Abbreviations

HIF, Hypoxia Inducible Factor;

ODDD, Oxygen Dependent Degradation Domain;

N- and C- terminal TAD, Transcriptional activation domain of HIF-1α

p300, Transcriptional coactivator;

CBP, CREB-binding protein;

SRC-1, Steroid receptor coactivator 1;

TIF2, Transcriptional intermediary factor 2;

HRE, Hypoxia responsive elements;

pVHL, Von Hippel-Lindau tumor suppressor;

PHD, Prolyl hydroxylase;

FIH, Factor inhibiting HIF;

HPCD, Homoprotocatechuate 2,3-dioxygenase;

HPCA, Homoprotocatechnic acid;

NDO, Naphthalene dioxygenase;

TrpH, Tryptophan hydroxylase;

TryH, Tyrosine hydroxylase;

PheH, Phenylalanine hydroxylase;

IPNS, Isopenicillin-N synthase;

ACV, δ-(L-α-aminoadipoyl)-L-cysteinyl-D-valine;

ACCO, aminocyclopropane carboxylate oxidase;

FOS, Fosfomycin oxidase;

AtsK, alkylsulfatase;

1.13 Bibliography

1. Rich, P. R. (2003) The molecular machinery of Keilin's respiratory chain, *Biochem. Soc. Trans. 31*, 1095-1105.

2. Semenza, G. L. (2009) Oxygen homeostasis, *Wiley Interdisciplinary Reviews: Systems Biology and Medicine 2*, 336-361.

3. Aragonés, J., Fraisl, P., Baes, M., and Carmeliet, P. (2009) Oxygen Sensors at the Crossroad of Metabolism, *Cell Metab. 9*, 11-22.

4. Webb, J. D., Coleman, M. L., and Pugh, C. W. (2009) Hypoxia, hypoxia-inducible factors (HIF), HIF hydroxylases and oxygen sensing, *Cell. Mol. Life Sci. 66*, 3539-3554.

5. Pugh, C. W. (2003) Oxygen sensing in cancer, *Ann. Med. 35*, 380-390.

6. Pugh, C. W., and Ratcliffe, P. J. (2003) Regulation of angiogenesis by hypoxia: role of the HIF system, *Nat. Med. 9*, 677-684.

7. Dann, C. E., and Bruick, R. K. (2005) Dioxygenases as O_2-dependent regulators of the hypoxic response pathway, *Biochem. Biophys. Res. Commun. 338*, 639-647.

8. Semenza, G. L. (2003) Targeting HIF-1 for cancer therapy, *Nat. Rev. Cancer 3*, 721-732.

9. Wang, G. L., Jiang, B. H., Rue, E. A., and Semenza, G. L. (1995) Hypoxia-Inducible Factor-1 is a basic-helix-loop-helix-pas heterodimer regulated by cellular O_2 tension, *PNAS 92*, 5510-5514.

10. Semenza, G. L. (2001) Hypoxia-inducible factor 1: oxygen homeostasis and disease pathophysiology, *Trends Mol. Med 7*, 345-350.

11. Wenger, R. H. (2002) Cellular adaptation to hypoxia: O_2 sensing protein hydroxylases, hypoxia inducible transcription factors, O_2 regulated gene expression., *FASEB J. 16*, 1151-1162.

12. Huang, L. E., and Bunn, H. F. (2003) Hypoxia-inducible factor and its biomedical relevance, *J. Biol. Chem. 278*, 19575-19578.

13. Pugh, C. W., Orourke, J. F., Nagao, M., Gleadle, J. M., and Ratcliffe, P. J. (1997) Activation of hypoxia-inducible factor-1; Definition of regulatory domains within the alpha subunit, *J. Biol. Chem. 272*, 11205-11214.

14. Jiang, B. H., Rue, E., Wang, G. L., Roe, R., and Semenza, G. L. (1996) Dimerization, DNA binding, and transactivation properties of hypoxia-inducible factor 1, *J. Biol. Chem. 271*, 17771-17778.

15. Jiang, B. H., Zheng, J. Z., Leung, S. W., Roe, R., and Semenza, G. L. (1997) Transactivation and inhibitory domains of hypoxia-inducible factor 1 alpha. Modulation of transcriptional activity by oxygen tension, *J. Biol. Chem. 272*, 19253-19260.

16. Ema, M., Taya, S., Yokotani, N., Sogawa, K., Matsuda, Y., and FujiiKuriyama, Y. (1997) A novel bHLH-PAS factor with close sequence similarity to hypoxia-inducible factor 1 alpha regulates the VEGF expression and is potentially involved in lung and vascular development, *PNAS 94*, 4273-4278.

17. Hogenesch, J. B., Chan, W. K., Jackiw, V. H., Brown, R. C., Gu, Y. Z., PrayGrant, M., Perdew, G. H., and Bradfield, C. A. (1997) Characterization of a subset of the basic-helix-loop-helix-PAS superfamily that interacts with components of the dioxin signaling pathway, *J. Biol. Chem. 272*, 8581-8593.

18. Flamme, I., Frohlich, T., vonReutern, M., Kappel, A., Damert, A., and Risau, W. (1997) HRF, a putative basic helix-loop-helix-PAS-domain transcription factor is closely related to hypoxia-inducible factor-1 alpha and developmentally expressed in blood vessels, *Mech. Dev. 63*, 51-60.

19. Tian, H., McKnight, S. L., and Russell, D. W. (1997) Endothelial PAS domain protein 1 (EPAS1), a transcription factor selectively expressed in endothelial cells, *Genes Dev. 11*, 72-82.

20. Erbel, P. J. A., Card, P. B., Karakuzu, O., Bruick, R. K., and Gardner, K. H. (2003) Structural basis for PAS domain heterodimerization in the basic helix-loop-helix-PAS transcription factor hypoxia-inducible factor, *PNAS 100*, 15504-15509.

21. Semenza, G. L., Agani, F., Booth, G., Forsythe, J., Iyer, N., Jiang, B. H., Leung, S., Roe, R., Wiener, C., and Yu, A. (1997) Structural and functional analysis of hypoxia-inducible factor 1, *Kidney Int. 51*, 553-555.

22. Giaccia, A., Siim, B. G., and Johnson, R. S. (2003) HIF-1 as a target for drug development, *Nat. Rev. Drug Discov. 2*, 803-811.

23. Semenza, G. L. (2001) HIF-1 and mechanisms of hypoxia sensing, *Curr. Opin. Cell Biol. 13*, 167-171.

24. Schofield, C. J., and Ratchliffe, P. J. (2004) Oxygen sensing by HIF-hydroxylases, *Nat. Rev. Mol. Cell Bio. 5*, 343-354.

25. Schofield, C. J., and Ratcliffe, P. J. (2005) Signalling hypoxia by HIF hydroxylases, *Biochem. Biophys. Res. Commun. 338*, 617-626.

26. Kaelin, W. G. (2005) Proline hydroxylation and gene expression, *Annu. Rev. Biochem. 74*, 115-128.

27. Hon, W. C., Wilson, M. I., Harlos, K., Claridge, T. D. W., Schofield, C. J., Pugh, C. W., Maxwell, P. H., Ratcliffe, P. J., Stuart, D. I., and Jones, E. Y. (2002) Structural basis for the recognition of hydroxyproline in HIF-1α by pVHL, *Nature 417*, 975-978.

28. Min, J. H., Yang, H. F., Ivan, M., Gertler, F., Kaelin, W. G., and Pavletich, N. P. (2002) Structure of an HIF-1 alpha-pVHL complex: Hydroxyproline recognition in signaling, *Science 296*, 1886-1889.

29. Lando, D., Peet, D. J., Gorman, J. J., Whelan, D. A., Whitelaw, M. L., and Bruick, R. K. (2002) FIH-1 is an asparaginyl hydroxylase enzyme that regulates the transcriptional activity of hypoxia-inducible factor, *Genes Dev. 16*, 1466-1471.

30. Lando, D., Peet, D. J., Whelan, D. A., Gorman, J. J., and Whitelaw, M. L. (2002) Asparagine hydroxylation of the HIF transactivation domain: A hypoxic switch, *Science 295*, 858-861.

31. McNeill, L. A., Hewitson, K. S., Claridge, T. D., Seibel, J. r. F., Horsfall, L. E., and Schofield, C. J. (2002) Hypoxia-inducible factor asparaginyl hydroxylase (FIH-1) catalyses hydroxylation at the beta-carbon of asparagine-803, *Biochem. J. 367*, 571-575.

32. Hewitson, K. S., McNeill, L. A., Riordan, M. V., Tian, Y., Bullock, A. N., Welford, R. W., Elkins, J. M., Oldham, N. J., Bhattacharya, S., Gleadle, J. M., Ratcliffe, P. J., Pugh, C. W., and Schofield, C. J. (2002) Hypoxia-inducible factor (HIF) asparagine hydroxylase is identical to factor inhibiting HIF (FIH) and is related to the cupin structural family, *J. Biol. Chem. 277*, 26351-26355.

33. Freedman, S. J., Sun, Z. Y. J., Poy, F., Kung, A. L., Livingston, D. M., Wagner, G., and Eck, M. J. (2002) Structural basis for recruitment of CBP/p300 by hypoxia-inducible factor-1 alpha, *PNAS 99*, 5367-5372.

34. Dames, S. A., Martinez-Yamout, M., De Guzman, R. N., Dyson, H. J., and Wright, P. E. (2002) Structural basis for Hif-1 alpha/CBP recognition in the cellular hypoxic response, *PNAS 99*, 5271-5276.

35. Hirsila, M., Koivunen, P., Gunzler, V., Kivirikko, K. I., and Myllyharju, J. (2003) Characterization of the human prolyl 4-hydroxylases that modify the hypoxia-inducible factor, *J. Biol. Chem. 278*, 30772-30780.

36. Koivunen, P., Hirsila, M., Kivirikko, K. I., and Myllyharju, J. (2006) The length of peptide substrates has a marked effect on hydroxylation by the hypoxia-inducible factor prolyl 4-hydroxylases, *J. Biol. Chem. 281*, 28712-28720.

37. Ehrismann, D., Flashman, E., Genn, D. N., Mathioudakis, N., Hewitson, K. S., Ratcliffe, P. J., and Schofield, C. J. (2007) Studies on the activity of the hypoxia-inducible-factor hydroxylases using an oxygen consumption assay, *Biochem. J. 401*, 227-234.

38. Wax, S. D., Tsao, L., Lieb, M. E., Fallon, J. T., and Taubman, M. B. (1996) SM-20 is a novel 40-kd protein whose expression in the arterial wall is restricted to smooth muscle, *Lab. Invest. 74*, 797-808.

39. Willam, C., Maxwell, P. H., Nichols, L., Lygate, C., Tian, Y. M., Bernhardt, W., Wiesener, M., Ratcliffe, P. J., Eckardt, K. U., and Pugh, C. W. (2006) HIF prolyl hydroxylases in the rat; organ distribution and changes in expression following hypoxia and coronary artery ligation, *J. Mol. Cell. Cardiol. 41*, 68-77.

40. Metzen, E., Berchner-Pfannschmidt, U., Stengel, P., Marxsen, J. H., Stolze, I., Klinger, M., Huang, W. Q., Wotzlaw, C., Hellwig-Burgel, T., Jelkmann, W., Acker, H., and Fandrey, J. (2003) Intracellular localisation of human HIF-1 alpha hydroxylases: implications for oxygen sensing, *J. Cell Sci. 116*, 1319-1326.

41. Takeda, K., Cowan, A., and Fong, G. H. (2007) Essential role for prolyl hydroxylase domain protein 2 in oxygen Homeostasis of the adult vascular system, *Circulation 116*, 774-781.

42. Takeda, K., and Fong, G. H. (2007) Prolyl hydroxylase domain 2 protein suppresses hypoxia-induced endothelial cell proliferation, *Hypertension 49*, 178-184.

43. Berra, E., Benizri, E., Ginouves, A., Volmat, V., Roux, D., and Pouyssegur, J. (2003) HIF prolyl-hydroxylase 2 is the key oxygen sensor setting low steady-state levels of HIF-1 alpha in normoxia, *Embo J. 22*, 4082-4090.

44. Schofield, C. J., and Zhang, Z. (1999) Structural and mechanistic studies on 2-oxoglutarate-dependent oxygenases and related enzymes, *Curr. Opin. Struct. Biol. 9*, 722-731.

45. Hegg, E. L., and Que, L. (1997) The 2-His-1-carboxylate facial triad - An emerging structural motif in mononuclear non-heme iron(II) enzymes, *Eur. J. Biochem. 250*, 625-629.

46. Koehntop, K. D., Emerson, J. P., and Que, L. (2005) The 2-His-1-carboxylate facial triad: a versatile platform for dioxygen activation by mononuclear non-heme iron(II) enzymes, *J. Biol. Inorg. Chem. 10*, 87-93.

47. Clifton, I. J., McDonough, M. A., Ehrismann, D., Kershaw, N. J., Granatino, N., and Schofield, C. J. (2006) Structural studies on 2-oxoglutarate oxygenases and related double-stranded beta-helix fold proteins, *J. Inorg. Biochem. 100*, 644-669.

48. Bugg, T. D. H. (2001) Oxygenases: mechanisms and structural motifs for O_2 activation, *Curr. Op. in Chem. Biol. 5*, 550-555.

49. Bugg, T. D. H. (2003) Dioxygenase enzymes: catalytic mechanisms and chemical models, *Tetrahedron 59*, 7075-7101.

50. Bugg, T. D. H., and Ramaswamy, S. (2008) Non-heme iron-dependent dioxygenases: unravelling catalytic mechanisms for complex enzymatic oxidations, *Curr. Op. in Chem. Biol. 12*, 134-140.

51. Dann, C. E., Bruick, R. K., and Deisenhofer, J. (2002) Structure of factor-inhibiting hypoxia-inducible factor 1: An asparaginyl hydroxylase involved in the hypoxic response pathway, *PNAS 99*, 15351-15356.

52. Elkins, J. M., Hewitson, K. S., McNeill, L. A., Seibel, J. F., Schlemminger, I., Pugh, C. W., Ratcliffe, P. J., and Schofield, C. J. (2003) Structure of factor-inhibiting hypoxia-inducible factor (HIF) reveals mechanism of oxidative modification of HIF-1 alpha, *J. Biol. Chem. 278*, 1802-1806.

53. Lee, C., Kim, S. J., Jeong, D. G., Lee, S. M., and Ryu, S. E. (2003) Structure of Human FIH-1 Reveals a Unique Active Site Pocket and Interaction Sites for HIF-1 and von Hippel-Lindau, *J. Biol. Chem. 278*, 7558-7563.

54. Proshlyakov, D. A., Henshaw, T. F., Monterosso, G. R., Ryle, M. J., and Hausinger, R. P. (2004) Direct Detection of Oxygen Intermediates in the Non-Heme Fe Enzyme Taurine/alpha-Ketoglutarate Dioxygenase, *J. Am. Chem. Soc. 126*, 1022-1023.

55. Fujimori, D. G., Barr, E. W., Matthews, M. L., Koch, G. M., Yonce, J. R., Walsh, C. T., Bollinger, J. M., Krebs, C., and Riggs-Gelasco, P. J. (2007) Spectroscopic evidence for a high-spin Br-Fe(IV)-Oxo intermediate in the alpha-ketoglutarate-dependent halogenase CytC3 from Streptomyces, *J. Am. Chem. Soc. 129*, 13408-+.

56. Riggs-Gelasco, P. J., Price, J. C., Guyer, R. B., Brehm, J. H., Barr, E. W., Bollinger, J. M., and Krebs, C. (2004) EXAFS spectroscopic evidence for an Fe = O unit in the Fe(IV) intermediate observed during oxygen activation by taurine :alpha-ketoglutarate dioxygenase, *J. Am. Chem. Soc. 126*, 8108-8109.

57. Price, J. C., Barr, E. W., Tirupati, B., Bollinger, J. M., and Krebs, C. (2003) The First Direct Characterization of a High-Valent Iron Intermediate in the Reaction of an α-Ketoglutarate-Dependent Dioxygenase: A High-Spin Fe(IV) Complex in Taurine/α-Ketoglutarate Dioxygenase (TauD) from Escherichia coli *Biochemistry 42*, 7497-7508.

58. Price, J. C., Barr, E. W., Glass, T. E., Krebs, C., and Bollinger, J. M. (2003) Evidence for Hydrogen Abstraction from C1 of Taurine by the High-Spin Fe(IV) Intermediate Detected during Oxygen Activation by Taurine:α-Ketoglutarate Dioxygenase (TauD), *J. Am. Chem. Soc. 125*, 13008-13009.

59. Hausinger, R. P. (2004) Fe(II)/alpha-Ketoglutarate-dependent hydroxylases and related enzymes, *Crit. Rev. Biochem. Mol. Biol. 39*, 21-68.

60. Ryle, M. J., and Hausinger, R. P. (2002) Non-heme iron oxygenases, *Curr. Op. in Chem. Biol. 6*, 193-201.

61. Abu-Omar, M. M., Loaiza, A., and Hontzeas, N. (2005) Reaction mechanisms of mononuclear non-heme iron oxygenases, *Chem. Rev. 105*, 2227-2252.

62. Costas, M., Mehn, M. P., Jensen, M. P., and Que, L. (2004) Dioxygen Activation at Mononuclear Nonheme Iron Active Sites: Enzymes, Models, and Intermediates, *Chem. Rev. 104*, 939-986.

63. Solomon, E. I., Brunold, T. C., Davis, M. I., Kemsley, J. N., Lee, S. K., Lehnert, N., Neese, F., Skulan, A. J., Yang, Y. S., and Zhou, J. (2000) Geometric and electronic structure/function correlations in non-heme iron enzymes, *Chem. Rev. 100*, 235-349.

64. Hanauske-Abel, H. M., and Günzler, V. (1982) A stereochemical concept for the catalytic mechanism of prolylhydroxylase : Applicability to classification and design of inhibitors, *J. Theor.Biol. 94*, 421-455.

65. Hewitson, K. S., McNeill, L. A., and Schofield, C. J. (2003) The role of iron and 2-oxoglutarate oxygenases in signaling, *Biochem. Soc. T. 31*, 510-515.

66. Welford, R. W. D., Kirkpatrick, J. M., McNeill, L. A., Puri, M., Oldham, N. J., and Schofield, C. J. (2005) Incorporation of oxygen into the succinate co-product of iron(II) and 2-oxoglutarate dependent oxygenases from bacteria, plants and humans, *FEBS Letters 579*, 5170-5174.

67. Kovaleva, E. G., and Lipscomb, J. D. (2008) Versatility of biological non-heme Fe(II) centers in oxygen activation reactions, *Nat Chem Biol 4*, 186-193.

68. Que, L. (2000) One motif-many different reactions, *Nat. Struct. Biol. 7*, 182-184.

69. Groce, S. L., and Lipscomb, J. D. (2005) Aromatic ring cleavage by homoprotocatechuate 2,3-dioxygenase: Role of His200 in the kinetics of interconversion of reaction cycle intermediates, *Biochemistry 44*, 7175-7188.

70. Groce, S. L., Miller-Rodeberg, M. A., and Lipscomb, J. D. (2004) Single-turnover kinetics of homoprotocatechuate 2,3-dioxygenase, *Biochemistry 43*, 15141-15153.

71. Kovaleva, E. G., and Lipscomb, J. D. (2007) Crystal structures of Fe^{2+} dioxygenase superoxo, alkylperoxo, and bound product intermediates, *Science 316*, 453-457.

72. Kovaleva, E. G., and Lipscomb, J. D. (2008) Intermediate in the O-O Bond Cleavage Reaction of an Extradiol Dioxygenase, *Biochemistry 47*, 11168-11170.

73. Senda, T., Sugiyama, K., Narita, H., Yamamoto, T., Kimbara, K., Fukuda, M., Sato, M., Yano, K., and Mitsui, Y. (1996) Three-dimensional structures of free form and two substrate complexes of an extradiol ring-cleavage type dioxygenase, the BphC enzyme from Pseudomonas sp strain KKS102, *J. Mol. Biol. 255*, 735-752.

74. Shu, L. J., Chiou, Y. M., Orville, A. M., Miller, M. A., Lipscomb, J. D., and Que, L. (1995) X-ray absorption spectroscopic studies of the Fe(II) active site of catechol 2,3-dioxygenase - Implications for the extradiol cleavage mechanism, *Biochemistry 34*, 6649-6659.

75. Groce, S. L., Miller, M. A., and Lipscomb, J. D. (1999) Transient kinetic studies of homoprotocatechuate 2,3-dioxygenase, *J. Inorg. Biochem. 74*, 149-149.

76. Ensley, B. D., Gibson, D. T., and Laborde, A. L. (1982) Oxidation of naphthalene by a multicomponent enzyme system from pseudomonas SP Strain NCIB9816, *J. Bacteriol. 149*, 948-954.

77. Carredano, E., Karlsson, A., Kauppi, B., Choudhury, D., Parales, R. E., Parales, J. V., Lee, K., Gibson, D. T., Eklund, H., and Ramaswamy, S. (2000) Substrate binding site of naphthalene 1,2-dioxygenase: Functional implications of indole binding, *J. Mol. Biol. 296*, 701-712.

78. Kauppi, B., Lee, K., Carredano, E., Parales, R. E., Gibson, D. T., Eklund, H., and Ramaswamy, S. (1998) Structure of an aromatic-ring-hydroxylating dioxygenase-naphthalene 1,2-dioxygenase, *Struct. Fold. Des. 6*, 571-586.

79. Ohta, T., Chakrabarty, S., Lipscomb, J. D., and Solomon, E. I. (2008) Near-IR MCD of the nonheme ferrous active site in naphthalene 1,2-dioxygenase: Correlation to crystallography and structural insight into the mechanism of Rieske dioxygenases, *J. Am. Chem. Soc. 130*, 1601-1610.

80. Wolfe, M. D., Parales, J. V., Gibson, D. T., and Lipscomb, J. D. (2001) Single turnover chemistry and regulation of O_2 activation by the oxygenase component of naphthalene 1,2-dioxygenase, *J. Biol. Chem. 276*, 1945-1953.

81. Karlsson, A., Parales, J. V., Parales, R. E., Gibson, D. T., Eklund, H., and Ramaswamy, S. (2003) Crystal structure of naphthalene dioxygenase: Side-on binding of dioxygen to iron, *Science 299*, 1039-1042.

82. Chakrabarty, S., Austin, R. N., Deng, D. Y., Groves, J. T., and Lipscomb, J. D. (2007) Radical intermediates in monooxygenase reactions of Rieske dioxygenases, *J. Am. Chem. Soc. 129*, 3514-+.

83. Wackett, L. P. (2002) Mechanism and applications of Rieske non-heme iron dioxygenases, *Enzyme Microb. Technol. 31*, 577-587.

84. Lee, K. (1999) Benzene-Induced Uncoupling of Naphthalene Dioxygenase Activity and Enzyme Inactivation by Production of Hydrogen Peroxide, *J. Bacteriol. 181*, 2719-2725.

85. Fitzpatrick, P. F. (2000) The aromatic amino acid hydroxylases, in *Advances in Enzymology, Vol 74*, pp 235-+, John Wiley & Sons Inc, New York.

86. Fitzpatrick, P. F. (1999) Tetrahydropterin-dependent amino acid hydroxylases, *Annu. Rev. Biochem. 68*, 355-381.

87. Pavon, J. A., Eser, B., Huynh, M. T., and Fitzpatrick, P. F. (2010) Single Turnover Kinetics of Tryptophan Hydroxylase: Evidence for a New Intermediate in the Reaction of the Aromatic Amino Acid Hydroxylases, *Biochemistry 49*, 7563-7571.

88. Pavon, J. A., and Fitzpatrick, P. F. (2006) Insights into the catalytic mechanisms of phenylalanine and tryptophan hydroxylase from kinetic isotope effects on aromatic hydroxylation, *Biochemistry 45*, 11030-11037.

89. Eser, B. E., Barr, E. W., Frantorn, P. A., Saleh, L., Bollinger, J. M., Krebs, C., and Fitzpatrick, P. F. (2007) Direct spectroscopic evidence for a high-spin Fe(IV) intermediate in tyrosine hydroxylase, *J. Am. Chem. Soc. 129*, 11334-+.

90. Dix, T. A., and Benkovic, S. J. (1985) Mechanism of uncoupled tetrahydropterin oxidation by phenylalanine hydroxylase, *Biochemistry 24*, 5839-5846.

91. Dix, T. A., and Benkovic, S. J. (1988) Mechanism of oxygen activation by pteridine dependent monooxygenases, *Acc. Chem. Res. 21*, 101-107.

92. Roach, P. L., Clifton, I. J., Hensgens, C. M. H., Shibata, N., Schofield, C. J., Hajdu, J., and Baldwin, J. E. (1997) Structure of isopenicillin N synthase complexed with substrate and the mechanism of penicillin formation, *Nature 387*, 827-830.

93. Dubus, A., Sami, M., Brown, T. J. N., Schofield, C. J., Baldwin, J. E., and Frere, J. M. (2000) Studies of isopenicillin N synthase enzymatic properties using a continuous spectrophotometric assay, *FEBS Letters 485*, 142-146.

94. Perry, D., Abraham, E. P., and Baldwin, J. E. (1988) Factors affecting the isopenicillin-N synthase reaction, *Biochem. J. 255*, 345-351.

95. Muller, I., Kahnert, A., Pape, T., Sheldrick, G. M., Meyer-Klaucke, W., Dierks, T., Kertesz, M., and Uson, I. (2004) Crystal Structure of the Alkylsulfatase AtsK: Insights into the Catalytic Mechanism of the Fe(II) alpha-Ketoglutarate-Dependent Dioxygenase Superfamily, *Biochemistry 43*, 3075-3088.

CHAPTER 2

UNCOUPLED O_2-ACTIVATION IN THE HUMAN HIF-ASPARAGINYL HYDROXYLASE, FIH, DOES NOT PRODUCE REACTIVE OXYGEN SPECIES

2.1 Introduction

Cellular oxygen-sensing in metazoans is directly controlled by enzymes which hydroxylate the alpha-subunit of the hypoxia inducible factor (HIFα or HIF-1α) (*1-3*). As the HIF-hydroxylases are key regulators of angiogenesis and basal metabolism, they are potential targets for treating diseases such as cancer and stroke (*4-6*). The two types of HIF-hydroxylase are the factor inhibiting HIF-1 (FIH) and prolyl hydroxylase (PHD) (*7-9*), both of which are Fe(II), α-ketoglutarate-dependent hydroxylases. The best characterized of these enzymes is the human enzyme FIH, which hydroxylates the Asn^{803} residue within the C-terminal transactivation domain (CTAD) of HIFα (*10*), thereby preventing transcriptional machinery from binding to HIFα.

αKG hydroxylases catalyze two half-reactions resulting in the transfer of oxidizing equivalents from O_2 to both αKG and the primary substrate (Scheme 2.1) (*4, 11, 12*). The first half-reaction is O_2-activation, in which the αKG/$[Fe]^{2+}$ is oxidatively decarboxylated to form succinate/$[FeO]^{2+}$ and CO_2 (*13, 14*). The second half-reaction is transfer of the oxidant from $[FeO]^{2+}$ to the prime substrate (*15, 16*), which may include reactions such as desaturation, demethylations, ring-closure, and hydroxylation (*11, 12, 17*); in the case of FIH, this reaction is the hydroxylation of the β-carbon of Asn^{803} (*10*). Tight coupling between these two half-reactions is challenging, and many of the αKG-

dependent hydroxylases exhibit reactions with O_2 that are uncoupled (*18-26*). In some cases this leads to auto-hydroxylation of residues within enzyme active sites (*18, 21, 22, 25*), however, more commonly, it leads to metal oxidation that can be rescued by ascorbate (*12, 23, 26*).

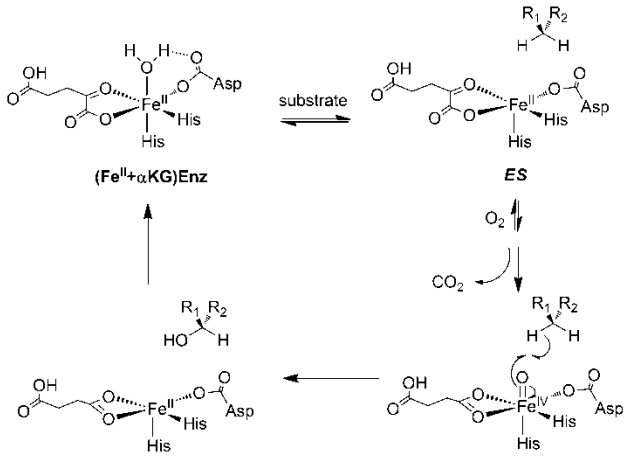

Scheme 2.1 Consensus chemical mechanism of αKG-dependent hydroxylases. The (Fe+αKG)Enzyme binds the primary substrate to form the *ES* complex.

The prevailing model for how αKG hydroxylases may achieve coupled turnover focuses on changes in the coordination number about the Fe(II) upon substrate binding. In this model, the Fe(II) is six-coordinate prior to prime substrate binding, coordinated by a His_2(Asp/Glu) facial triad, a bidentate αKG, and a single H_2O ligand. Once the prime substrate binds, the H_2O ligand (*17*) is released to form a five-coordinate Fe(II) center which is ready to react with O_2. Crystal structures of several αKG hydroxylases support this model (*12, 27-29*), as does mechanistic data indicating that poor substrates stimulate uncoupling (*20, 24, 26, 30*). Perhaps the strongest evidence comes from advanced spectroscopic studies that clearly show this coordination change occurs upon substrate binding (*31-33*). Tight coupling would be highly beneficial to an O_2-sensing enzyme, such as FIH.

There are three criteria for effective O_2-sensing by HIF hydroxylases. First, the $K_{M(O2)}$ should lie above the physiological pO_2, so that the rate of HIF hydroxylation is proportional to the pO_2. As the reported $K_{M(O2)}$ for FIH is much higher than the cellular pO_2 under physiological conditions (*34*, *35*), it appears that FIH is well suited for its regulatory role by this first criterion. Second, uncoupling between the two half-reactions must be low, ideally such that no molecule of O_2 reacts without HIF hydroxylation, due to the potential for oxidative damage. Although αKG hydroxylases are mechanistically predisposed to some uncoupling between O_2-activation and substrate hydroxylation (*12*, *36*), and FIH can autohydroxylate in the absence of prime substrate (*18*), the extent of uncoupling during steady-state turnover by FIH is unknown. Third, release of reactive oxygen species (ROS) from the active site should be minimal in order to avoid oxidative damage to the cell. The propensity of FIH to produce ROS has never been tested.

Here we use chemical methods to test the uncoupling and ROS production from human FIH in comparison to AtsK, a metabolic αKG hydroxylase involved in bacterial sulfur metabolism (*37*). As metabolic enzymes are expected to favor fast catalysis over tight coupling, we felt that AtsK would be an instructive contrast to FIH. We observed that FIH does not uncouple during turnover conditions, nor does it release ROS under any tested conditions. FIH does, however, autohydroxylate in a slow reaction in the absence of substrate, forming an inactive form FIH. In contrast, AtsK uncouples under turnover conditions and releases H_2O_2.

2.2 Experimental Procedures

2.2.1 Materials

The prime substrate for FIH was a 39-residue peptide corresponding to HIF$\alpha^{788\text{-}826}$ with a Cys^{800}→Ala point mutation, which corresponds to the C-terminal transactivation domain of HIF-1α (CTAD). The CTAD sequence used (Asn^{803} underlined) was DESGL-PQLTS-YDAEV-NAPIQ-GSRNL-LQGEE-LLRAL-DQVN, which was unmodified at the peptide termini. CTAD peptide was purchased from EZBiolabs as a desalted product, and was further purified by reverse-phase HPLC. Hexylsulfate ($HexSO_4$) and NADH were obtained from Acros Organics. The enzymes used in coupled assays were from commercial sources: alcohol dehydrogenase and Cu/Zn superoxide dismutase were from MP Biomedicals, horseradish peroxidase was from Fluka. A succinate detection kit was purchased from R-Biopharm.

2.2.2 Protein Expression, Purification and Activity

AtsK and FIH were expressed and purified as previously described (*19, 37*). AtsK activity was measured continuously with both oxygen sensor using a Clark-type electrode and coupling the enzyme reaction with NADH/alcohol dehydrogenase at 25°C. In O_2 consumption assay, 200 μM ascorbate, 1 mM αKG, 0-1 mM $HexSO_4$ and 100 μM $FeSO_4$ were premixed in 1 mL volume with 10 mM HEPES pH 7.00, and the reaction was initiated by adding 1 μM AtsK, and oxygen consumption was monitored. AtsK activity was also monitored by coupling the enzyme reaction with 160 μM NADH and 5 unit/mL alcohol dehydrogenase in 100 μL volume by monitoring the absorbance change of NADH at 340 nm in UV-Visible(UV-Vis) Spectrometer.

FIH activity was monitored by a quenched time point assay and analyzed by LC-MS. In a 50 µL reaction volume, 2 mM ascorbate, 0.1 mM DTT, 5 unit/mL catalase, 500 µM αKG, 25 µM $FeSO_4$, 0-600 µM CTAD were preincubated at 37°C and 0.5-5 µM of FIH was added to initiate the reaction. At certain time points 5 µL aliquots were taken and the reaction was quenched with 45 µL 0.1% formic acid. For each reaction 5-10 samples were prepared on a 3-10 min time scale and analyzed by LC-MS using a C_8 column. The +3 charge-state of parental and and hydroxylated CTAD peaks were observed at m/z of 1419.1 and 1424.4 respectively, as expected for the anticipated mass gain of 16 amu in the product. The ratio of hydroxylated CTAD peak intensity to overall peak intensity was calculated for each sample and the rate was calculated from a linear fit of these time points.

2.2.3 Uncoupling

2.2.3.1 Absence of prime substrate

Small volumes of an AtsK stock (0.38 mM) were injected into a 1.00 mL solution containing 100 µM $FeSO_4$, 200 µM ascorbate, 1 mM αKG and were mixed in 10 mM HEPES buffer pH 7.00, 25 °C. The FIH assay was performed with 50 µM $FeSO_4$, 500 µM αKG, and 11.7 µM FIH in 50 mM HEPES, pH 7.50, 37°C. O_2 consumption was monitored by a Clark-type electrode (YSI Incorporated).

2.2.3.2 Presence of prime substrate

The coupling ratio of each enzyme was determined in the presence of varied concentrations of primary substrate. For AtsK, the amount of consumed oxygen was

compared to the amount of product formed by oxygen consumption and NADH coupled assays, respectively. The coupling ratio of FIH was obtained by comparing the amount of succinate formed to the amount of hydroxylated peptide. Succinate was measured by UV-Vis spectroscopy using a succinate detection kit and hydroxylated CTAD was analyzed by LC-MS.

2.2.4 ROS Production

2.2.4.1 H_2O_2 / O_2^- assays

Hydrogen peroxide production was detected by coupling H_2O_2 oxidation of 50 μM 2,2'-azino-bis(3-ethylbenzthiazoline-6-sulfonic acid) (ABTS) with 1 Unit/mL horseradish peroxidase (HRP). Hydrogen peroxide production was continuously monitored at 405 nm. Ascorbic acid was excluded from the reaction mixtures to prevent reduction of $ABTS^+$. Superoxide detection was accomplished in a same manner of peroxide detection, by the use of 100 Unit/mL Cu/Zn superoxide dismutase (Cu/Zn SOD) to convert O_2^- into H_2O_2. The reaction conditions for H_2O_2 and O_2^- detection included the coupling reagents with the respective enzyme assays; for AtsK: 11.4 μM AtsK, 1 mM αKG, 0-100 μM $HexSO_4$, 100 μM $FeSO_4$; for FIH: 5 μM FIH, 500 μM αKG, 50 μM $FeSO_4$, 0-100 μM CTAD.

2.2.4.2 $OH^\bullet$ radical assay

Hydroxyl radical detection of AtsK and FIH was achieved by mixing enzyme activity assay solutions with 15 mM 2-deoxyribose (*38*). Primary substrate concentrations were varied for AtsK, 0-600 μM $HexSO_4$; and for FIH, 0-120 μM CTAD. The reactions were

initiated by adding enzyme then incubating at 37 °C for 1 hour. Reactions were quenched with 100 µl 1% thiobarbituric acid in 50 mM NaOH and 100 µL 2.8 % trichloroacetic acid in water. The solution was heated at 100 °C for 20 minutes. After cooling down to room temperature, the absorbance at 532 nm was measured. The zero substrate sample was treated as a reference.

2.2.5 Inactivation and Rescue of Inactivated Enzyme

2.2.5.1 1 Inactivation of AtsK

Inactivation of AtsK was tested by changing the concentration of AtsK in a reaction from 1 to 10 µM, in the NADH-coupled assay detected at 340 nm. 1 mM αKG, 1mM $HexSO_4$, 100 µM Fe(II), 0-2 mM ascorbic acid, 1-10 µM AtsK, 30 µM NADH and 30 units of alcohol dehydrogenase were used in a 100 µL reaction volume.

2.2.5.2 Inactivation and rescue of autohydroxylated FIH

Autohydroxylated FIH was prepared to test for re-activation conditions. Under anaerobic conditions, 50 mM HEPES (pH 7.50) αKG (100 µM), FIH (49 µM) and $FeSO_4$ (50 µM) were added to a septum-sealed UV cuvette. An initial UV-Vis absorption spectrum was collected; the septum was then removed to introduce air and initiate the reaction. The characteristic absorption peak of autohydroxylated FIH (λ_{max} = 583 nm) grew over several hours (*18*). Autohydroxylated FIH was tested for activity in an assay mixture containing αKG (500 µM), $FeSO_4$ (25 µM), CTAD (70 µM), autohydroxylated FIH (5 µM), and a mild reductant. The mild reductants ascorbate (0 - 2 mM) and DTT (0 - 0.1 mM) were tested for their ability to re-activate auto-hydroxylated FIH. Samples were analyzed for hydroxylated CTAD by LC-ESI-MS.

2.3 Results

Uncoupling for FIH and AtsK was evaluated by comparing the steady-state kinetic signatures of the two half reactions. As O_2 reacts with αKG to form succinate and CO_2 in the first half-reaction, the stoichiometry of O_2-activation was measured by O_2 consumption or succinate formation. This assumes that O_2 is only activated by oxidative decarboxylation of αKG. The rate of prime substrate hydroxylation was monitored by mass spectrometry for FIH or by a UV-Vis assay for AtsK. A fully coupled reaction would exhibit an [O_2]:[hydroxylated product] ratio of unity; deviations from this ratio would indicate that O_2 was being activated in the absence of substrate hydroxylation.

Uncoupling for AtsK and FIH was measured with variable concentrations of substrate. The solution conditions for AtsK included 0 – 1000 μM $HexSO_4$, with up to 3.0 μM AtsK. AtsK was tightly coupled under steady-state conditions, as the number of enzyme turnovers was equivalent by both Clark electrode and by the UV-Vis assay. These assays indicated a coupling ratio of 1.04 ± 0.07 in the steady-state for AtsK (Figure 2.1A). As the $K_{M(HexSO4)}$ is 15 μM for AtsK, the measured steady-state coupling ratio for AtsK reflected that of an *ES* complex, indicating that once AtsK bound $HexSO_4$ and entered its catalytic cycle it completed the hydroxylation with relatively high fidelity (ca. 96%). This indicated that AtsK turnover was much faster than uncoupling from the ES complex.

Similarly, FIH was tightly coupled as shown by the stoichiometry of succinate to hydroxylated peptide present in quenched reactions. FIH (2 μM) was incubated with CTAD (200 μM) and the reaction quenched at several time points for analysis. These

assays indicated a coupling ratio of 1.03 ± 0.17 in the steady-state for FIH (Figure 2.1B). FIH distributed between predominantly an (Fe^2+αKG)FIH form at low [CTAD], and an *ES* complex at high [CTAD], as we measured the $K_{M(CTAD)}$ as 77 μM (*39*). Nevertheless, FIH exhibited a tightly coupled reaction under steady-state conditions, indicating that O_2-activation by FIH is tightly controlled. It should be noted that the succinate assay used to measure O_2-activation by FIH was less precise than the simpler UV-Vis assay used for AtsK, due to the many reaction components and manipulations needed.

The consumption of O_2 by AtsK and FIH in the absence of prime substrate was directly monitored by use of a Clark electrode (Figure 2.2). Small volumes of enzyme (1-3 μL) were injected into thermostated 1.00 mL reaction buffer containing $FeSO_4$ (100 μM), ascorbate (200 μM), and αKG (1mM). Despite the tight coupling ratios observed during steady-state turnover, O_2 consumption was not absolutely tied to substrate hydroxylation for either enzyme. In the case of AtsK, O_2 was consumed within 30 seconds at a molar stoichiometry of 2.5 (+/- 0.2) O_2 per AtsK active site (Figure 2.3). Such a rapid reaction with O_2 is reminiscent of the fast inactivation observed for several other αKG hydroxylases, such as TauD and TfdA (*25*, *26*).

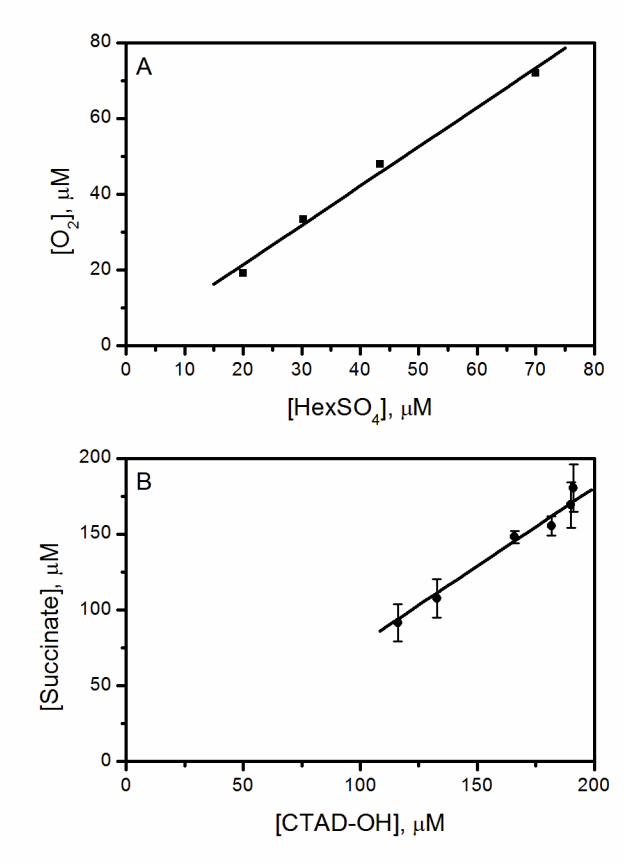

Figure 2.1 Coupling of O_2 to prime substrate for AtsK and FIH. A) O_2 consumption vs. $HexSO_4$ hydroxylation for AtsK. AtsK (0.38 – 3.0 μM), ascorbate (200 μM), αKG (1 mM), $FeSO_4$ (100 μM), $HexSO_4$ (1 mM), NADH (160 μM), alcohol dehydrogenase (5 Unit/mL) in 10 mM HEPES (10 mM, pH 7.00). B) Succinate production vs. CTAD hydroxylation for FIH. FIH (2.0 μM), ascorbate (2000 μM), DTT (100 μM), αKG (500 μM), $FeSO_4$ (50 μM), CTAD (240 μM) in HEPES (50 mM, pH 7.50).

In contrast, injections of FIH at a final concentration of 11.7 μM consumed no measurable O_2 on the minutes timescale (Figure 2.2A). Although we were unable to measure any uncoupled O_2-consumption for FIH on the minutes timescale, we did reproduce the autohydroxylation reaction (*18*). Autohydroxylation required O_2, and formed a hydroxylated Trp^{296} residue on FIH (*18*), which is formed via hydroxylase activity in the absence of CTAD.

Although the coupling ratios for both FIH and AtsK were near unity during the steady-state, the consumption of O_2 by AtsK in the absence of prime substrate suggested that ROS may be produced by the resting form of AtsK, (Fe+ αKG)AtsK. As an enzyme will partition amongst various forms depending on substrate concentrations, ROS formation was measured while varying prime substrate concentrations for both FIH and AtsK. The tested ROS species were superoxide (O_2^-), hydrogen peroxide (H_2O_2), and hydroxyl radical ($OH^\bullet$), which may form depending on the number of electrons transferred to O_2.

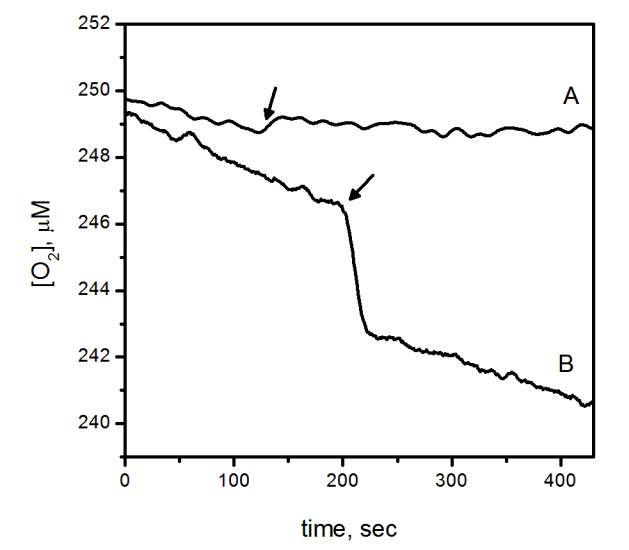

Figure 2.2 Oxygen consumption of FIH and AtsK measured with O_2 sensor; A) FIH (11.7 µM) mixed with $FeSO_4$ (50 µM), αKG (500 µM) in 50 mM HEPES pH 7.5 B) AtsK (1.14 µM) mixed with ascorbate (200 µM), $FeSO_4$ (100µM), αKG (1 mM) in 10 mM HEPES pH 7.00.

Both H_2O_2 and O_2^- were assayed by a peroxidase/ABTS assay in which H_2O_2 was indicated by a characteristic absorption at 405 nm due to the formation of ABTS+. In the

absence of $HexSO_4$, AtsK (11.4 µM) produced 0.12 µM H_2O_2; this was much less than the anticipated 2.5 equivalents of O_2 consumed by AtsK. Under steady-state conditions, AtsK produced up to 0.47 µM H_2O_2, with [$HexSO_4$] ranging from 0 – 800 µM. Notably, H_2O_2 production was a saturable function of [$HexSO_4$], with an apparent half-maximal value of 10 µM $HexSO_4$ (Figure 2.4). As this is similar to the reported $K_{M(HexSO4)}$ (*37*), it suggested that H_2O_2 was also released from the *ES* complex of AtsK, (Fe^2+αKG+$HexSO_4$)AtsK.

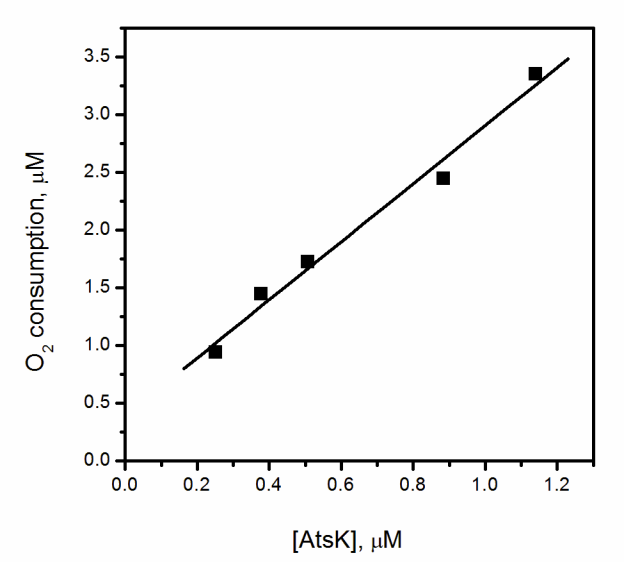

Figure 2.3 Oxygen consumption of AtsK in the absence of HexSO4. AtsK (0.2-1.2 µM) mixed with ascorbate (200 µM), FeSO4 (100 µM) and αKG (1 mM) in 10 mM HEPES pH 7.00.

FIH (5 µM) failed to produce measurable levels of H_2O_2 under any tested condition. FIH concentrations were varied between 5 and 50 µM in the absence of CTAD to test for H_2O_2 production by (Fe^{2+}+αKG)FIH, however H_2O_2 was not detected even at 50 µM FIH. FIH was also tested under steady-state conditions with 50 µM CTAD; however,

H_2O_2 was not detected suggesting that the *ES* complex, (Fe^2+αKG+CTAD)FIH, did not produce H_2O_2. This was consistent with the near unity coupling ratio for FIH (Figure 2.4 inset).

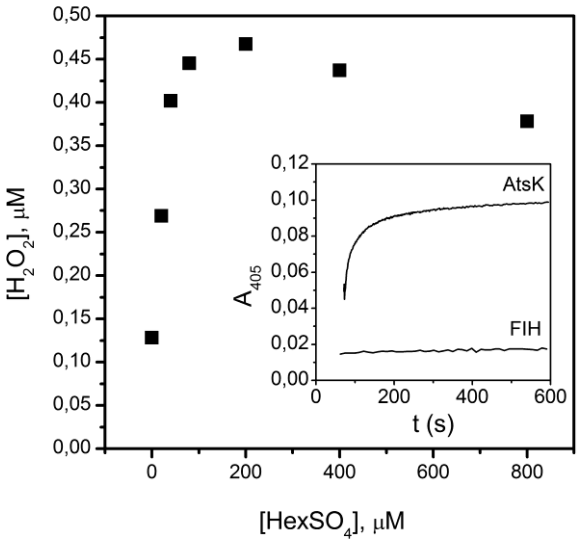

Figure 2.4 H_2O_2 produced by AtsK (11.4 μM) during steady state turnover. Inset) Timecourse for H_2O_2 production by AtsK (upper line) and FIH (lower line). AtsK (11.4 μM) was added into a reaction mixture containing $FeSO_4$ (100 μM), αKG (1 mM), $HexSO_4$ (100 μM), ABTS (50 μM) and HRP (1 unit/mL) in 10 mM HEPES pH 7.00. FIH (5 μM) was added into a solution wich has $FeSO_4$ (25 μM), αKG (500 μM), CTAD (50 μM), ABTS (50 μM) and HRP (1 unit/mL) in 50 mM HEPES pH 7.50.

Superoxide was measured by the use of Cu/Zn SOD to convert two equivalents of O_2^- into one equivalent of H_2O_2 for the peroxidase/ABTS assay. Neither AtsK nor FIH produced detectable O_2^- by this coupled assay in the absence of prime substrate; experiments in the presence of added prime substrate similarly yielded no detectable O_2^-.

Hydroxyl radicals were tested by the deoxyribose method, a qualitative colorimetric assay that compares $OH^{\bullet}$ production to a baseline condition by normalized absorptivities (A/A_0); an increase in A/A_0 would indicate that more $OH^{\bullet}$ radical were produced. AtsK (1.14 µM) was tested at varied concentrations of $HexSO_4$ (0-600 µM). This allowed a comparison of different enzyme forms, with free enzyme prevalent at sub-saturating concentrations of $HexSO_4$, and an *ES* complex prevalent at saturation. A plot of the normalized data indicated a slight decrease in $OH^{\bullet}$ production in the presence of $HexSO_4$, however this was independent of [$HexSO_4$] (A/A_0 = 0.91 +/- 0.05) (Figure 2.5A). This showed that $OH^{\bullet}$ radical production was not a function of enzyme form, suggesting that neither the free enzyme nor the *ES* complex produced diffusible $OH^{\bullet}$. Similarly, FIH (0.5 µM) was assayed for $OH^{\bullet}$ production at varied CTAD concentrations. The normalized data was a line of zero slope with respect to [CTAD] (A/A_0 = 1.03 +/- 0.03) (Figure 2.5B). This indicated that $OH^{\bullet}$ radical production was not a function of enzyme form. As with AtsK, this suggested that FIH did not produce diffusible $OH^{\bullet}$ radicals.

During steady-state kinetics assays, we noted a biphasic time course for AtsK, indicating enzyme inactivation. Inactivation could result from the oxidation of the iron pool into Fe(III), or from specific changes to AtsK. Oxidation of iron was excluded as the reason for inactivation by serial injections of AtsK (0.5-1 µM, 1.25-2.5 µL) into a 1.0 mL reaction solution containing $HexSO_4$ (1 mM) and $FeSO_4$ (100 µM); ascorbate was omitted to simplify data interpretation. Each injection of AtsK consumed O_2 for approximately 60 seconds, followed by a return to baseline; subsequent AtsK injections were similarly active (Figure 2.6A). This showed that the Fe(II) and $HexSO_4$ in solution

were sufficient for turnover, and that diluted AtsK (1 μM) itself became inactive within one minute.

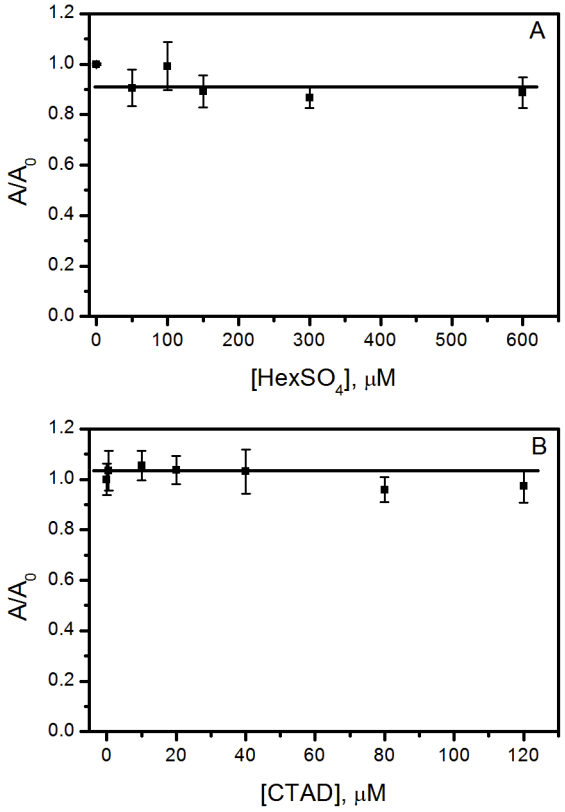

Figure 2.5 Hydroxyl radical assays of AtsK and FIH. A) AtsK (1.14 μM), ascorbate (200 μM), αKG (1 mM), $FeSO_4$ (100 μM), $HexSO_4$ (0-600 μM), 2-deoxyribose (15 mM) in 10 mM HEPES pH 7.0 B) FIH (0.5 μM), ascorbate (2 mM), αKG (500 μM), $FeSO_4$ (25 μM), CTAD (0-120 μM), 2-deoxyribose (15 mM) in 50 mM HEPES pH 7.50.

As AtsK is a tetramer (*29*), we tested de-oligomerization as the cause of the rapid inactivation. Timecourses for varied concentrations of AtsK (0.5 – 10 μM) were monitored by either the UV-Vis assay or the O_2-consumption assay. High concentrations of AtsK (5 – 10 μM) were active for hundreds of seconds, whereas low concentrations

(0.5 – 1 μM) inactivated within 50 seconds (Figure 2.6 A, B), suggesting that de-oligomerization was the root cause of the rapid inactivation.

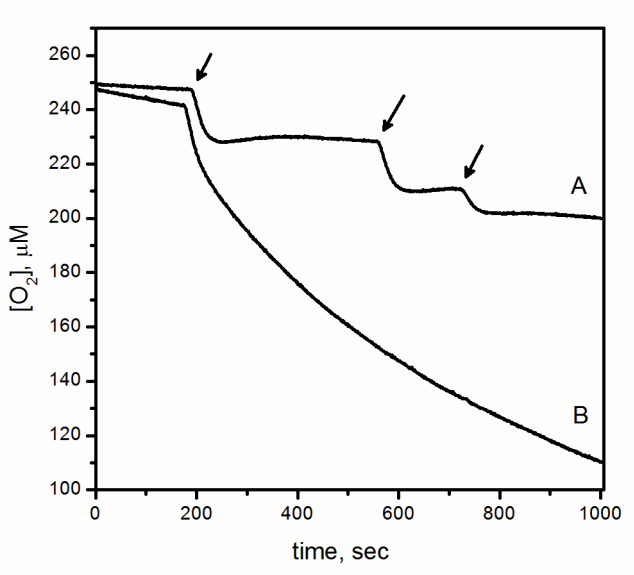

Figure 2.6 Inactivation of AtsK measured by O_2-electrode. A) Sequential injection of AtsK (1 μM, 1 μM, 0.5 μM) into a mixture of $FeSO_4$ (100 μM), ascorbate (200 μM), αKG (1 mM), HexSO4 (1 mM) in 10 mM HEPES pH 7.00. B) Injection of high concentration of AtsK (7 μM) into same reaction conditions as in A.

FIH exhibited linear progress curves for more than 4 minutes in steady-state assays that included ascorbate, indicating that enzyme inactivation was not a rapid process. However, we previously observed that FIH would autohydroxylate over several hours to form an Fe(III) form of the enzyme called 'purple FIH' in which Fe(III) was coordinated by the hydroxy-group of hydroxylated Trp^{296} (*18*). As Saari and Hausinger noted that inactivated TfdA was partially rescued by ascorbate (*26*), we tested two common reductants for their ability to rescue auto-hydroxylated FIH. First, we tested auto-hydroxylated FIH for activity; purple FIH (5 μM) exhibited no activity following

incubation with CTAD (70 μM), $FeSO_4$ (25 μM) and αKG (500 μM), indicating that this enzyme form was inactive. Next, we tested ascorbate (2 mM) and/or DTT (100 μM) for their ability to re-activate purple FIH by including these reductants in purple FIH assay mixtures, however no activity was observed with these mild reductants (Table 2.1).

Table 2.1 Effect of reducing agents on auto-hydroxylated FIH.

FIH (μM)	Ascorbate (mM)	DTT (mM)	υ (μM/min)
5 (purple)	0	0.1	0.05±0.04
5 (purple)	2	0.1	0.06±0.05
5 (purple)	2	0	0.06±0.08
5 (fresh)	0	0	4.4±0.4
5 (fresh)	2	0.1	7.3±0.5

2.4 Discussion

Although the αKG hydroxylases are mechanistically predisposed to uncouple the oxidative and reductive parts of their catalytic cycle, the rate and products of uncoupling depend greatly on the identity of the enzyme and on reaction conditions. The reported coupling ratio during turnover was within error of unity for all reported examples (*20*, *26*, *40*, *41*), indicating that uncoupling occurs on less than ~ 5% of turnovers in the presence of prime substrate. However, reactivity toward O_2 in the absence of prime substrate is variable, as some αKG oxygenases release ROS whereas some autohydroxylate, suggesting that structural differences may control both the rates and products of uncoupling. Neither FIH nor AtsK were significantly uncoupled during turnover;

however they differed in both their reactivity toward O_2 in the absence of prime substrate, as well as in their uncoupling products.

Coupling between O_2-activation and substrate hydroxylation likely relies on three structural factors. The first being local structures which link the binding of prime substrate to coordination changes at Fe, such as proposed for hydrogen bonding between the facial triad and the Fe-bound H_2O (*31*). In a highly organized active site, the (Fe^{2+}+αKG) form of enzyme would be unable to react with O_2 until prime substrate bound, and would tightly couple O_2 activation to substrate oxidation. The second factor is a closed active site to prevent solvent access, such as by loop closure or the binding of a large substrate. The (Fe^{2+}+αKG+Substrate) form of enzyme, the *ES* complex, would be tightly coupled if solvent were unable to reach reactive intermediates, such as $(FeO)^{2+}$. The third factor is the presence of oxidizable residues near the active site which may react with $(FeO)^{2+}$ or scavenge any generated ROS. Any ROS formed by O_2-activation in the absence of prime substrate could then damage the protein rather than diffusing away, and has been proposed as a general protective strategy for αKG-dependent hydroxylases (*36*).

The free enzyme forms of AtsK and FIH were quite distinct in their propensity to react with O_2, suggesting differences in their structures. As described below, the primary factor is likely to be hydrogen bonding between the facial triad and the coordinated H_2O. In the context of the inner-sphere O_2-activation model, the Fe(II) in the free enzyme (eg: (Fe+αKG)FIH) should be 6-coordinate due to a H_2O ligand which is hydrogen bonded to

the Asp/Glu ligand. In order for free enzyme to react with O_2, this H_2O ligand must be released in the absence of prime substrate. As (Fe+αKG)FIH was unreactive toward O_2 on the minutes timescale (Figure 2.2), the H_2O-ligand is likely to be tightly bound in FIH. In contrast, (Fe^{2+}αKG)AtsK consumed 2.5 equivalents of O_2 (Figure 2.3), suggesting weaker hydrogen bonding from the facial triad in AtsK.

While the reactivity data presented herein do not directly probe the strength of this hydrogen bond, the structural data for FIH and AtsK are consistent with weakened hydrogen bonding in AtsK. In particular, while Asp^{201} of the facial triad in FIH forms a hydrogen bond to the Fe-bound H_2O (*27*), the orientation of AtsK Asp^{110} precludes any hydrogen-bond from the facial triad of AtsK (*29, 31*). The confluence of structural data with our reactivity data suggest that hydrogen bonding from the facial triad is a significant factor in deactivating FIH towards uncoupled O_2-activation.

Differential solvent access to the active sites of FIH and AtsK is unlikely to be the origin of the very different uncoupling behavior in the absence of prime substrate, as both active sites are highly solvent exposed. The crystal structures of AtsK suggested that the active site would be very solvent accessible, as a 'lid' formed by residues 80 – 102 was so disordered in the crystal structure that it could not be refined (*29*). This is also consistent with the broad substrate tolerance of AtsK, and suggests that solvent access to the active site should be facile. In a similar vein, FIH has no structural obstruction to solvent access to the active site in the (Fe+ αKG)FIH enzyme form, as the active site only becomes closed upon binding of the prime substrate, CTAD (*27*). As a consequence, any

uncoupled O_2-activation in the absence of prime substrate should lead to a highly solvent exposed $(FeO)^{2+}$ center in both AtsK and FIH. That AtsK released ROS, but FIH did not, indicated that some combination of slow initial reactivity and internal scavenging (see below) is most likely operative in FIH.

The only ROS produced by (Fe+αKG)AtsK was H_2O_2, suggesting that simple hydrolysis of the $(FeO)^{2+}$ intermediate formed H_2O_2 and regenerated the Fe^{2+} cofactor. ROS have been implicated during uncoupling of αKG oxygenases, but seldom observed. Two negative examples are enzymes structurally related to AtsK, which also inactivated during turnover: TFdA and TauD. The irreversible inactivation of TfdA was suggested to involve oxidative damage from hydroxyl radicals, however diffusible $OH^{\bullet}$ was not observed (*26*); neither H_2O_2 nor O_2^- were observed during uncoupling by TauD (*41*). The rare positive example is for CS2, which releases H_2O_2 in the absence of substrate as does AtsK (*40*). A crucial difference between AtsK and CS2 is that unlike CS2, AtsK also released H_2O_2 during normal turnover. This may relate to the size of the active site pocket, as the AtsK active site is highly disordered (*29*) and may therefore be more prone to hydrolytic attack at the FeO^{2+} intermediate than CS2.

The presence of a sacrificial site in FIH may explain the absence of diffusible ROS from this enzyme. FIH autohydroxylation led to irreversibly inactivated enzyme on the timescale of hours. The autohydroxylated form of FIH, in which the Fe(III) is coordinated by the hydroxylated ring of Trp^{296} (*18, 19*), could not be rescued by the addition of common reducing agents nor by excess αKG (Table 2.1). Irreversible

inactivation by 'sacrificial' reactivity near the active site has precedent in the autohydroxylation reactions of TauD, AlkB and TfdA, where new chromophores arise from Fe(III) coordination of the newly formed hydroxylated residue, and for which no reactivation pathway has been identified (*21*, *22*, *25*). We propose that FIH is deactivated from aberrant O_2 reactivity by strong hydrogen bonding from the facial triad, and further insured against ROS release by the internal reaction with Trp^{296}.

2.5 Conclusions

FIH is a proximate O_2-sensor for human cells, controlling vital processes such as basal metabolism and angiogenesis. Understanding the link between O_2-activation and substrate hydroxylation is crucial to developing therapies targeting FIH function. Our findings show that FIH minimizes uncoupled O_2 reactivity at two levels: through an inherently low reactivity in the absence of prime substrate; and through presentation of a sacrificial acceptor (Trp^{296}) near the active site. The tight control over O_2-reactivty for FIH is in contrast to the facile production of H_2O_2 by the bacterial enzyme AtsK, both in the presence and absence of the prime substrate for AtsK. We propose that this low reactivity for FIH may be due to strong hydrogen bonding between the coordinated water and the facial triad. Such tight control over O_2-activation by FIH is compatible with the significance of O_2 and O_2-derived species to both gene expression and cellular toxicity.

2.6 Appendix

2.6.1 Supplemental

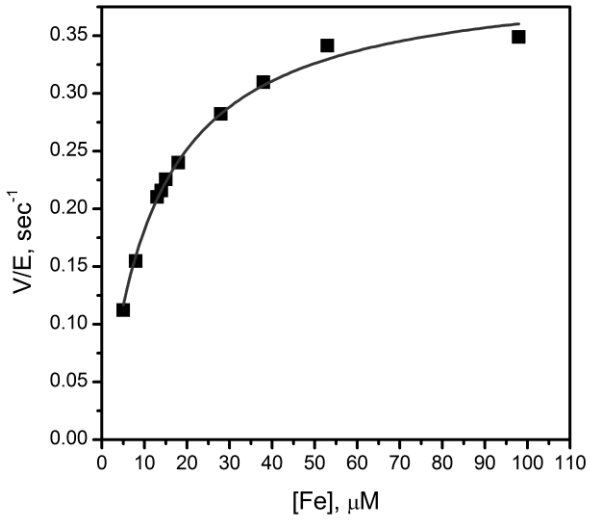

Figure 2.7 AtsK (1.14 μM), ascorbate (200 μM), αKG (1 mM), $FeSO_4$ (0-100 μM), $HexSO_4$ (1 mM) in 10 mM Hepes pH 7.00. Reaction was initiated by adding the enzyme and oxygen consumption was monitored

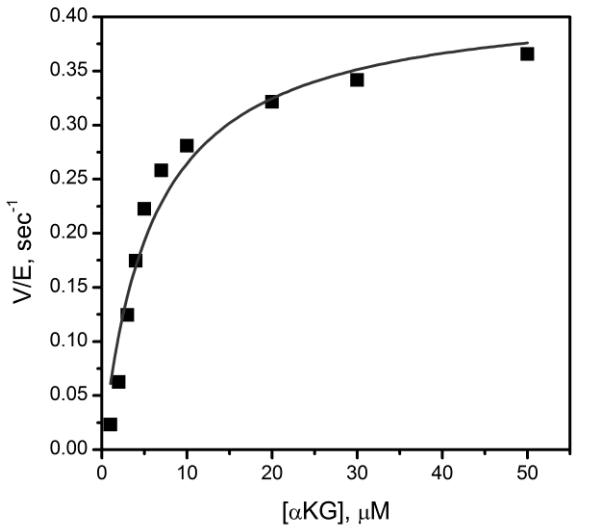

Figure 2.8 AtsK (1.14 μM), ascorbate (200 μM), αKG (0-100 μM), $FeSO_4$ (100 μM), $HexSO_4$ (1 mM) in 10 mM Hepes pH 7.00. Reaction was initiated by adding the enzyme and oxygen consumption was monitored.

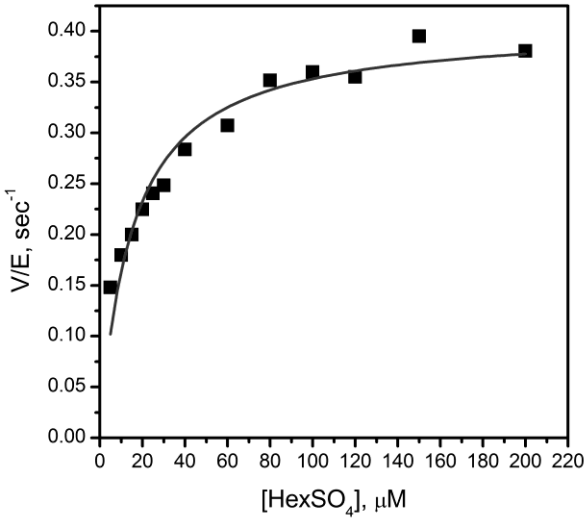

Figure 2.9 AtsK (1.14 μM), ascorbate (200 μM), αKG (1 mM), $FeSO_4$ (100 μM), $HexSO_4$ (0-200 μM) in 10 mM Hepes pH 7.00. Reaction was initiated by adding the enzyme and oxygen consumption was monitored

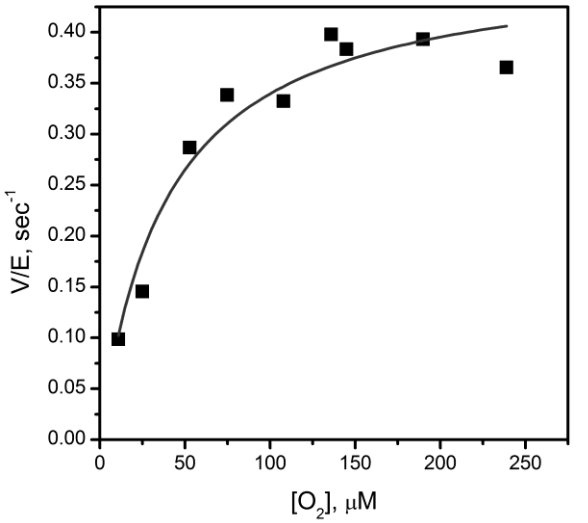

Figure 2.10 AtsK (1.14 μM), ascorbate (200 μM), αKG (1 mM), $FeSO_4$ (0-100 μM), $HexSO_4$ (1 mM), O_2 (0-100%) in 10 mM Hepes pH 7.00. Reaction was initiated by adding the enzyme and oxygen consumption was monitored.

Table 2.2 Summary of Michaelis-Menten kinetics of AtsK

	k_{cat} (sec^{-1})	K_m (μM)	K_d (μM)
Fe(II)	0.41 ± 0.01		12 ± 4
αKG	0.42 ± 0.03	5.9 ± 1.2	
$HexSO_4$	0.41 ± 0.02	15 ± 2	
O_2	0.47 ± 0.03	40 ± 9	

2.6.2 Abbreviations

ABTS, 2,2'-azino-bis(3-ethylbenzthiazoline-6-sulfonic acid);

αKG, alpha-ketoglutarate;

AtsK, oxygenative alkylsulfatase;

CS2, clavaminate synthase-2;

CTAD, C-terminal transactivation domain of HIFα;

ESI-MS, electrospray ionization mass spectrometry;

HEPES, 4-(2-hydroxyethyl)-1-piperazineethanesulfonic acid;

FIH-1, the factor inhibiting HIF;

$HexSO_4$, hexylsulfate;

HIF, Hypoxia Inducible Factor;

HRP, horseradish peroxidase;

SOD, superoxide dismutase;

TauD, taurine dioxygenase;

TfdA, (2, 4-dichlorophenoxy)acetate dioxygenase.

2.7 Bibliography

1. Bruick, R. K. (2003) Oxygen sensing in the hypoxic response pathway: regulation of the hypoxia-inducible transcription factor, *Genes Dev. 17*, 2614-2623.

2. Ozer, A., and Bruick, R. K. (2007) Non-heme dioxygenases: cellular sensors and regulators jelly rolled into one?, *Nat. Chem. Biol. 3*, 144-153.

3. Semenza, G. L. (2004) Hydroxylation of HIF-1: Oxygen sensing at the molecular level, *Physiology 19*, 176-182.

4. Hanauske-Abel, H. M., and Günzler, V. (1982) A stereochemical concept for the catalytic mechanism of prolylhydroxylase : Applicability to classification and design of inhibitors, *J. Theor. Biol. 94*, 421-455.

5. Hewitson, K. S., and Schofield, C. J. (2004) The HIF pathway as a therapeutic target, *Drug Discov. Today 9*, 704-711.

6. Nagel, S., Talbot, N. P., Mecinovic, J., Smith, T. G., Buchan, A. M., and Schofield, C. J. (2010) Therapeutic manipulation of the HIF hydroxylases., *Antioxid. Redox Signaling 12*, 481-501.

7. Hewitson, K. S., McNeill, L. A., Riordan, M. V., Tian, Y., Bullock, A. N., Welford, R. W., Elkins, J. M., Oldham, N. J., Bhattacharya, S., Gleadle, J. M., Ratcliffe, P. J., Pugh, C. W., and Schofield, C. J. (2002) Hypoxia-inducible factor (HIF) asparagine hydroxylase is identical to factor inhibiting HIF (FIH) and is related to the cupin structural family, *J. Biol. Chem. 277*, 26351-26355.

8. Bruick, R. K., and McKnight, S. L. (2001) A Conserved Family of Prolyl-4-Hydroxylases That Modify HIF, *Science 294*, 1337-1340.

9. Ivan, M., Kondo, K., Yang, H., Kim, W., Valiando, J., Ohh, M., Salic, A., Asara, J. M., Lane, W. S., and Kaelin Jr, W. G. (2001) HIFα Targeted for VHL-Mediated Destruction by Proline Hydroxylation: Implications for O_2 Sensing, *Science 292*, 464-468.

10. McNeill, L. A., Hewitson, K. S., Claridge, T. D., Seibel, J. r. F., Horsfall, L. E., and Schofield, C. J. (2002) Hypoxia-inducible factor asparaginyl hydroxylase (FIH-1) catalyses hydroxylation at the beta-carbon of asparagine-803, *Biochem. J. 367*, 571-575.

11. Costas, M., Mehn, M. P., Jensen, M. P., and Que, L. (2004) Dioxygen Activation at Mononuclear Nonheme Iron Active Sites: Enzymes, Models, and Intermediates, *Chem. Rev. 104*, 939-986.

12. Hausinger, R. P. (2004) Fe(II)/alpha-Ketoglutarate-dependent hydroxylases and related enzymes, *Crit. Rev. Biochem. Mol. Biol. 39*, 21-68.

13. Price, J. C., Barr, E. W., Tirupati, B., Bollinger, J. M., and Krebs, C. (2003) The First Direct Characterization of a High-Valent Iron Intermediate in the Reaction of an α-Ketoglutarate-Dependent Dioxygenase: A High-Spin Fe(IV) Complex in Taurine/α-Ketoglutarate Dioxygenase (TauD) from Escherichia coli *Biochemistry 42*, 7497-7508.

14. Proshlyakov, D. A., Henshaw, T. F., Monterosso, G. R., Ryle, M. J., and Hausinger, R. P. (2004) Direct Detection of Oxygen Intermediates in the Non-Heme Fe Enzyme Taurine/alpha-Ketoglutarate Dioxygenase, *J. Am. Chem. Soc. 126*, 1022-1023.

15. Hoffart, L. M., Barr, E. W., Guyer, R. B., Bollinger, J. M., and Krebs, C. (2006) Direct spectroscopic detection of a C-H-cleaving high-spin Fe(IV) complex in a prolyl-4-hydroxylase, *PNAS 103*, 14738-14743.

16. Price, J. C., Barr, E. W., Glass, T. E., Krebs, C., and Bollinger, J. M. (2003) Evidence for Hydrogen Abstraction from C1 of Taurine by the High-Spin Fe(IV) Intermediate Detected during Oxygen Activation by Taurine:α-Ketoglutarate Dioxygenase (TauD), *J. Am. Chem. Soc. 125*, 13008-13009.

17. Solomon, E. I., Brunold, T. C., Davis, M. I., Kemsley, J. N., Lee, S. K., Lehnert, N., Neese, F., Skulan, A. J., Yang, Y. S., and Zhou, J. (2000) Geometric and electronic structure/function correlations in non-heme iron enzymes, *Chem. Rev. 100*, 235-349.

18. Chen, Y. H., Comeaux, L. M., Eyles, S. J., and Knapp, M. J. (2008) Auto-hydroxylation of FIH-1: an Fe(II), alpha-ketoglutarate-dependent human hypoxia sensor, *Chem. Commun.*, 4768-4770.

19. Chen, Y. H., Comeaux, L. M., Herbst, R. W., Saban, E., Kennedy, D. C., Maroney, M. J., and Knapp, M. J. (2008) Coordination changes and auto-hydroxylation of FIH-1: Uncoupled O_2-activation in a human hypoxia sensor, *J. Inorg. Biochem. 102*, 2120-2129.

20. Counts, D. F., Cardinale, G. J., and Udenfriend, S. (1978) Prolyl hydroxylase half reaction: peptidyl prolyl-independent decarboxylation of alpha-ketoglutarate, *PNAS 75*, 2145-2149.

21. Henshaw, T. F., Feig, M., and Hausinger, R. P. (2004) Aberrant activity of the DNA repair enzyme AlkB, *J. Inorg. Biochem. 98*, 856-861.

22. Liu, A., Ho, R. Y. N., Que, L., Ryle, M. J., Phinney, B. S., and Hausinger, R. P. (2001) Alternative Reactivity of an alpha-Ketoglutarate-Dependent Iron(II) Oxygenase: Enzyme Self-Hydroxylation, *J. Am. Chem. Soc. 123*, 5126-5127.

23. Myllyla, R., Majamaa, K., Gunzler, V., Hanauske-Abel, H. M., and Kivirikko, K. I. (1984) Ascorbate is consumed stoichiometrically in the uncoupled reactions catalyzed by prolyl 4-hydroxylase and lysyl hydroxylase, *J. Biol. Chem. 259*, 5403-5405.

24. Rao, N. V., and Adams, E. (1978) Partial reaction of prolyl hydroxylase. (Gly-PRO-Ala)n stimulates alpha-ketoglutarate decarboxylation without prolyl hydroxylation, *J. Biol. Chem. 253*, 6327-6330.

25. Ryle, M. J., Liu, A., Muthukumaran, R. B., Ho, R. Y. N., Koehntop, K. D., McCracken, J., Que, L., and Hausinger, R. P. (2003) O2- and alpha-Ketoglutarate-Dependent Tyrosyl Radical Formation in TauD, an alpha-Keto Acid-Dependent Non-Heme Iron Dioxygenase *Biochemistry 42*, 1854-1862.

26. Saari, R. E., and Hausinger, R. P. (1998) Ascorbic Acid-Dependent Turnover and Reactivation of 2,4-Dichlorophenoxyacetic Acid/alpha-Ketoglutarate Dioxygenase Using Thiophenoxyacetic Acid *Biochemistry 37*, 3035-3042.

27. Dann, C. E., Bruick, R. K., and Deisenhofer, J. (2002) Structure of factor-inhibiting hypoxia-inducible factor 1: An asparaginyl hydroxylase involved in the hypoxic response pathway, *PNAS 99*, 15351-15356.

28. Elkins, J. M., Ryle, M. J., Clifton, I. J., Dunning Hotopp, J. C., Lloyd, J. S., Burzlaff, N. I., Baldwin, J. E., Hausinger, R. P., and Roach, P. L. (2002) X-ray Crystal Structure of Escherichia coli Taurine/alpha-Ketoglutarate Dioxygenase Complexed to Ferrous Iron and Substrates, *Biochemistry 41*, 5185-5192.

29. Muller, I., Kahnert, A., Pape, T., Sheldrick, G. M., Meyer-Klaucke, W., Dierks, T., Kertesz, M., and Uson, I. (2004) Crystal Structure of the Alkylsulfatase AtsK: Insights into the Catalytic Mechanism of the Fe(II) alpha-Ketoglutarate-Dependent Dioxygenase Superfamily, *Biochemistry 43*, 3075-3088.

30. Welford, R. W. D., Schlemminger, I., McNeill, L. A., Hewitson, K. S., and Schofield, C. J. (2003) The Selectivity and Inhibition of AlkB, *J. Biol. Chem. 278*, 10157-10161.

31. Neidig, M. L., Brown, C. D., Light, K. M., Fujimori, D. G., Nolan, E. M., Price, J. C., Barr, E. W., Bollinger, J. M., Krebs, C., Walsh, C. T., and Solomon, E. I. (2007) CD and MCD of CytC3 and Taurine Dioxygenase: Role of the Facial Triad in α-KG-Dependent Oxygenases, *J. Am. Chem. Soc. 129*, 14224-14231.

32. Zhou, J., Kelly, W. L., Bachmann, B. O., Gunsior, M., Townsend, C. A., and Solomon, E. I. (2001) Spectroscopic studies of substrate interactions with clavaminate synthase 2, a multifunctional alpha-KG-dependent non-heme iron enzyme: Correlation with mechanisms and reactivities, *J. Am. Chem. Soc. 123*, 7388-7398.

33. Pavel, E. G., Zhou, J., Busby, R. W., Gunsior, M., Townsend, C. A., and Solomon, E. I. (1998) Circular dichroism and magnetic circular dichroism spectroscopic studies of the non-heme ferrous active site in clavaminate synthase and its interaction with alpha-ketoglutarate cosubstrate, *J. Am. Chem. Soc. 120*, 743-753.

34. Koivunen, P., Hirsila, M., Gunzler, V., Kivirikko, K. I., and Myllyharju, J. (2004) Catalytic properties of the asparaginyl hydroxylase (FIH) in the oxygen sensing pathway are distinct from those of its prolyl 4-hydroxylases, *J. Biol. Chem. 279*, 9899-9904.

35. Ehrismann, D., Flashman, E., Genn, D. N., Mathioudakis, N., Hewitson, K. S., Ratcliffe, P. J., and Schofield, C. J. (2007) Studies on the activity of the hypoxia-inducible-factor hydroxylases using an oxygen consumption assay, *Biochem. J. 401*, 227-234.

36. Ryle, M. J., and Hausinger, R. P. (2002) Non-heme iron oxygenases, *Curr. Op. in Chem. Biol. 6*, 193-201.

37. Kahnert, A., and Kertesz, M. A. (2000) Characterization of a Sulfur-regulated Oxygenative Alkylsulfatase from *Pseudomonas putida* S-313*, *J. Biol. Chem. 275*, 31661-31667.

38. Halliwell, B., Gutteridge, J. M. C., and Aruoma, O. I. (1987) The deoxyribose method: A simple "test-tube" assay for determination of rate constants for reactions of hydroxyl radicals, *Anal. Biochem. 165*, 215-219.

39. Saban, E., Chen, Y.-H., Hangasky, J., Taabazuing, C., Holmes, B. E., and Knapp, M. J. (2011) The second coordination sphere of FIH controls hydroxylation, *Biochemistry 50*, 4733-4740.

40. Salowe, S. P., Marsh, E. N., and Townsend, C. A. (1990) Purification and characterization of clavaminate synthase from Streptomyces clavuligerus: an unusual oxidative enzyme in natural product biosynthesis, *Biochemistry 29*, 6499-6508.

41. McCusker, K. P., and Klinman, J. P. (2009) Modular behavior of tauD provides insight into the origin of specificity in alpha-ketoglutarate-dependent nonheme iron oxygenases, *PNAS 106*, 19791-19795.

CHAPTER 3

THE SECOND COORDINATION SPHERE OF FIH CONTROLS HYDROXYLATION

3.1 Introduction

A small number of Fe(II), α-ketoglutarate (αKG)-dependent dioxygenases directly control cellular oxygen sensing in humans (*1-3*). These enzymes hydroxylate specific residues within the α-subunit of the hypoxia inducible factor (HIF), thereby affecting the transcriptional level of hundreds of genes (*4*). The best characterized of these enzymes is 'factor inhibiting HIF-1' (FIH), which hydroxylates the β-carbon of HIF-Asn^{803} (*5*); HIF-Asn^{803} lies within the C-terminal transactivation domain (CTAD) of HIFα. Hydroxylating HIF-Asn^{803} turns off HIF-dependent gene expression and is a key step in down-regulating angiogenesis. Understanding the chemical basis of how FIH reacts with HIFα and O_2 is crucial to understanding tissue O_2 homeostasis, and holds potential for treating disease states such as cancer or stroke (*6-8*). According to the consensus chemical mechanism (Scheme 3.1), O_2 binds to (Fe^{II}+αKG)FIH only after HIFα binds (*9, 10*). In this mechanism, the active site Fe(II) of FIH is proposed to change its coordination geometry upon binding HIFα, thereby creating a binding site for O_2. A close correlation between pO_2 and HIF hydroxylation would then result, as the rate would be proportional to pO_2. X-ray crystallography of FIH in various substrate-bound states revealed a structural linkage between HIF-binding and O_2 activation through changes in multiple hydrogen-bonding interactions (*11-13*). Controlling oxygenation chemistry through varied hydrogen bonding to atoms coordinated to the metal has been found in

other enzymes and models (*14-16*), suggesting that the structural changes in FIH might also have functional significance.

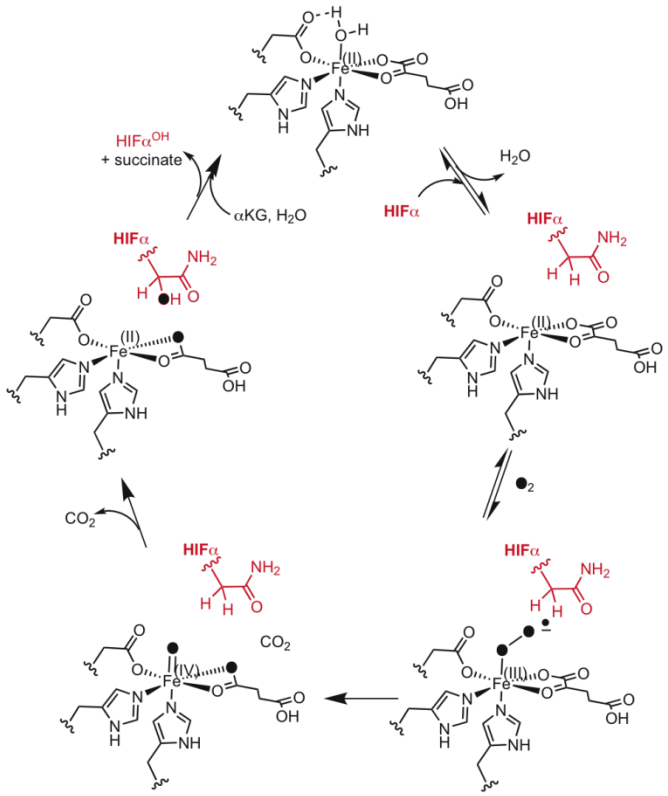

Scheme 3.1 Consensus chemical mechanism

The chemistry within the FIH active site occurs at the Fe(II) cofactor, making the extended coordination environment of this metal the focus of our investigation. FIH provides a primary coordination sphere of His^{199}, Asp^{201}, and His^{279}, forming a facial triad (*17*), with other coordination sites occupied by H_2O or αKG (Figure 3.1). The secondary coordination sphere is comprised of those residues that form hydrogen bonds to the ligands. Spectroscopic and structural data from FIH and related enzymes suggest

that coordination changes at Fe are crucial to turnover (*9*, *18*, *19*). Based on evidence from related enzymes, these key coordination geometries are proposed to be a six-coordinate (6C) center for the (Fe^{II}+αKG)FIH, and a five-coordinate (5C) center for (Fe^{II}+αKG+CTAD)FIH.

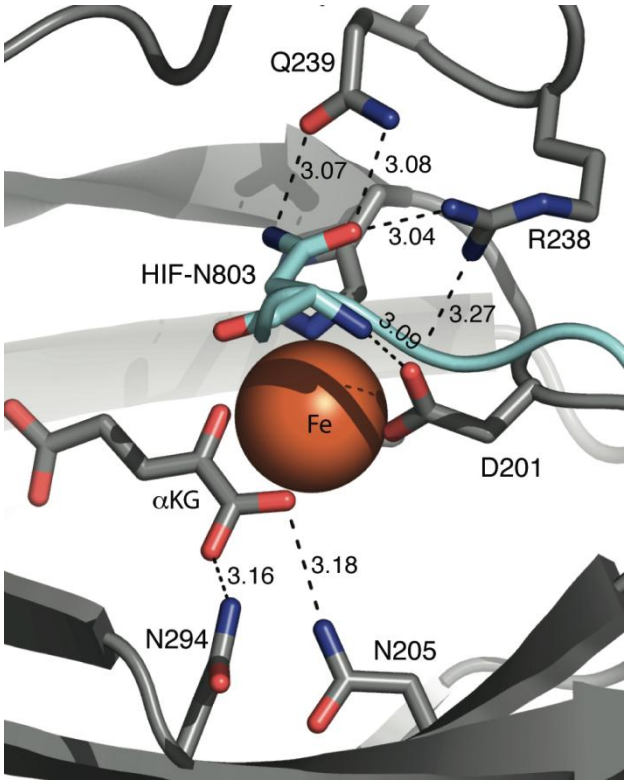

Figure 3.1 Hydrogen bonding network in the active site of wild type FIH (PDB 1H2K). FIH (gray) and CTAD (cyan) shown as strands; hydrogen bond distances (Å), FIH residues, and HIF-Asn^{803} are noted.

Hydrogen bonds between surrounding residues, substrates, and iron ligands may comprise a functionally significant second-coordination sphere for FIH, both for priming as well as for oxidative decarboxylation. X-ray crystal structures of FIH imply that the single H_2O-ligand is lost from the 6C (Fe^{II}+αKG)FIH upon binding CTAD, which would prime the Fe(II) to react with O_2 (*11-13*). Concomitant alterations in nearby hydrogen

bonds between Arg^{238}, Asp^{201}, and the H_2O ligand suggest that these second-sphere interactions may be necessary for priming. We prepared and characterized the isosteric mutant Arg^{238}→Met in order to determine how loss of this hydrogen bond linkage affected priming of the Fe(II) to react with O_2.

Decarboxylating α-ketoacids generally requires stabilization of negative charge within the transition state (*18-20*). Notably, a Lys or Arg is positioned as a hydrogen bond donor to the C1-carboxylate of αKG in most structures of the αKG dioxygenase superfamily (*9*). In the case of FIH, Asn^{205} and Asn^{294} appear to fulfill this role via hydrogen-bond donation to the C-1 carboxylate. We prepared and characterized the single-point Asn → Ala mutants to test how loss of each hydrogen bond affected O_2-activation in normal turnover as well as autohydroxylation.

Subsequent to O_2-activation, CTAD hydroxylation likely proceeds via a hydrogen transfer/rebound steps involving a putative $[FeO]^{2+}$ oxidant observed in related enzymes (*21, 22*). Precise substrate positioning is necessary to ensure that the putative $[FeO]^{2+}$ oxidant attacks the proper C-H bond. The side chain of the HIFα-Asn^{803} residue is located directly above the open coordination site of the Fe(II) in FIH, and forms a hydrogen bond pair to FIH-Gln^{239}. This interaction may be crucial for substrate positioning, such that the $[FeO]^{2+}$ oxidant reacts selectively with the β-carbon of HIF-Asn^{803}. Although Gln^{239} is not strictly a second-sphere residue in FIH, the Gln239→Asn mutant was included in the present study as a way to investigate the role of CTAD positioning on catalysis.

Testing the functional role of the second-sphere is crucial to understand the intricate relationship between the overall structure and function of FIH. This manuscript reports the activity, metal binding, and catalytic precision of second-sphere point mutants of FIH. Our results indicate that several second-sphere residues are key to tuning the O_2-reactivity of FIH.

3.2 Materials and Methods

3.2.1 Protein expression and purification

FIH and its mutants were expressed from *E. coli* with an N-terminal His_6 tag and purified as previously described (*23*). Following purification via Ni-NTA column chromatography, the His_6 tag was removed by thrombin digestion. Exogenous metal was removed by prolonged incubation with EDTA, and then FIH was further purified by size-exclusion chromatography to yield the FIH dimer.

3.2.2 Differential Scanning Calorimetry

DSC experiments were performed using a MicroCal VP-DSC microcalorimeter (*24*). 50 mM Hepes buffer pH 7.50 was used and 50 µM samples were heated in the calorimeter over a 25-75 ºC range at a scan rate of 60°C/hour. A buffer scan was subtracted from each dataset to correct for base-line drift. Data analysis was performed using Origin Microcal software,(*25*) the results of which are provided in the supplementary material.

3.2.3 Metal Binding

The experimental protocol was modified from Marletta et al. (*26*). Citrate was used as a chelator to buffer the concentration of free Co(II) ion, $[Co(H_2O)_6]^{2+}$, for which stability

constants are reported (*27*). Co(II) binding to FIH was monitored by fluorescence quenching in a deoxygenated solution at room temperature. FIH was present in a fluorescence cuvette as a 200 μL solution of 1.00 mM sodium citrate, 20 μM FIH, 100 μM α-ketoglutarate, and 50 mM HEPES pH 7.50. Small volumes of $CoCl_2$ were added from a solution of 1.00 mM $CoCl_2$ and 1.00 mM sodium citrate, 50 mM HEPES pH 7.50. Following addition of Co(II), the cuvette was gently rocked by hand and the fluorescence measured over several minutes until a steady reading was obtained. Samples were excited at 280 nm and the fluorescence intensity was measured at 340 nm. Data fitting and results are provided in the supplementary material.

3.2.4 EPR

X-band EPR spectra were recorded on a Bruker Elexsys E-500 ESR Spectrometer equipped with a Bruker ER 4118CF-O LHe/LN_2 cryostat. EPR samples were prepared by reconstituting enzymes with $CuSO_4$ in a FIH:Cu^{2+} ratio of 1:0.9; the $CuSO_4$ solution was slowly added to the enzyme solution to prevent precipitation. Similarly, FIH(Cu+αKG) was prepared by adding αKG slowly as the final step. Samples totaling 300 μL of 1 mM enzyme, 0.9 mM $CuSO_4$ and 1 mM αKG in 50 mM Hepes, pH 7.50, were frozen in quartz tubes with liquid nitrogen. The spectra were obtained by averaging 4 scans at 9.438 GHz frequency, 20 mW power, 20 G modulation amplitude, 100 GHz modulation frequency and a 327 ms time constant. The microwave power was varied to ensure the samples were not saturated under reported conditions.

3.2.5 UV-Vis Spectroscopy

Enzyme stocks, $FeSO_4$, and αKG were made anaerobic under an Argon flush. 50 mM HEPES pH 7.50 was also made anaerobic by a repeating cycle of vacuum and nitrogen flush. (Fe^{II}+αKG)FIH spectra were obtained on anaerobic samples containing FIH (250 μM), $FeSO_4$ (230 μM) and αKG (500 μM) in buffer. Apo FIH spectra were recorded for similar samples by omitting αKG and $FeSO_4$, and used as background spectra.

3.2.6 Activity Assays

Initial rate measurements were performed in 50 mM HEPES pH 7.50 and incubated at 37 °C in 50 μL reaction volume. Reaction buffer included 2.00 mM ascorbate, 100 μM DTT, 5 unit/mL catalase, 600 μM αKG, 25 μM $FeSO_4$, and 0-600 μM CTAD. The reaction was initiated by adding the enzyme (0.5-5 μM), and at certain time points 5 μL aliquots were taken and quenched in 45 μL 0.1% formic acid. For each reaction 10 time points were collected and quenched, then analyzed by LC-ESI-MS. Samples were first loaded onto a C8 column for desalting, and CTAD and hydroxylated CTAD ($CTAD^{OH}$) were detected by ESI-MS to determine the mole fraction of peptide that had been converted to product, $\chi_{CTAD\text{-}OH}$. Product concentrations were calculated as $[CTAD^{OH}] = \chi_{(CTAD\text{-}OH)} \times [CTAD]_0$, and used to determined initial rates, which were then used for Michaelis-Menten fits.

3.2.7 Autohydroxylation

Autohydroxylation was measured as described previously, with minor changes (*28*). FIH (100 μM), $FeSO_4$ (500 μM), and αKG (500 μM) were anaerobically incubated in 50 mM HEPES pH 7.50 for 20 min. Autohydroxylation was initiated by adding an equal volume

of buffer that had been equilibrated under air, and the reaction monitored at 583 nm. Competitive autohydroxylation assays included 50 μM CTAD that was pre-incubated with the FIH.

3.2.8 Coupling

A Hamilton PRP-X300 anion exclusion column and UV detection at 210 nm was used to separate and detect succinate yield from quenched steady-state reactions of FIH. The concentration of hydroxylated CTAD, $CTAD^{OH}$, was determined as per the activity assays. The coupling ratio was defined as C = [succinate]/[$CTAD^{OH}$].

3.3 Results

Inspection of the X-ray crystal structure of FIH revealed hydrogen-bonding networks surrounding the Fe, which were centered on either αKG or CTAD. Asn^{205} and Asn^{294} residues donate hydrogen-bonds to the C-1 carboxylate of αKG, suggesting that these second-sphere residues may stabilize charge buildup during decarboxylation. Arg^{238} and Gln^{239} make hydrogen bonds with CTAD, suggesting that these residues may position the HIF-Asn^{803}, or may play a role in priming the Fe for oxygenation chemistry (Figure 3.1). The role of these hydrogen bonds was tested by functional assays and electronic spectroscopy of point mutants.

Table 3.1 Kinetic parameters for WT-FIH and its mutants for αKG and the synthetic peptide CTAD (39 residues).[a,b]

	k_{cat} (min^{-1})[a]	$K_{M(\alpha KG)}$ (μM)[b]	$K_{M(CTAD)}$ (μM)[a]	$k_{cat}/K_{M(CTAD)}$ ($\mu M^{-1}min^{-1}$)[a]
WT-FIH	31 ± 4	22 ± 6	77 ± 22	0.41 ± 0.1
N205A	10.2 ± 0.5	7.5 ± 2	43 ± 8	0.24 ± 0.07
N294A	2.2 ± 0.1	14 ± 2	137 ± 26	0.016 ± 0.004
Q239N	0.123 ± 0.002	24 ± 4	38 ± 2	0.0032 ± 0.0002
R238M[c]	-	-	-	-

[a] Assays in which CTAD was the varied substrate were performed with FIH and mutants (0.5-5 μM), ascorbate (2 mM), DTT (100 μM), catalase (5 unit/mL), αKG (500 μM), $FeSO_4$ (25-50 μM), CTAD (0-600 μM) in 50 mM HEPES pH 7.50 at 37 °C. CTAD corresponds to a Cys→Ala point mutant of HIF-1α$^{788-826}$

[b] Assays in which αKG was the varied substrate were as above, with these exceptions: CTAD (200 μM), and αKG varied (3 – 160 μM).

[c] R238M was too slow to assay initial rates.

The effect of hydrogen bonding network on turnover was investigated by steady-state kinetics (Table 3.1). Saturating conditions were determined for ascorbate, αKG and Fe(II) and then initial rates of WT-FIH and its mutants were acquired by varying the CTAD concentration. DTT and catalase were used in the steady-state assays to prevent ferroxidase chemistry by Fe(II) in solution. WT-FIH showed k_{cat} of 31 min^{-1} with a $k_{cat}/K_{M(CTAD)}$ of 0.41 μM^{-1} min^{-1}, similar to previously reported values (Figure 3.2) (*29-31*). Each of the mutants had a modest effect on $K_{M(CTAD)}$, as both k_{cat} and k_{cat}/K_M were diminished by a similar factor for each mutant: N205A (3-fold), N294A (15-fold), and

Q239N (150-fold) (Figure 3.2 and Figure 3.3). R238M exhibited very low activity, which we could only detect through endpoint assays.

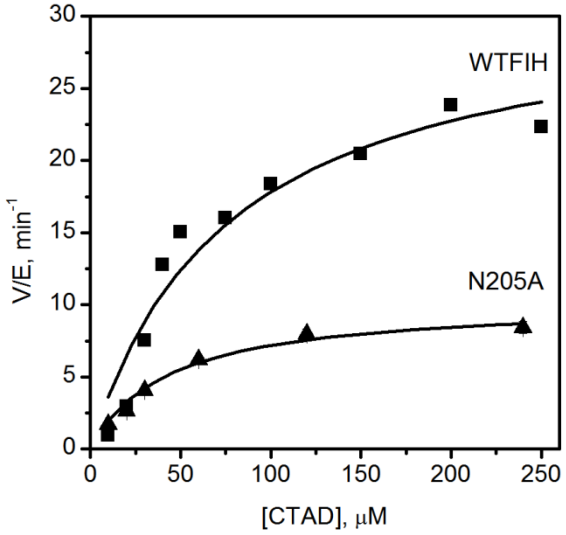

Figure 3.2 Steady state kinetics of WT-FIH and N205A. WT-FIH (0.5 μM), N205A (1 μM), ascorbate (2 mM), DTT (100 μM), catalase (5 unit/mL), αKG (500 μM), $FeSO_4$ (25 μM), CTAD (0-250 μM) in 50 mM HEPES pH 7.50.

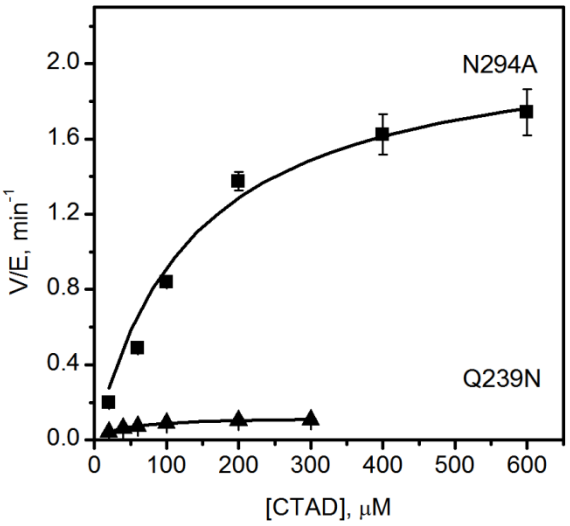

Figure 3.3 Steady-state kinetics of N294A and Q239N. N294A (5 μM), Q239N (5 μM), ascorbate (2 mM), DTT (100 μM), catalase (5 unit/mL), αKG (500 μM), $FeSO_4$ (50 μM), CTAD (0-600 μM) in 50 mM HEPES pH 7.50.

Endpoint assays showed that CTAD-centered mutants were impaired in terms of product yield, relative to WT-FIH and the αKG-centered mutants (Table 3.2). WT-FIH hydroxylated 94% of CTAD during prolonged incubations; the αKG-centered mutants, N205A and N294A, were nearly as thorough as WT-FIH, converting over 79% of CTAD to product. In contrast, both CTAD-centered mutants were significantly compromised in their ability to hydroxylate CTAD, as Q239N and R238M converted less than 25% of CTAD to hydroxylated product.

The ratio of succinate production to CTAD hydroxylation was measured, to check for coupling between O_2-activation and hydroxylation (Table 3.2). As O_2-activation produces succinate, but might not lead to hydroxylated CTAD, uncoupling between these two enzymatic steps would lead to elevated coupling ratios, C = [succinate]/[$CTAD^{OH}$]. WT-FIH was tightly coupled (*43*), with *C* equal to unity within experimental uncertainty (*C* = 0.98 ± 0.03). The Q205A and Q294A point mutants exhibited slightly elevated *C* values, however Q239N exhibited a coupling ratio was appreciably greater than unity (*C* = 3.1 ± 0.4).

Table 3.2 Coupling and yield of hydroxylated CTAD by FIH variants.

	C^{a}	% $CTAD^{OH\ b}$
WT-FIH	0.98 ± 0.03	94%
N205A	1.08 ± 0.04	90
N294A	1.3 ± 0.1	79
Q239N	3.1 ± 0.4	23
R238M	n.d.	5

[a] C = [succinate]/[$CTAD^{OH}$] as determined under steady-state turnover conditions; see text for details. Not determined (n.d.).

[b] Qualitative endpoints: FIH (100μM) $FeSO_4$ (500 μM), αKG (500μM), CTAD (50 μM) 50 mM HEPES, pH 7.50.

FIH will slowly activate O_2 in the absence of CTAD, autohydroxylating Trp^{296} to form an Fe(III)-O-Trp^{296} chromophore with λ_{max} = 583 nm (*23, 28*). While the rate-limiting step in autohydroxylation is not known, priming of the (Fe^{II}+αKG)FIH is a likely requirement to permit O_2-activation. WT-FIH and the point mutants were tested for autohydroxylation rates in the absence of CTAD in order to determine how the priming of Fe(II) changed upon mutation. The autohydroxylation rates for the point mutants were only moderately altered from WT-FIH (Table 3.3), suggesting that the second coordination sphere had minor effects on steps directly involved in autohydroxylation. It is notable that both αKG-centered mutants exhibited 2-fold increases in the autohydroxylation rates relative to that for WT-FIH.

Table 3.3 Autohydroxylation rates for FIH variants.

	auto-hydroxylation initial rates (μM/min)	
	0 CTAD	50 μM CTAD
WT FIH	0.0442 ± 0.0007	0.0265 ± 0.0008
N205A	0.100 ± 0.002	0.078 ± 0.001
N294A	0.0816 ± 0.0008	0.068 ± 0.002
Q239N	0.034 ± 0.001	0.0564 ± 0.0008
R238M	0.0262 ± 0.0008	0.0183 ± 0.0013

100 μM FIH, 500 μM $FeSO_4$, 500μM αKG, 0 or 50 μM CTAD, 50 mM HEPES, pH 7.50.

We felt that a competition assay, in which autohydroxylation was monitored in the presence of CTAD, would be an interesting way to further test the effect of second-sphere mutations on positioning. In the competition assay, HIF-Asn^{803} and Trp^{296} were both present as hydroxylation targets (Table 3.3). The rate of autohydroxylation for WT-FIH, and most of the point mutants, decreased in the presence of CTAD. The lone exception to this was the CTAD-centered mutant Q239N, which underwent autohydroxylation 60% faster in the presence of CTAD than in its absence. This increased autohydroxylation rate for Q239N strongly suggested that CTAD binding primed Fe(II) to react with O_2, but that HIF-Asn^{803} was improperly oriented to receive the oxidant in this point mutant.

The ability of WT-FIH and its mutants to stabilize negative charge on C-1 of αKG was analyzed spectroscopically by the energy of the metal to ligand charge transfer (MLCT) transition. UV-Vis absorption spectra of (Fe^{II}+αKG)FIH form of each enzyme was measured, with the spectrum of the apo enzyme subtracted as a background. Each of the (Fe^{II}+αKG)FIH samples exhibited an MLCT peak near 500 nm (Figure 3.4). This absorption band has been attributed to three overlapping transitions between populated Fe $T_{2g}(\pi)$ orbitals and empty π* orbitals delocalized over the C1 carboxylate and C2 keto group of αKG (*18*). WT-FIH displayed an MLCT maximum at 500 nm, similar to that of other αKG hydroxylases such as TauD (530 nm) (*32*) and CS2 (476 nm) (*33*). In αKG-centered mutants this MLCT was blue shifted (Table 3.4), with the MLCT peaks for N205A and N294A appearing at 485 and 490 nm respectively. This blue shift indicated that the αKG π* orbitals in these point mutants were destabilized from WT-FIH, consistent with the hydrogen-bonds donated by Asn^{205} and Asn^{294} pulling electron density away from the keto-group of αKG.

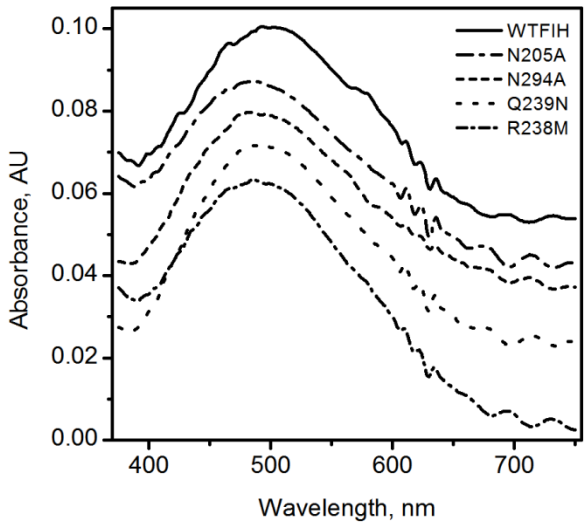

Figure 3.4 UV-Vis spectra of (Fe^{II}+αKG)FIH under anaerobic conditions after subtraction of (Fe^{II})FIH spectra. FIH & mutants (250 μM), $FeSO_4$ (230 μM), αKG (250 μM) in 50 mM HEPES pH 7.50.

Table 3.4 MLCT transitions in FIH variants.

	λ_{max} (nm)
WT FIH	500
N205A	485
N294A	490
Q239N	495
R238M	488

FIH (250 μM), $FeSO_4$ (230 μM), αKG (250 μM) in 50 mM HEPES pH 7.50.

Substrate centered mutations also showed blue-shifted MLCT bands (Table 3.4). Charge transfer complexes of Q239N and R238M appeared at 495 and 488 nm respectively. The slight shift in the MLCT energy for Q239N is consistent with the short distance between residue 239 and αKG, suggesting only minor structural perturbations. The larger shift observed for R238M is similar in magnitude to that observed for N294A, and may be tentatively attributed to polarization effects from the loss of the positive charge at residue 238.

Cu(II) was used as a spectroscopic probe for the electronic fine structure in FIH. EPR spectra of both (Cu)FIH and (Cu+αKG)FIH were measured for WT-FIH and each point mutant (Table 3.5). The spectra of the point mutants were similar to that of WT-FIH, with some heterogeneity evident in the (Cu)FIH samples that diminished significantly in the (Cu+αKG)FIH samples. As FIH only provided three protein derived ligands, heterogeneity in the (Cu)FIH samples likely arose due to the presence of two or three solvent-derived ligands with variable bond lengths to the Cu(II). The WT (Cu)FIH sample exhibited an axial spectrum with apparent g_{eff} and $A_{\|}$ values ($g_{\perp}$ = 2.06; $g_{\|}$ = 2.3; $A_{\|}$ = 148.1 G) appropriate for a "Type 2" Cu(II) site with mixed N and O-donor ligands (Figure 3.5) (*34*). Spectra of the WT (Cu+αKG)FIH sample exhibited increased anisotropy in g_{eff} ($g_{\perp}$ = 2.06, $g_{\|}$ = 2.35) and reduced hyperfine coupling ($A_{\|}$ = 136.4 G) as compared to (Cu)FIH (Figure 3.6). The small $A_{\|}$ is similar to that reported for other αKG hydroxylases (*35*-*37*), where it was attributed to an O-rich anionic ligand set and distorted planarity (*37*). The spectra for the (Cu+αKG)FIH point mutants were nearly identical to

those of WT-FIH, showing that the point mutations did not alter the metal coordination geometry in the (Cu+αKG)FIH enzyme form.

Table 3.5 EPR spectral parameters for (Cu)FIH and (Cu+αKG)FIH.

	EPR parameters		
	$g_{\|\|}$	$g_{\perp}$	$A_{\|\|}$ (G)
(Cu)FIH	2.30	2.06	146.2
(Cu)N205A	2.31	2.06	131.0
(Cu)N294A	2.31	2.06	134.6
(Cu)Q239N	2.29	2.06	135.0
(Cu)R238M	2.31	2.06	144.8
(Cu+αKG)FIH	2.35	2.06	136.4
(Cu+αKG)N205A	2.35	2.06	136.4
(Cu+αKG)N294A	2.35	2.07	136.4
(Cu+αKG)Q239N	2.35	2.07	136.8
(Cu+αKG)R238M	2.35	2.07	136.1

Parameters observed using Spincount(*44*)

Global enzyme stability was not altered by point mutation, as shown by the irreversible melting temperatures ($T_{M(app)}$) determined by DSC (Table 3.). The $T_{M(app)}$ of wild type FIH was 54.5 °C, whereas the $T_{M(app)}$ for the mutants were, in fact, slightly higher. Substrate centered mutants R238M and Q239N had slightly higher $T_{M(app)}$ than wild type, 56.2 and 56.7 °C respectively. The $T_{M(app)}$ of αKG centered mutants N205A and N294A were 58.6 and 58.9 °C respectively, again indicating that the second sphere mutations did not alter overall protein stability.

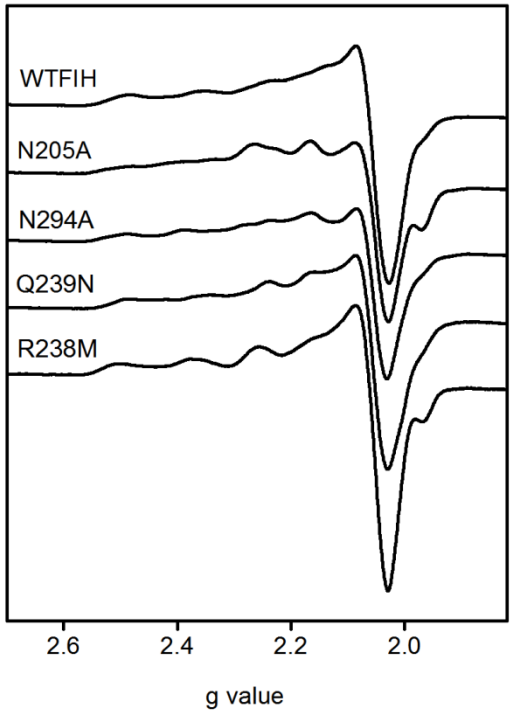

Figure 3.5 X-band EPR spectra of (Cu^{II})FIH variants. FIH and point mutants (1 mM), $CuSO_4$ (0.9 mM) in 50 mM HEPES pH 7.50. 9.438 GHz, 20 mW power, 20 G modulation amplitude, 100 GHz modulation frequency, 327 ms time constant, 77 K.

The metal binding of FIH was slightly affected by point mutation, as shown by the Co(II) titrations (Table 3.). The equilibrium dissociation constant for (Co^{2+}+αKG)FIH was 1.38(6) × 10^{-7}, indicating a relatively strong affinity for Co^{2+}. Each of the point mutants exhibited a similar dissociation constant, with K_D ranging from 1.0 – 1.9 × 10^{-7}. This indicated that the primary coordination sphere of the active site was not altered by mutagenesis in the secondary sphere.

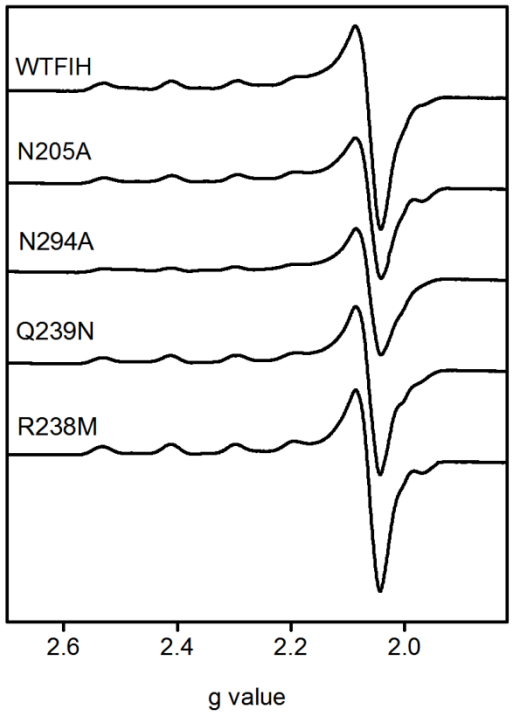

Figure 3.6 X-band EPR spectra of (Cu^{II}+αKG)FIH variants. FIH and mutants (1 mM), $CuSO_4$ (0.9 mM), αKG (1 mM) in 50 mM HEPES pH 7.50. 9.438 GHz frequency, 20 mW power, 20G modulation amplitude, 100 GHz modulation frequency, 327 ms time constant at 77 K.

3.4 Discussion

Hydrogen bonding networks have been shown to be crucial to the function of enzymes reacting with O_2-derived species, such as lipoxygenase and SOD (*15*, *16*), as well as for O_2-activating models (*14*). In the case of FIH, hydrogen bonding was observed between the facial triad ligands of Fe(II), the αKG, and various second-sphere residues, suggesting a functional role in tuning the chemistry of the Fe(II) center. In addition Gln^{239} hydrogen bonds to the CTAD substrate, and its role in substrate positioning has been included. The present work combines kinetics and spectroscopy to show that these second sphere hydrogen bonds play roles in promoting oxidative decarboxylation, priming Fe(II) to bind O_2, and positioning HIF-Asn^{803}.

The steady-state rate constants, k_{cat} and $k_{cat}/K_{M(CTAD)}$, were diminished for each point mutant of FIH (Table 3.1), indicating a reduction in the rate of one or more steps during turnover. These rate constants can be interpreted within the context of an ordered sequential mechanism, which is the consensus chemical mechanism for αKG hydroxylases (*9, 10*). A minimal kinetic model (Scheme 3.2) for FIH in the presence of saturating αKG involves separate microscopic steps for binding S = CTAD (k_1) and O_2 (k_2), with an irreversible chemical step (k_3) followed by product release (k_4).

$$E \underset{}{\overset{k_1}{\rightleftharpoons}} ES \overset{k_2}{\rightleftharpoons} ES(O_2) \overset{k_3}{\longrightarrow} \overset{k_4}{\longrightarrow} E + P$$

Scheme 3.2 Minimal kinetic model for FIH

The steady-state rate constants are composites of the above microscopic steps. All steps after substrate binding contribute to k_{cat}, while $k_{cat}/K_{M(CTAD)}$ is a function of all steps up through the first irreversible step. The reduced values to both k_{cat} and $k_{cat}/K_{M(CTAD)}$ for

each point mutant suggests that the second coordination sphere plays a significant role in determining k_3, the common microscopic step. This first irreversible step may be oxidative decarboxylation of αKG to form the $[FeO]^{2+}$ intermediate, as seen for TauD (*38, 39*), or a another step forming an Fe(II) center, as implied for PHD (*40*). In the absence of additional mechanistic probes such as kinetic isotope effects, we turned to the use of electronic spectroscopy and inactivation kinetics to test the effect of the second sphere residues.

Point mutations to second sphere residues were non-perturbing to the protein structure and primary coordination of the metal center in mutated FIH, as shown by the thermodynamic stability and electronic spectroscopy of each mutant. EPR spectra of the point mutants showed that the metal center in (Cu+αKG)FIH retained a virtually identical ground-state electronic environment to WT-FIH (Figure 3.6). The MLCT transitions for (Fe^{II}+αKG)FIH variants revealed that the αKG was a bidentate ligand to Fe(II), while also providing a view of the changing Lewis acidity of the C2-position of αKG (Figure 3.4). As nucleophilic attack of superoxide at C2 is thought to be a key step in O_2-activation by αKG-dependent oxygenases (*41*), the Lewis acidity of the keto group is essential for oxidative decarboxylation. The blue shifts in the MLCT energies for point mutants indicated that the αKG π* orbitals were destabilized in the N294A and N205A mutants, suggesting that the hydrogen bonds found in WT-FIH serve to pull electron density away from the C2 position of αKG.

Oxidative decarboxylation is promoted by stabilizing negative charge buildup in the transition state, as shown for enzymes (*20*) and model complexes (*41*). Structural analysis and the MLCT shifts in FIH indicate that both Asn^{205} and Asn^{294} pull electron density away from αKG, although the Fe(II) likely plays the predominant role in activating αKG for decarboxylation. Asn^{294} plays a more significant role than Asn^{205} in stabilizing charge, as shown by the relative values for k_{cat}: WT > N205A > N294A (Table 3.1). This may be due to Asn^{294} being the sole residue pulling electron density away from the distal O of the C1 carboxylate of αKG, while both Asn^{205} and Fe(II) pull electron density from the proximal O of the C1 carboxylate (Figure 3.1).

The significant decrease in the steady-state rate constants for CTAD-centered mutants may arise from changes in Fe(II) priming or CTAD positioning. The consensus chemical mechanism suggests that mutations affecting priming should principally reduce $k_{cat}/K_{M(CTAD),}$ as steps up through O_2-activation determine this rate constant. Conversely, mutations affecting positioning should reduce k_{cat}, as steps following O_2-binding determine this rate constant. Although the structure of FIH with CTAD bound suggests that there may be hydrogen bonds with specific roles, such as those between Gln^{239} and HIF-Asn^{803} (positioning), and Arg^{238} and Asp^{201} (priming), the kinetics data is less clear as each point mutation reduced k_{cat} as well as $k_{cat}/K_{M(CTAD)}$ when compared to WT FIH. This may arise from an effect on a chemical step common to both rate constants, such as O_2-activation, or from the extended hydrogen bond network linking Asp^{201} to HIF-Asn^{803} thorugh Arg^{238} and Gln^{239} (Figure 3.1). It appears that positioning the sidechain of HIF-

Asn^{803} is integral to the priming of Fe(II), and may even be a design feature to ensure tight coupling between O_2-activation and substrate hydroxylation.

While priming could not be separated from substrate positioning by steady-state kinetics, the two roles could be distinguished by the coupling ratio, and by analysis of hydroxylation products, as shown for TauD (*42*). A functional view of priming is the abilty of FIH to activate O_2 only once CTAD binds, leading to close coupling between the production of succinate and $CTAD^{OH}$. In the case of WT-FIH, breakdown in priming leads solely to autohydroxylation as FIH does not release reactive oxygen species (*23*, *28*, *43*). This was supported by our observation of a coupling value of unity (C = 0.98 ± 0.03) for WT-FIH, and a near-unity coupling ratio for N205A and N294A.

Positioning HIF-Asn^{803} in the proper registry within the active site is crucial to ensure that the $[FeO]^{2+}$ oxidant attacks the correct residue and forms the $CTAD^{OH}$ product. The Q239N mutant exhibited notable effects on the coupling ratio, indicating that Gln^{239} was crucial for local positioning (

Table 3.2). Q239N was the only mutant in which the coupling ratio differed significantly from unity (3.1 ± 0.4), and the only mutant that autohydroxylated faster in the presence of CTAD. These observations indicate that, while Q239N was able to activate O_2, the HIF-Asn^{803} sidechain was improperly positioned to form normal product.

FIH serves a crucial role in sensing hypoxia within human cells. As an O_2-sensing enzyme, it must maintain tight coupling between O_2-activation and substrate hydroxylation, which it achieves by hydrogen bonding between ligands to the Fe and the second coordination sphere. These second sphere hydrogen bonds play roles in promoting O_2-activation as well as maintaining the structural registry between CTAD and Fe. Hydrogen bonds from Asn^{205} and Asn^{294} pulled electron density away from αKG, as shown by the LMCT transitions; removal of either hydrogen bond in the Asn→Ala point mutants slightly accelerated autohydroxylation, but made normal turnover much slower in the case of Asn^{294}→Ala. It is likely that autohydroxylation rates reflect the intrinsic reactivity of αKG, whereas the rate of normal turnover is more dependent on precise positioning of CTAD. For this reason, the rate constants for normal turnover are greatly reduced in Gln^{239}→Asn and Arg^{238}→Met, both CTAD-centered mutants. By virtue of their respective locations relative to Asp^{201} and HIF-Asn^{803}, it is likely that Arg^{238} is necessary for priming of the Fe(II) in response to CTAD binding, whereas Gln^{239} is more involved in positioning HIF-Asn^{803}. The second sphere interactions play a significant role in O_2-sensing function of FIH by tuning the chemistry at the Fe(II) center.

3.5 Appendix

3.5.1 Supplemental

3.5.1.1 Thermal stability of FIH variants

The thermal stability of FIH variants was measured by differential scanning calorimetry, as described in the text.

Table 3.5 DSC melting temperature analysis of FIH and its mutants.

	$T_{M(app)}$ (°C)
WTFIH	54.5
N205A	58.6
N294A	58.9
R238M	56.7
Q239N	56.2

FIH (50 μM) in 50 mM HEPES pH 7.50, temperature range: 25-75 °C, scan rate: 60 °C/hour.

3.5.1.2 Co^{II} Binding thermodynamics to FIH variants

3.5.1.2.1 Metal titration data fitting

The binding affinity of (Co^{2+}+αKG)FIH for Co^{2+} was obtained by competitive titration in 50 mM HEPES, pH 7.50 at 23ºC. A 200 μL solution of apo FIH (20 μM), citrate (1.00 mM), and αKG (100 μM) was temperature equilibrated in a fluorescence cuvette, while a separate solution of $CoCl_2$ (1.00 mM) with citrate (1.00 mM) in buffer was loaded into a titrating syringe. As FIH-1 utilizes αKG as a co-substrate as well as a bidentate ligand for metal, αKG was included to complete the relevant ligand set of (Co^{2+}+αKG)FIH.

This experiment used citrate to buffer the concentration of free Co^{2+}, or $Co(H_2O)_6^{2+}$, as the log β values for Co(II) binding to citrate are well defined (1). Upon addition of small volumes of $CoCl_2$, apo FIH bound the available αKG and Co^{2+}. The fluorescence intensity of FIH-1 at 340 nm (F340) was plotted against $\log[Co^{2+}]_{free}$, exhibiting the sigmoidal shape characteristic of a binding equilibrium. The binding curve was fitted to a simple 1:1 binding equilibrium in which the Co^{2+} dissociation constant of (Co^{2+}+αKG)FIH (K_D) is with respect to $Co(H_2O)_6^{2+}$ (Eq. S1). The fluorescence intensity (F340) was fitted to Eq. S2 (2) which yielded log K_D (x) relative to the log[Co^{2+}]free (c), using a cooperativity parameter (B) which accounted for both chemical cooperativity involved with dimeric FIH-1 as well as the spectroscopic cooperativity involved with fluorescence signal from the eight Trp residues of FIH. The results are in Table 3..

$$(Co^{2+} + \alpha KG)FIH \leftrightarrow Co(H_2O)_6^{2+} + apoFIH \quad (S1)$$

$$F_{340} = F_{min} + (F_{max} - F_{min})/(1+10^{(c-x)B}) \quad (S2)$$

Table 3.6 Co^{II} binding affinity of FIH-1 mutants in the presence of αKG

	K_D (M)	B
WTFIH	1.38(6)x10^{-7}	2.2 ± 0.2
N205A	1.63(3) x10^{-7}	1.6 ± 0.1
N294A	1.01(4) x10^{-7}	2.3 ± 0.2
R238M	1.45(8) x10^{-7}	1.9 ± 0.2
Q239N	1.9(2) x10^{-7}	1.3 ± 0.1

$CoCl_2$ (1 mM) / citrate (1 mM) was titrated into FIH (20 μM), αKG (100 μM) in 50 mM HEPES pH 7.50.

3.5.1.2.2 References:

1. Martell, A. E., and Smith, R. M. (eds). (1974) Critical stability constants, Plenum Press, New York

2. Mills, S. A., and Marletta, M. A. (2005) Biochemistry 44, 13553-13559

3.5.2 Abbreviations

αKG, alpha-ketoglutarate;

CTAD, C-terminal transactivation domain of HIFα;

DSC, differential scanning calorimetry;

EPR, electron paramagnetic resonance;

FIH, factor inhibiting HIF-1;

HIF, hypoxia inducible factor;

LC-ESI-MS, liquid chromatography – electrospray ionization mass spectrometry;

MLCT, metal-to-ligand charge transfer;

NTA, nitrilotriacetate;

SOD, superoxide dismutase

3.6 Bibliography

1. Bruick, R. K., and McKnight, S. L. (2001) A conserved family of prolyl-4-hydroxylases that modify HIF, *Science 294*, 1337-1340.

2. Ozer, A., and Bruick, R. K. (2007) Non-heme dioxygenases: cellular sensors and regulators jelly rolled into one?, *Nat. Chem. Biol. 3* 144-153.

3. Semenza, G. L. (2004) Hydroxylation of HIF-1: Oxygen sensing at the molecular level, *Physiology 19*, 176-182.

4. Mole, D. R., Blancher, C., Copley, R. R., Pollard, P. J., Gleadle, J. M., Ragoussis, J., and Ratcliffe, P. J. (2009) Genome-wide Association of Hypoxia-inducible Factor (HIF)-1 alpha and HIF-2 alpha DNA Binding with Expression Profiling of Hypoxia-inducible Transcripts, *J. Biol. Chem. 284*, 16767-16775.

5. McNeill, L. A., Hewitson, K. S., Claridge, T. D., Seibel, J. F., Horsfall, L. E., and Schofield, C. J. (2002) Hypoxia-inducible factor asparaginyl hydroxylase (FIH-1) catalyses hydroxylation at the beta-carbon of asparagine-803, *Biochem. J. 367*, 571-575.

6. Hanauske-Abel, H. M., and Gunzler, V. (1982) A stereochemical concept for the catalytic mechanism of prolylhydroxylase : Applicability to classification and design of inhibitors, *J. Theor. Biol. 94*, 421-455.

7. Hewitson, K. S., and Schofield, C. J. (2004) The HIF pathway as a therapeutic target, *Drug Discovery Today 9*, 704-711

8. Nagel, S., Talbot, N. P., Mecinovic, J., Smith, T. G., Buchan, A. M., and Schofield, C. J. (2010) Therapeutic Manipulation of the HIF Hydroxylases, *Antioxid. Redox Signal. 12*, 481-501.

9. Hausinger, R. P. (2004) FeII/alpha-ketoglutarate-dependent hydroxylases and related enzymes, *Crit. Rev. Biochem. Mol. Biol. 39*, 21-68.

10. Solomon, E. I., Brunold, T. C., Davis, M. I., Kemsley, J. N., Lee, S. K., Lehnert, N., Neese, F., Skulan, A. J., Yang, Y. S., and Zhou, J. (2000) Geometric and electronic structure/function correlations in non-heme iron enzymes, *Chem. Rev. 100*, 235-350.

11. Dann, C. E., Bruick, R. K., and Deisenhofer, J. (2002) Structure of factor-inhibiting hypoxia-inducible factor 1: An asparaginyl hydroxylase involved in the hypoxic response pathway, *PNAS. USA 99*, 15351-15356.

12. Elkins, J. M., Hewitson, K. S., McNeill, L. A., Seibel, J. F., Schlemminger, I., Pugh, C. W., Ratcliffe, P. J., and Schofield, C. J. (2003) Structure of factor-inhibiting hypoxia-inducible factor (HIF) reveals mechanism of oxidative modification of HIF-1 alpha, *J. Biol. Chem. 278,* 1802-1806.

13. Lee, C., Kim, S. J., Jeong, D. G., Lee, S. M., and Ryu, S. E. (2003) Structure of human FIH-1 reveals a unique active site pocket and interaction sites for HIF-1 and von Hippel-Lindau, *J. Biol. Chem. 278*, 7558-7563.

14. Shook, R. L., and Borovik, A. S. (2008) The effects of hydrogen bonds on metal-mediated O_2 activation and related processes, *Chem. Commun.*, 6095-6107.

15. Tomchick, D. R., Phan, P., Cymborowski, M., Minor, W., and Holman, T. R. (2001) Structural and functional characterization of second-coordination sphere mutants of soybean lipoxpgenase-1, *Biochemistry 40*, 7509-7517.

16. Miller, A. F. (2008) Redox tuning over almost 1 V in a structurally conserved active site: Lessons from Fe-containing superoxide dismutase, *Acc. Chem. Res. 41*, 501-510.

17. Hegg, E. L., and Que, L. (1997) The 2-His-1-carboxylate facial triad - An emerging structural motif in mononuclear non-heme iron(II) enzymes, *Eur. J. Biochem. 250*, 625-629.

18. Pavel, E. G., Zhou, J., Busby, R. W., Gunsior, M., Townsend, C. A., and Solomon, E. I. (1998) Circular dichroism and magnetic circular dichroism spectroscopic studies of the non-heme ferrous active site in clavaminate synthase and its interaction with alpha-ketoglutarate cosubstrate, *J. Am. Chem. Soc. 120*, 743-753.

19. Zhou, J., Kelly, W. L., Bachmann, B. O., Gunsior, M., Townsend, C. A., and Solomon, E. I. (2001) Spectroscopic studies of substrate interactions with clavaminate synthase 2, a multifunctional alpha-KG-dependent non-heme iron enzyme: Correlation with mechanisms and reactivities, *J. Am. Chem. Soc. 123*, 7388-7398.

20. Walsh, C. T. (1979) *Enzymatic Reaction Mechanisms*, W. H. Freeman & Co., San Francisco.

21. Price, J. C., Barr, E. W., Tirupati, B., Bollinger, J. M., Jr., and Krebs, C. (2003) The first direct characterization of a high-valent iron intermediate in the reaction of an alpha-ketoglutarate-dependent dioxygenase: a high-spin FeIV complex in taurine/alpha-ketoglutarate dioxygenase (TauD) from Escherichia coli, *Biochemistry 42*, 7497-7508.

22. Proshlyakov, D. A., Henshaw, T. F., Monterosso, G. R., Ryle, M. J., and Hausinger, R. P. (2004) Direct detection of oxygen intermediates in the non-heme Fe enzyme taurine/alpha-ketoglutarate dioxygenase, *J. Am. Chem. Soc. 126*, 1022-1023.

23. Chen, Y. H., Comeaux, L. M., Herbst, R. W., Saban, E., Kennedy, D. C., Maroney, M. J., and Knapp, M. J. (2008) Coordination changes and auto-hydroxylation of FIH-1: uncoupled O_2-activation in a human hypoxia sensor, *J. Inorg. Biochem. 102*, 2120-2129.

24. Plotnikov, V. V., Brandts, J. M., Lin, L. N., and Brandts, J. F. (1997) A new ultrasensitive scanning calorimeter, *Anal. Biochem. 250*, 237-244.

25. Northrop, D. B. (1981) The Expression of Isotope effects on Enzyme-Catalyzed Reactions, *Ann. Rev. Biochem. 50*, 103-131.

26. Mills, S. A., and Marletta, M. A. (2005) Metal binding characteristics and role of iron oxidation in the ferric uptake regulator from Escherichia coli, *Biochemistry 44*, 13553-13559.

27. Martell, A. E., and Smith, R. M. (1974) *Critical Stability Constants*, Plenum Press, New York, New York.

28. Chen, Y. H., Comeaux, L. M., Eyles, S. J., and Knapp, M. J. (2008) Auto-hydroxylation of FIH-1: an Fe(II), alpha-ketoglutarate-dependent human hypoxia sensor, *Chem. Commun.*, 4768-4770.

29. Ehrismann, D., Flashman, E., Genn, D. N., Mathioudakis, N., Hewitson, K. S., Ratcliffe, P. J., and Schofield, C. J. (2007) Studies on the activity of the hypoxia-inducible-factor hydroxylases using an oxygen consumption assay, *Biochem. J. 401*, 227-234.

30. Koivunen, P., Hirsila, M., Gunzler, V., Kivirikko, K. I., and Myllyharju, J. (2004) Catalytic properties of the asparaginyl hydroxylase (FIH) in the oxygen sensing pathway are distinct from those of its prolyl 4-hydroxylases, *J. Biol. Chem. 279*, 9899-9904.

31. Linke, S., Stojkoski, C., Kewley, R. J., Booker, G. W., Whitelaw, M. L., and Peet, D. J. (2004) Substrate requirements of the oxygen-sensing asparaginyl hydroxylase factor-inhibiting hypoxia-inducible factor, *J. Biol. Chem. 279*, 14391-14397.

32. Ryle, M. J., Padmakumar, R., and Hausinger, R. P. (1999) Stopped-Flow Kinetic Analysis of Escherichia coli Taurine/α-Ketoglutarate Dioxygenase: Interactions with α-Ketoglutarate, Taurine, and Oxygen, *Biochemistry 38*, 15278-15286.

33. Zhou, J., Gunsior, M., Bachmann, B. O., Townsend, C. A., and Solomon, E. I. (1998) Substrate Binding to the α-Ketoglutarate-Dependent Non-Heme Iron Enzyme Clavaminate Synthase 2: Coupling Mechanism of Oxidative Decarboxylation and Hydroxylation, *J. Am. Chem. Soc. 120*, 13539-13540.

34. Peisach, J., and Blumberg, W. E. (1974) Structural Implications Derived from Analysis of Electron-Paramagnetic Resonance-Spectra of Natural and Artificial Copper Proteins, *Arch. Biochem. Biophys. 165*, 691-708.

35. Bleijlevens, B., Shivarattan, T., Sedgwick, B., Rigby, S. E. J., and Matthews, S. J. (2007) Replacement of non-heme Fe(II) with Cu(II) in the alpha-ketoglutarate dependent DNA repair enzyme AlkB: Spectroscopic characterization of the active site, *Journal of Inorganic Biochemistry 101*, 1043-1048.

36. Hegg, E. L., Whiting, A. K., Saari, R. E., McCracken, J., Hausinger, R. P., and Que, L. (1999) Herbicide-degrading alpha-keto acid-dependent enzyme TfdA: Metal coordination environment and mechanistic insights, *Biochemistry 38*, 16714-16726.

37. Whiting, A. K., Que, L., Saari, R. E., Hausinger, R. P., Fredrick, M. A., and McCracken, J. (1997) Metal coordination environment of a Cu(II)-substituted alpha-keto acid-dependent dioxygenase that degrades the herbicide 2,4-D, *J. Am. Chem. Soc. 119*, 3413-3414.

38. Grzyska, P. K., Ryle, M. J., Monterosso, G. R., Liu, J., Ballou, D. P., and Hausinger, R. P. (2005) Steady-state and transient kinetic analyses of taurine/alpha-ketoglutarate dioxygenase: Effects of oxygen concentration, alternative sulfonates, and active-site variants on the fe(IV)-oxo intermediate, *Biochemistry 44*, 3845-3855.

39. Price, J. C., Barr, E. W., Glass, T. E., Krebs, C., and Bollinger, J. M., Jr. (2003) Evidence for hydrogen abstraction from C1 of taurine by the high-spin Fe(IV) intermediate detected during oxygen activation by taurine:alpha-ketoglutarate dioxygenase (TauD), *J. Am. Chem. Soc. 125*, 13008-13009.

40. Flashman, E., Hoffart, L. M., Hamed, R. B., Bollinger, J. M., Krebs, C., and Schofield, C. J. (2010) Evidence for the slow reaction of hypoxia-inducible factor prolyl hydroxylase 2 with oxygen, *FEBS J. 277*, 4089-4099.

41. Mehn, M. P., Fujisawa, K., Hegg, E. L., and Que, L. (2003) Oxygen activation by nonheme iron(II) complexes: alpha-keto carboxylate versus carboxylate, *J. Am. Chem. Soc. 125*, 7828-7842.

42. McCusker, K. P., and Klinman, J. P. (2010) An Active-Site Phenylalanine Directs Substrate Binding and C-H Cleavage in the alpha-Ketoglutarate-Dependent Dioxygenase TauD, *J. Am. Chem. Soc. 132*, 5114-5120.

43. Saban, E., Flagg, S. C., and Knapp, M. J. (2011) Uncoupled O_2-activation in the human HIF-asparaginyl hydroxylase, FIH, does not produce reactive oxygen species, *J. Inorg. Biochem. 105*, 630-636.

44. Hendrich, M. P. Spincount software, Carnegie Mellon Univ.

CHAPTER 4

SOLVENT ISOTOPE EFFECTS ON FIH

4.1 Introduction

Solvent isotope effects (SIE) can be seen when enzymatic rates are measured in H_2O, D_2O or mixture of these solvents. Solvent isotope effects are more global when compared to substrate isotope effects which use one or few isotopic positions. Because the physical properties of D_2O are different, replacing H_2O with D_2O might affect the enzyme stability, conformational change, substrate binding and kinetic & equilibrium constants associated with enzymatic reactions. Overall change is termed as solvent isotope effects which is expressed as ratios of the rate constants in two solvents (*1, 2*). When the kinetic parameters k_H/k_D, V_H/V_D or $(V/K)_H/(V/K)_D$ are larger than unity (larger in H_2O) a normal solvent isotope effect is observed. When the parameters are less than unity (larger in D_2O), it is called an inverse solvent isotope effect.

Acid dissociation constant for H_2O ($1x10^{-14}$) is about ten times larger than that of D_2O ($1x10^{-15}$). While the pH of H_2O is 7.00, pD of D_2O is 7.41 which is a significant isotope effect and might have important consequences on pH and pD sensitive rate constants. Generally pD values are corrected by a factor of 0.4 (pD=pH+0.4) and thus accurate measurements of pH and pD are required for sensitive solvent isotope effects (*3-6*).

If the enzyme structure /function is maintained by hydrogen bonding network, conformation and stability can change in heavy water. Because the intermolecular hydrogen bond length is longer in D_2O, conformation and stability can slightly alter in

heavy water (*7*). So the overall structure might not be perturbed but loss of activity is possible due to instability of protein in heavy water. If substrate binding is pH sensitive or causes a conformational change, solvent isotope effect would be expected. SIE on microscopic rate constants of enzyme catalyzed reactions would affect steady-state parameters k_{cat} and k_{cat}/K_M. The best way to determine SIE on k_{cat} and k_{cat}/K_M is to measure them as a function of substrate. If pH profile of an enzyme is considered in which the enzyme rate follows a bell shaped curve, monitoring the effects of SIE at one pH and one pD will not be enough. When the steady-state parameters of an enzyme do not change over a couple of pH/pD units, the most stable pH region can be chosen and the SIE studies can be done at that pH range. Otherwise wide range of pH range should be selected because SIE requires sensitive measurements.

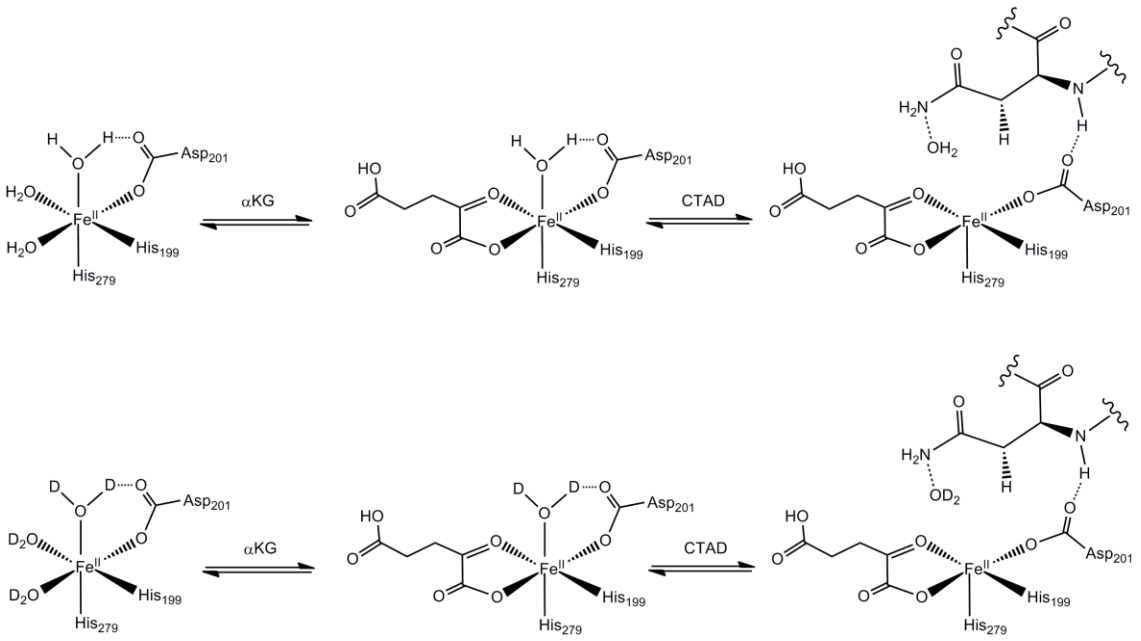

Scheme 4.1 Steps of FIH between the resting state and substrate binding which might show solvent isotope effect.

SIE measurements in a wide pH range would also give information about the ionization states of enzyme and/or substrate. Substrate binding, enzyme/substrate ionization state and/or product release might all show solvent isotope effects if those steps are pH or solvent dependent.

Examples of solvent isotope studies on nonheme iron enzymes showed no significant effects. An ethylene forming enzyme ACCO showed only background SIE (*8*) and TauD did not show any SIE (*9*). Although there is no significant SIE among these enzymes, FIH will be tested for any solvent isotope effects.

In the case of FIH, water release upon CTAD binding is the most interesting step because iron center needs to be five-coordinate for binding and activation of oxygen (Scheme 4.1). If the rate determining step is the water release upon CTAD binding, changing H_2O with D_2O might show a solvent isotope effect. Properties of normal and heavy water are different in the following ways: First, OH intramolecular bond length is longer than OD by about 0.03 Å or 3%. Second, intermolecular hydrogen bonding distance in H_2O is shorter than in D_2O by 0.07 Å or 4%. Also the distance between hydrogen atoms on neighboring molecules is about 2% longer for H_2O than in D_2O. Finally, the number of hydrogen bonds per water molecule is less in H_2O than in D_2O (3.62 vs. 3.76). So there is an overall change geometrically (*7*).

If these geometrical differences are applied, hydrogen bonds are stronger in D_2O which results in higher density, viscosity and boiling point (*3*). Zero-point vibrational energy of water molecules are decreased when they are deuterated. In terms of energy, D_2O exchange from the Fe(II) center should be slower which would cause normal solvent isotope effects. However, when the hydrogen bonding property of D_2O is taken into account, it might exchange faster than normal water. Stronger hydrogen bonding in D_2O can weaken Fe-D_2O bond causing a faster exchange and slower isotope effect (inverse SIE) with a higher k_{cat} but no change in K_m. If this step is not the rate limiting step, SIE=1 would be expected.

Substrate binding might also be affected by heavy water. Because CTAD is a pretty large substrate, hydrogen bonding interactions between CTAD and FIH would change upon changing H_2O with D_2O. Because D_2O forms stronger hydrogen bonds, the interaction between FIH and CTAD would be more pronounced. To test this mechanism, one pH/pD point will not be enough to compare because a solvent isotope effect seen might not be only due to substrate binding step. Interpretation of SIE is generally hard so in addition to wide pH profile control experiments should be done.

4.2 Materials and Methods

4.2.1 Activity assays and pH profile

Initial rate measurements were performed in 50 mM HEPES (pH 6.50, 6.90, 7.40 and 7.80) and incubated at 37 °C in 50 µL reaction volume. Reaction buffer included 2.00 mM ascorbate, 500 µM αKG, 25 µM $FeSO_4$, and 0-300 µM CTAD. The reaction was

initiated by adding the enzyme (0.5 µM), and at certain time points 5 µL aliquots were taken and quenched in 45 µL 0.1% formic acid. For each reaction 10 time points were collected and quenched, then analyzed by LC-ESI-MS. Samples were first loaded onto a C8 column for desalting, and CTAD and hydroxylated CTAD ($CTAD^{OH}$) were detected by ESI-MS to determine the mole fraction of peptide that had been converted to product, $\chi_{CTAD\text{-}OH}$. Product concentrations were calculated as $[CTAD^{OH}] = \chi_{(CTAD\text{-}OH)} \times [CTAD]_0$, and used to determine initial rates, which were then used for Michaelis-Menten fits. The steady-state parameter k_{cat} vs. pH was fitted to equation 4.1 to obtain a kinetic pK_a value of FIH.

$$k_{cat} = \frac{enzH * 10^{-pH} + enz * 10^{-pKa}}{10^{-pH} + 10^{-pKa}} \qquad \text{Eq. 4.1}$$

4.2.2 Solvent isotope effects

For solvent isotope effect studies, MALDI was chosen over LC-ESI-MS. Because in ESI-MS, +3 charge states caused misinterpretation of data. During the HPLC run, deuterated samples were back exchanged to some extent. CTAD and $CTAD^{OH}$ m/z appeared in two places due to H_2O and D_2O and this has led the data being not useful. To avoid these problems SIE measurements were performed like in the previous part by using MALDI with the following changes. Reaction buffer (50 mM Hepes pH 7.0) included 2.00 mM ascorbate, 500 µM αKG, 25 µM $FeSO_4$, and 0-200 µM CTAD. The reaction was initiated by adding the enzyme (0.5 µM), and at certain time points 5 µL aliquots were taken and quenched in 5-15 µL freshly prepared saturated sinapinic acid solution in 75% ACN+0.2% TFA (in H_2O). For the measurements in D_2O, buffer solution of 50 mM Hepes pD 7.0 was prepared by dissolving Hepes salt in D_2O and adjusting the pH by

NaOH to 6.60 (pD was corrected by adding 0.4 to pH reading). The reaction buffer (50 mM Hepes pD 7.0) included 2.00 mM ascorbate, 500 µM αKG, 25 µM $FeSO_4$, and 0-200 µM CTAD (all reagents were prepared in D_2O, CTAD was in 50 mM Hepes pD 7.0 buffer). The reaction was initiated by adding the enzyme (0.5 µM in 50 mM Hepes pH 7.0), and at certain time points 5 µL aliquots were taken and quenched in 5-15 µL freshly prepared saturated sinapinic acid solution in 75% ACN+0.2% TFA (in D_2O). Based on the volume percentages, the deuterium content was calculated to be around 90% for SIE measurements. Measurements were done in triplicate.

The matrix quenched samples were then spotted on the target and analyzed by two different MALDI (Bruker Daltonics Omniflex III MALDI TOF and Autoflex III MALDI TOF) mass spectrometers. Omniflex and Autoflex are low and high resolution instruments respectively. The tuning parameters for both instruments were as the following;

	Omniflex	**Autoflex**
Ion Source 1	19 kV	19 kV
Ion Source 2	17.30 kV	17.30 kV
Lens	9.4 kV	9.4 kV
Reflector	0 kV	20 kV
Detector Mode	Linear	Reflective
Shots	1000	1000

Analysis of the data was done by taking the ratios of hydroxylated CTAD intensity to overall intensity to determine concentration as it was done in the previous part. Calculated and observed masses of CTAD in H_2O and D_2O are summarized in Table 4.1.

Table 4.1 Calculated and observed CTAD mass in H_2O and D_2O

Sequence	Backbone	Fast exchangable	Sum	Mono mass	Avg mass	Back bone deuterated mass	Fully deuterated mass	Observed mass in H_2O	Observed mass in D_2O
DESGL PQLTS YDAEV NAPIQ GSRNL LQGEE LLRAL DQVN	**36**	**38**	**74**	4252.13	4254.58	4290.81	4329.04	4255	4326

The residues that have fast exchangeable protons: STYCDEHWKQNR

4.3 Results and Discussion

Obtaining a wide pH profile for an enzyme is generally hard due to the limitations of buffer capacities. Two or three component buffers can be used to make the buffer work in a wider pH range. In this case ionic strength should be controlled. Because all of the previous studies have been done in 50 mM Hepes, we have chosen to stay in Hepes within its buffer capacity (useful pH range for Hepes is 6.8-8.2). 50 mM Hepes pH 6.50, 6.90, 7.40 and 7.80 buffers were prepared by dissolving Hepes salt in water and adjusting the pH by NaOH to the according values. The lowest pH point was little off the buffer capacity but at the end of each initial assay the final pH values were checked to make sure reaction is occurred at that pH. The Michaelis-Menten fits can be seen in Figure 4.1.

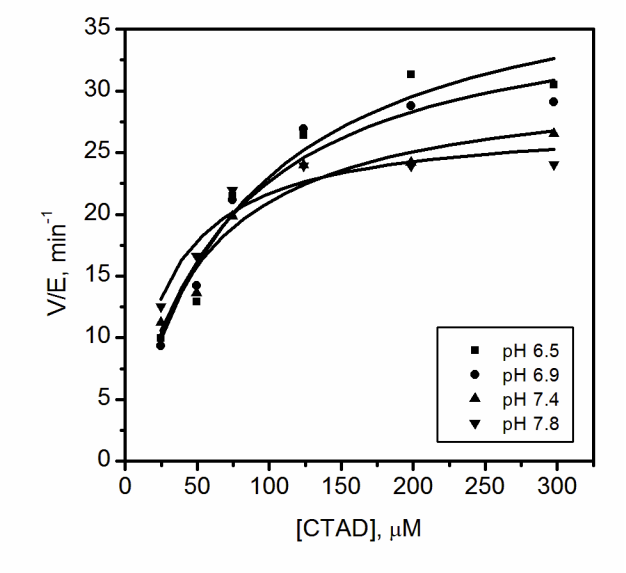

Figure 4.1 Michaelis-Menten fits of FIH at different pHs. FIH(0.5 μM), αKG(500 μM), Ascorbate (2 mM), Fe (25 μM), CTAD (0-300 μM) were mixed in 50 mM Hepes 6.5, 6.9, 7.4 and 7.8 buffers.

When the steady-state parameters k_{cat} and k_{cat}/K_M were plotted as a function of pH, no drastic change is observed (Figure 4.2 and Figure 4.3). This small pH range did not give a kinetic pK_a so we chose to work around pH 7.0. Log-log plots of k_{cat} vs. pH was almost linear.

Table 4.2 Steady-state parameters of FIH at different pHs.

	k_{cat}, min^{-1}	K_{cat}/K_M, $\mu M^{-1}min^{-1}$
pH 6.5	41.3 ± 4.2	0.52 ± 0.15
pH 6.9	37.7 ± 3.2	0.57 ± 0.14
pH 7.4	31 ± 2	0.65 ± 0.15
pH 7.8	29 ± 2	0.92 ± 0.23

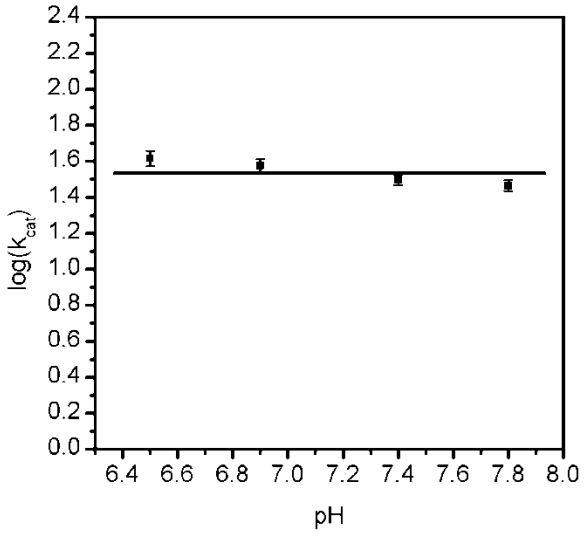

Figure 4.2 log(k_{cat}) vs. pH. FIH showed no pK_a over pH 6.4-7.8 range.

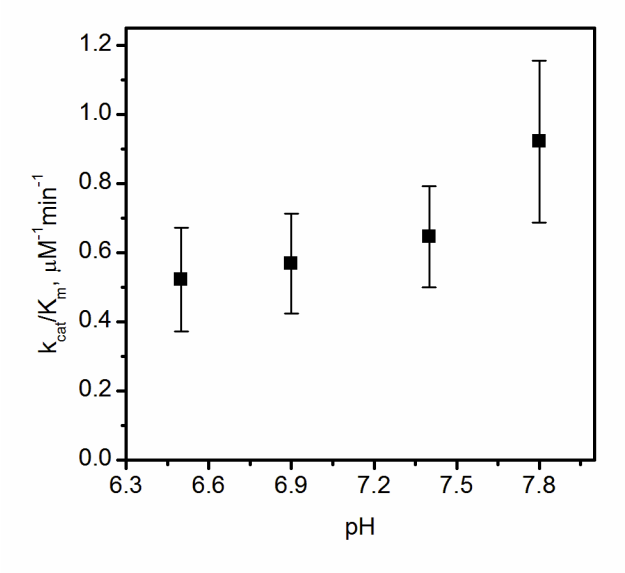

Figure 4.3 k_{cat}/K_M of FIH in pH 6-4-7.8 range.

The steady-state parameters and fitting parameters were summarized in Table 4.2. For the solvent isotope effect studies pH 7.0 was chosen because k_{cat}/K_M does not change around that pH value. If the k_{cat}/K_M value deviates within small pH range, that would cause insensitive SIE measurements. If any SIE was to be observed, that might be due to pH changes. So k_{cat}/K_M should not change drastically within a small region for the control experiments. After preparing 50 mM Hepes pH/pD 7.0 initial assays were done according to the protocol mentioned in methods. H_2O data showed a similar Michaelis-Menten curve with the data in pH profile studies. FIH has a k_{cat} of 34.1±1.8 min^{-1} and K_m value of 88.2±10.9 µM in 50 mM Hepes pH 7.0 (Figure 4.4). However the D_2O data behaved differently so Michaelis-Menten type kinetics was not observed Figure 4.4. Up to 50 µM CTAD concentration reaction is faster in D_2O than in H_2O. When the CTAD concentration was increased, a proinhibition type behaviour was observed. Because there is not any inhibitior in the reaction mixture, CTAD itself inhibited FIH. This type of behaviour due to heavy water could not be addressed; a proinhibition kinetics model (equation 4.2) was used to obtain K_i value for CTAD. The steady-state parameters are summarized in Table 4.3.

$$\frac{V}{E} = \frac{k_{cat}}{1 + \frac{K_m}{[S]} + \frac{[S]}{K_i}} \qquad \text{Eq. 4.2}$$

Omniflex MALDI instrument gave low resolution spectra in which CTAD and hydroxylated CTAD peaks were not separated enough. The data was still useful to obtain initial rates but to make things sure, SIE measurements were repeated with a high resolution Autoflex MALDI. The comparison of low and high resolution instruments can be seen in Figure 4.5. Interestingly Autoflex MALDI gave the same results. So the

inhibition behaviour seen is not due to resolving issues at high CTAD concentrations. SIE measurements were repeated several times in both high and low resolution instruments, in all of which a proinhibition can be observed (Figure 4.6). To address this proinhibiton behaviour, all of the reagents were prepared fresh several times including the buffer. CTAD is also purified, lyophilized and dissolved in pD 7.0 buffer but the results were same.

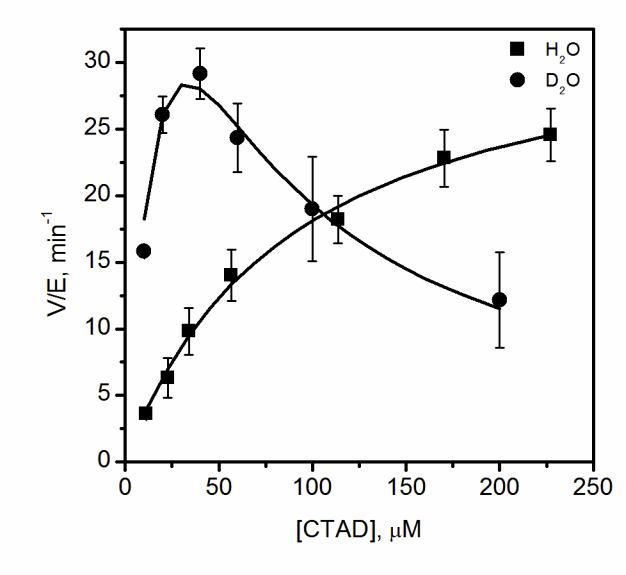

Figure 4.4 Solvent Isotope Effects on FIH. H_2O data (■); FIH(0.5 μM), αKG(500 μM), Ascorbate (2 mM), Fe (25 μM), CTAD (0-250 μM) were mixed in 50 mM Hepes pH 7. D_2O data (●); FIH(0.5 μM), αKG(500 μM), Ascorbate (2 mM), Fe (25 μM), CTAD (0-250 μM) were mixed in 50 mM Hepes pD 7. αKG, Ascorbate and Fe(II) solution were prepared in D_2O, CTAD was in 50 mM Hepes pD 7 buffer and FIH was in 50 mM Hepes pH 7 buffer. D_2O content is 90%.

Table 4.3 Steady-state parameters of FIH in pH 7.0 and pD 7.0.

	k_{cat}	K_m	K_i
pH 7.0	34.1 ± 1.8	88.2 ± 10.9	
pD 7.0	92.3 ± 34.8	37.1 ± 21.6	29.3 ± 13.9

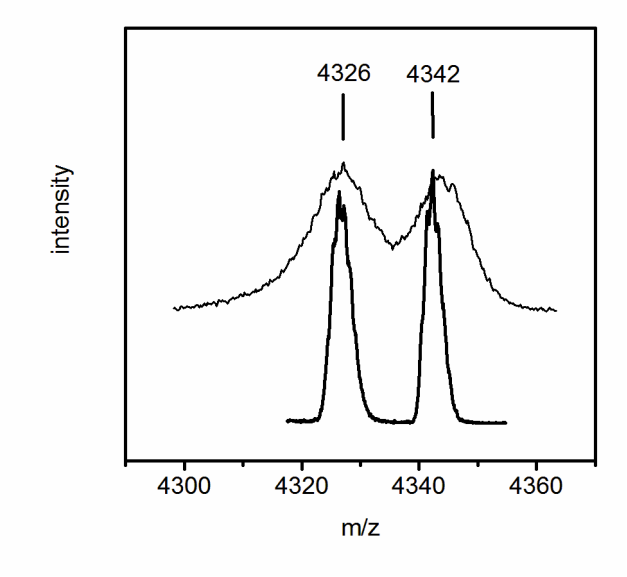

Figure 4.5 Comparison of low resolution and high resolution MALDI instruments. CTAD m/z is 4326 and CTAD-OH m/z is 4342 in D_2O

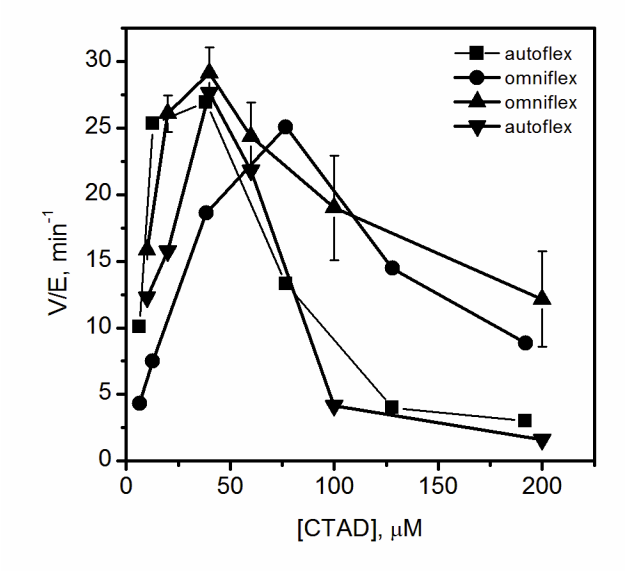

Figure 4.6 FIH(0.5 μM), αKG(500 μM), Ascorbate (2 mM), Fe (25 μM), CTAD (0-250 μM) were mixed in 50 mM Hepes pD 7. αKG, Ascorbate and Fe(II) solution were prepared in D_2O, CTAD was in 50 mM Hepes pD 7 buffer and FIH was in 50 mM Hepes pH 7 buffer. D_2O content is 90%. Autoflex is high resolution MALDI, Omniflex is low resolution MALDI.

4.4 Conclusions and Future Directions

These studies could not be completed due to time limitation. If the substrate inhibition at high concentrations could be addressed, FIH might still show faster rates in heavy water which means an inverse solvent isotope effect. SIE measurements in a wider pH range would also give better answers to our questions. Afterall for the preliminary efforts, FIH behaves different in heavy water, probably showing an inverse SIE.

CTAD inhibition at high concentrations might be due to stronger hydrogen bonding interactions in heavy water, so product release after hydroxylation might be prevented. To test this behaviour, really high concentrations of CTAD should be tested for any inhibition in H_2O.

If the water release upon CTAD binding is the rate limiting step, it would help us to better understand the regulatory role of FIH. It would also elucidate how oxygen is activated. In the absence of substrate, oxygen can still bind to iron center and do slow oxidative reaction like auto-hydroxylation. When the substrate is present, water release opens a coordination site for oxygen binding. Determining the rate limiting step for oxygen activation will provide more insights into oxygen sensor FIH and other nonheme iron enzymes in which oxygen is activated in a controlled manner.

As we have seen in the previous chapters there is not only one factor for oxygen activation. In chapter 2; how activated oxygen is tightly coupled to CTAD hydroxylation in FIH was tested, in chapter 3; the impact of hydrogen bonding network on the second

coordination sphere was studied and in chapter 4; the rate determining step for the oxygen activation was investigated by means of solvent isotope studies.

Overall this thesis provided insights into how oxygen is activated and controlled in FIH which is one of the primary oxygen sensors in human body. Understanding the mechanism of how activated oxygen is controlled in human oxygen sensor FIH would draw new pathways in hypoxia sensing and its related diseases.

4.5 Bibliography

1. Cleland, W. W., O'Leary, M. H., and Northrop, D. B. (1977) *Isotope effects on enzyme-catalyzed reactions*, University Park Press.

2. Schowen, K. B., and Schowen, R. L. (1982) Solvent isotope effects on enzyme systems, *Methods Enzymol. 87*, 551-606.

3. Cook, P. F. (1991) *Enzyme mechanism from isotope effects*, CRC Press.

4. Northrop, D. B. (1991) Intrinsic isotope effects in enzyme catalyzed reactions, in *Enzyme mechanism from isotope effects* (Cook, P. F., Ed.), pp 181-202, CRC Press, Boca Raton.

5. Kohen, A., and Limbach, H. H. (2006) *Isotope effects in chemistry and biology*, Taylor & Francis.

6. Glasoe, P. K., and Long, F. A. (1960) Use of glass electrodes to measure acidities in deuterium oxide, *J. Phys. Chem. 64*, 188-190.

7. Soper, A. K., and Benmore, C. J. (2008) Quantum Differences between Heavy and Light Water, *Phys. Rev. Lett. 101*, 065502.

8. Mirica, L. M., and Klinman, J. P. (2008) The nature of O_2 activation by the ethylene-forming enzyme 1-aminocyclopropane-1-carboxylic acid oxidase, *PNAS 105*, 1814-1819.

9. Grzyska, P. K., Ryle, M. J., Monterosso, G. R., Liu, J., Ballou, D. P., and Hausinger, R. P. (2005) Steady-State and Transient Kinetic Analyses of Taurine/alpha-Ketoglutarate Dioxygenase: Effects of Oxygen Concentration, Alternative Sulfonates, and Active-Site Variants on the Fe(IV)-oxo Intermediate *Biochemistry 44*, 3845-3855.

BIBLIOGRAPHY

1. Abu-Omar, M. M., Loaiza, A., and Hontzeas, N. (2005) Reaction mechanisms of mononuclear non-heme iron oxygenases, *Chem. Rev.* 105, 2227-2252.

2. Aragonés, J., Fraisl, P., Baes, M., and Carmeliet, P. (2009) Oxygen Sensors at the Crossroad of Metabolism, *Cell Metab.* 9, 11-22.

3. Berra, E., Benizri, E., Ginouves, A., Volmat, V., Roux, D., and Pouyssegur, J. (2003) HIF prolyl-hydroxylase 2 is the key oxygen sensor setting low steady-state levels of HIF-1 alpha in normoxia, *Embo J.* 22, 4082-4090.

4. Bleijlevens, B., Shivarattan, T., Sedgwick, B., Rigby, S. E. J., and Matthews, S. J. (2007) Replacement of non-heme Fe(II) with Cu(II) in the alpha-ketoglutarate dependent DNA repair enzyme AlkB: Spectroscopic characterization of the active site, *J. Inorg. Biochem.* 101, 1043-1048.

5. Bruick, R. K. (2003) Oxygen sensing in the hypoxic response pathway: regulation of the hypoxia-inducible transcription factor, *Genes Dev.* 17, 2614-2623.

6. Bruick, R. K., and McKnight, S. L. (2001) A Conserved Family of Prolyl-4-Hydroxylases That Modify HIF, *Science* 294, 1337-1340.

7. Bugg, T. D. H. (2001) Oxygenases: mechanisms and structural motifs for O2 activation, *Curr. Op. in Chem. Biol.* 5, 550-555.

8. Bugg, T. D. H. (2003) Dioxygenase enzymes: catalytic mechanisms and chemical models, *Tetrahedron* 59, 7075-7101.

9. Bugg, T. D. H., and Ramaswamy, S. (2008) Non-heme iron-dependent dioxygenases: unravelling catalytic mechanisms for complex enzymatic oxidations, *Curr. Op. in Chem. Biol.* 12, 134-140.

10. Carredano, E., Karlsson, A., Kauppi, B., Choudhury, D., Parales, R. E., Parales, J. V., Lee, K., Gibson, D. T., Eklund, H., and Ramaswamy, S. (2000) Substrate binding site of naphthalene 1,2-dioxygenase: Functional implications of indole binding, *J. Mol. Biol.* 296, 701-712.

11. Chakrabarty, S., Austin, R. N., Deng, D. Y., Groves, J. T., and Lipscomb, J. D. (2007) Radical intermediates in monooxygenase reactions of Rieske dioxygenases, *J. Am. Chem. Soc.* 129, 3514.

12. Chen, Y. H., Comeaux, L. M., Eyles, S. J., and Knapp, M. J. (2008) Auto-hydroxylation of FIH-1: an Fe(II), alpha-ketoglutarate-dependent human hypoxia sensor, *Chem. Commun.*, 4768-4770.

13. Chen, Y. H., Comeaux, L. M., Herbst, R. W., Saban, E., Kennedy, D. C., Maroney, M. J., and Knapp, M. J. (2008) Coordination changes and auto-hydroxylation of FIH-1: Uncoupled O-2-activation in a human hypoxia sensor, *J. Inorg. Biochem.* 102, 2120-2129.

14. Cleland, W. W., O'Leary, M. H., and Northrop, D. B. (1977) *Isotope effects on enzyme-catalyzed reactions*, University Park Press.

15. Clifton, I. J., McDonough, M. A., Ehrismann, D., Kershaw, N. J., Granatino, N., and Schofield, C. J. (2006) Structural studies on 2-oxoglutarate oxygenases and related double-stranded beta-helix fold proteins, *J. of Inorg. Biochem.* 100, 644-669.

16. Cook, P. F. (1991) *Enzyme mechanism from isotope effects*, CRC Press.

17. Costas, M., Mehn, M. P., Jensen, M. P., and Que, L. (2004) Dioxygen Activation at Mononuclear Nonheme Iron Active Sites: Enzymes, Models, and Intermediates, *Chem. Rev.* 104, 939-986.

18. Counts, D. F., Cardinale, G. J., and Udenfriend, S. (1978) Prolyl hydroxylase half reaction: peptidyl prolyl-independent decarboxylation of alpha-ketoglutarate, *PNAS* 75, 2145-2149.

19. Dames, S. A., Martinez-Yamout, M., De Guzman, R. N., Dyson, H. J., and Wright, P. E. (2002) Structural basis for Hif-1 alpha/CBP recognition in the cellular hypoxic response, *PNAS* 99, 5271-5276.

20. Dann, C. E., and Bruick, R. K. (2005) Dioxygenases as O2-dependent regulators of the hypoxic response pathway, *Biochem. Biophys. Res. Commun.* 338, 639-647.

21. Dann, C. E., Bruick, R. K., and Deisenhofer, J. (2002) Structure of factor-inhibiting hypoxia-inducible factor 1: An asparaginyl hydroxylase involved in the hypoxic response pathway, *PNAS* 99, 15351-15356.

22. Dix, T. A., and Benkovic, S. J. (1985) Mechanism of uncoupled tetrahydropterin oxidation by phenylalanine hydroxylase, *Biochemistry* 24, 5839-5846.

23. Dix, T. A., and Benkovic, S. J. (1988) Mechanism of oxygen activation by pteridine dependent monooxygenases, *Accounts Chem. Res.* 21, 101-107.

24. Dubus, A., Sami, M., Brown, T. J. N., Schofield, C. J., Baldwin, J. E., and Frere, J. M. (2000) Studies of isopenicillin N synthase enzymatic properties using a continuous spectrophotometric assay, *FEBS Lett.* 485, 142-146.

25. Ehrismann, D., Flashman, E., Genn, D. N., Mathioudakis, N., Hewitson, K. S., Ratcliffe, P. J., and Schofield, C. J. (2007) Studies on the activity of the hypoxia-inducible-factor hydroxylases using an oxygen consumption assay, *Biochem. J.* 401, 227-234.

26. Elkins, J. M., Hewitson, K. S., McNeill, L. A., Seibel, J. F., Schlemminger, I., Pugh, C. W., Ratcliffe, P. J., and Schofield, C. J. (2003) Structure of factor-inhibiting hypoxia-inducible factor (HIF) reveals mechanism of oxidative modification of HIF-1 alpha, *J. Biol. Chem.* 278, 1802-1806.

27. Elkins, J. M., Ryle, M. J., Clifton, I. J., Dunning Hotopp, J. C., Lloyd, J. S., Burzlaff, N. I., Baldwin, J. E., Hausinger, R. P., and Roach, P. L. (2002) X-ray Crystal Structure of Escherichia coli Taurine/alpha-Ketoglutarate Dioxygenase Complexed to Ferrous Iron and Substrates, *Biochemistry* 41, 5185-5192.

28. Ema, M., Taya, S., Yokotani, N., Sogawa, K., Matsuda, Y., and FujiiKuriyama, Y. (1997) A novel bHLH-PAS factor with close sequence similarity to hypoxia-inducible factor 1 alpha regulates the VEGF expression and is potentially involved in lung and vascular development, *PNAS* 94, 4273-4278.

29. Ensley, B. D., Gibson, D. T., and Laborde, A. L. (1982) Oxidation of naphthalene by a multicomponent enzyme system from pseudomonas SP Strain NCIB9816, *J. Bacteriol.* 149, 948-954.

30. Erbel, P. J. A., Card, P. B., Karakuzu, O., Bruick, R. K., and Gardner, K. H. (2003) Structural basis for PAS domain heterodimerization in the basic helix-loop-helix-PAS transcription factor hypoxia-inducible factor, *PNAS* 100, 15504-15509.

31. Eser, B. E., Barr, E. W., Frantorn, P. A., Saleh, L., Bollinger, J. M., Krebs, C., and Fitzpatrick, P. F. (2007) Direct spectroscopic evidence for a high-spin Fe(IV) intermediate in tyrosine hydroxylase, *J. Am. Chem. Soc.* 129, 11334.

32. Fitzpatrick, P. F. (1999) Tetrahydropterin-dependent amino acid hydroxylases, *Annu. Rev. Biochem.* 68, 355-381.

33. Fitzpatrick, P. F. (2000) The aromatic amino acid hydroxylases, in *Advances in Enzymology*, 74, 235, John Wiley & Sons Inc, New York.

34. Flamme, I., Frohlich, T., vonReutern, M., Kappel, A., Damert, A., and Risau, W. (1997) HRF, a putative basic helix-loop-helix-PAS-domain transcription factor is closely related to hypoxia-inducible factor-1 alpha and developmentally expressed in blood vessels, *Mech. Dev.* 63, 51-60.

35. Flashman, E., Hoffart, L. M., Hamed, R. B., Bollinger Jr, J. M., Krebs, C., and Schofield, C. J. (2010) Evidence for the slow reaction of hypoxia-inducible factor prolyl hydroxylase 2 with oxygen, *FEBS J.* 277, 4089-4099.

36. Freedman, S. J., Sun, Z. Y. J., Poy, F., Kung, A. L., Livingston, D. M., Wagner, G., and Eck, M. J. (2002) Structural basis for recruitment of CBP/p300 by hypoxia-inducible factor-1 alpha, *PNAS* 99, 5367-5372.

37. Fujimori, D. G., Barr, E. W., Matthews, M. L., Koch, G. M., Yonce, J. R., Walsh, C. T., Bollinger, J. M., Krebs, C., and Riggs-Gelasco, P. J. (2007) Spectroscopic evidence for a high-spin Br-Fe(IV)-Oxo intermediate in the alpha-ketoglutarate-dependent halogenase CytC3 from Streptomyces, *J. Am. Chem. Soc.* 129, 13408.

38. Giaccia, A., Siim, B. G., and Johnson, R. S. (2003) HIF-1 as a target for drug development, *Nat. Rev. Drug Discov.* 2, 803-811.

39. Glasoe, P. K., and Long, F. A. (1960) Use of glass electrodes to measure acidities in deuterium oxide, *J. Phys. Chem.* 64, 188-190.

40. Groce, S. L., and Lipscomb, J. D. (2005) Aromatic ring cleavage by homoprotocatechuate 2,3-dioxygenase: Role of His200 in the kinetics of interconversion of reaction cycle intermediates, *Biochemistry* 44, 7175-7188.

41. Groce, S. L., Miller, M. A., and Lipscomb, J. D. (1999) Transient kinetic studies of homoprotocatechuate 2,3-dioxygenase, *J. Inorg. Biochem.* 74, 149-149.

42. Groce, S. L., Miller-Rodeberg, M. A., and Lipscomb, J. D. (2004) Single-turnover kinetics of homoprotocatechuate 2,3-dioxygenase, *Biochemistry* 43, 15141-15153.

43. Grzyska, P. K., Ryle, M. J., Monterosso, G. R., Liu, J., Ballou, D. P., and Hausinger, R. P. (2005) Steady-State and Transient Kinetic Analyses of Taurine/alpha-Ketoglutarate Dioxygenase: Effects of Oxygen Concentration, Alternative Sulfonates, and Active-Site Variants on the Fe(IV)-oxo Intermediate, *Biochemistry* 44, 3845-3855.

44. Halliwell, B., Gutteridge, J. M. C., and Aruoma, O. I. (1987) The Deoxyribose Method - A Simple Test-Tube Assay for Determination of Rate Constants for Reactions of Hydroxyl Radicals, *Anal. Biochem.* 165, 215-219.

45. Hanauske-Abel, H. M., and Günzler, V. (1982) A stereochemical concept for the catalytic mechanism of prolylhydroxylase : Applicability to classification and design of inhibitors, *J. Theor. Biol.* 94, 421-455.

46. Hausinger, R. P. (2004) Fe(II)/alpha-Ketoglutarate-dependent hydroxylases and related enzymes, *Crit. Rev. Biochem. Mol. Biol.* 39, 21-68.

47. Hegg, E. L., Whiting, A. K., Saari, R. E., McCracken, J., Hausinger, R. P., and Que, L. (1999) Herbicide degrading alpha-keto acid dependent enzyme Tfda: Metal coordination environment and mechanistic insights., *Biochemistry* 38, 16714-16726.

48. Hegg, E. L., and Que, L. (1997) The 2-His-1-carboxylate facial triad - An emerging structural motif in mononuclear non-heme iron(II) enzymes, *Eur. J. Biochem.* 250, 625-629.

49. Hendrich, M. P. *Spincount software,* Carnegie Mellon Univ.

50. Henshaw, T. F., Feig, M., and Hausinger, R. P. (2004) Aberrant activity of the DNA repair enzyme AlkB, *J. Inorg. Biochem.* 98, 856-861.

51. Hewitson, K. S., McNeill, L. A., Riordan, M. V., Tian, Y., Bullock, A. N., Welford, R. W., Elkins, J. M., Oldham, N. J., Bhattacharya, S., Gleadle, J. M., Ratcliffe, P. J., Pugh, C. W., and Schofield, C. J. (2002) Hypoxia-inducible factor (HIF) asparagine hydroxylase is identical to factor inhibiting HIF (FIH) and is related to the cupin structural family, *J. Biol. Chem.* 277, 26351-26355.

52. Hewitson, K. S., McNeill, L. A., and Schofield, C. J. (2003) The role of iron and 2-oxoglutarate oxygenases in signaling, *Biochem. Soc. T.* 31, 510-515.

53. Hewitson, K. S., and Schofield, C. J. (2004) The HIF pathway as a therapeutic target, *Drug Discov. Today* 9, 704-711.

54. Hirsila, M., Koivunen, P., Gunzler, V., Kivirikko, K. I., and Myllyharju, J. (2003) Characterization of the human prolyl 4-hydroxylases that modify the hypoxia-inducible factor, *J. Biol. Chem.* 278, 30772-30780.

55. Hoffart, L. M., Barr, E. W., Guyer, R. B., Bollinger, J. M., and Krebs, C. (2006) Direct spectroscopic detection of a C-H-cleaving high-spin Fe(IV) complex in a prolyl-4-hydroxylase, *PNAS* 103, 14738-14743.

56. Hogenesch, J. B., Chan, W. K., Jackiw, V. H., Brown, R. C., Gu, Y. Z., PrayGrant, M., Perdew, G. H., and Bradfield, C. A. (1997) Characterization of a subset of the basic-helix-loop-helix-PAS superfamily that interacts with components of the dioxin signaling pathway, *J. Biol. Chem.* 272, 8581-8593.

57. Hon, W. C., Wilson, M. I., Harlos, K., Claridge, T. D. W., Schofield, C. J., Pugh, C. W., Maxwell, P. H., Ratcliffe, P. J., Stuart, D. I., and Jones, E. Y. (2002) Structural basis for the recognition of hydroxyproline in HIF-1a by pVHL, *Nature* 417, 975-978.

58. Huang, L. E., and Bunn, H. F. (2003) Hypoxia-inducible factor and its biomedical relevance, *J. Biol. Chem.* 278, 19575-19578.

59. Ivan, M., Kondo, K., Yang, H., Kim, W., Valiando, J., Ohh, M., Salic, A., Asara, J. M., Lane, W. S., and Kaelin Jr, W. G. (2001) HIFa Targeted for VHL-Mediated Destruction by Proline Hydroxylation: Implications for O2 Sensing, *Science* 292, 464-468.

60. Jiang, B. H., Rue, E., Wang, G. L., Roe, R., and Semenza, G. L. (1996) Dimerization, DNA binding, and transactivation properties of hypoxia-inducible factor 1, *J. Biol. Chem.* 271, 17771-17778.

61. Jiang, B. H., Zheng, J. Z., Leung, S. W., Roe, R., and Semenza, G. L. (1997) Transactivation and inhibitory domains of hypoxia-inducible factor 1 alpha. Modulation of transcriptional activity by oxygen tension, *J. Biol. Chem.* 272, 19253-19260.

62. Kaelin, W. G. (2005) Proline hydroxylation and gene expression, *Annu. Rev. Biochem.* 74, 115-128.

63. Kahnert, A., and Kertesz, M. A. (2000) Characterization of a Sulfur-regulated Oxygenative Alkylsulfatase from Pseudomonas putida S-313*, *J. Biol. Chem.* 275, 31661-31667.

64. Karlsson, A., Parales, J. V., Parales, R. E., Gibson, D. T., Eklund, H., and Ramaswamy, S. (2003) Crystal structure of naphthalene dioxygenase: Side-on binding of dioxygen to iron, *Science* 299, 1039-1042.

65. Kauppi, B., Lee, K., Carredano, E., Parales, R. E., Gibson, D. T., Eklund, H., and Ramaswamy, S. (1998) Structure of an aromatic-ring-hydroxylating dioxygenase-naphthalene 1,2-dioxygenase, *Struct. Fold. Des.* 6, 571-586.

66. Koehntop, K. D., Emerson, J. P., and Que, L. (2005) The 2-His-1-carboxylate facial triad: a versatile platform for dioxygen activation by mononuclear non-heme iron(II) enzymes, *J. Biol. Inorg. Chem.* 10, 87-93.

67. Kohen, A., and Limbach, H. H. (2006) *Isotope effects in chemistry and biology*, Taylor & Francis.

68. Koivunen, P., Hirsila, M., Gunzler, V., Kivirikko, K. I., and Myllyharju, J. (2004) Catalytic Properties of the Asparaginyl Hydroxylase (FIH) in the Oxygen Sensing Pathway Are Distinct from Those of Its Prolyl 4-Hydroxylases, *J. Biol. Chem.* 279, 9899-9904.

69. Koivunen, P., Hirsila, M., Kivirikko, K. I., and Myllyharju, J. (2006) The length of peptide substrates has a marked effect on hydroxylation by the hypoxia-inducible factor prolyl 4-hydroxylases, *J. Biol. Chem.* 281, 28712-28720.

70. Kovaleva, E. G., and Lipscomb, J. D. (2007) Crystal structures of Fe^{2+} dioxygenase superoxo, alkylperoxo, and bound product intermediates, *Science* 316, 453-457.

71. Kovaleva, E. G., and Lipscomb, J. D. (2008) Versatility of biological non-heme Fe(II) centers in oxygen activation reactions, *Nat. Chem. Biol.* 4, 186-193.

72. Kovaleva, E. G., and Lipscomb, J. D. (2008) Intermediate in the O-O Bond Cleavage Reaction of an Extradiol Dioxygenase, *Biochemistry* 47, 11168-11170.

73. Lando, D., Peet, D. J., Gorman, J. J., Whelan, D. A., Whitelaw, M. L., and Bruick, R. K. (2002) FIH-1 is an asparaginyl hydroxylase enzyme that regulates the transcriptional activity of hypoxia-inducible factor, *Genes Dev.* 16, 1466-1471.

74. Lando, D., Peet, D. J., Whelan, D. A., Gorman, J. J., and Whitelaw, M. L. (2002) Asparagine hydroxylation of the HIF transactivation domain: A hypoxic switch, *Science* 295, 858-861.

75. Lee, C., Kim, S. J., Jeong, D. G., Lee, S. M., and Ryu, S. E. (2003) Structure of Human FIH-1 Reveals a Unique Active Site Pocket and Interaction Sites for HIF-1 and von Hippel-Lindau, *J. Biol. Chem.* 278, 7558-7563.

76. Lee, K. (1999) Benzene-Induced Uncoupling of Naphthalene Dioxygenase Activity and Enzyme Inactivation by Production of Hydrogen Peroxide, *J. Bacteriol.* 181, 2719-2725.

77. Linke, S., Stojkoski, C., Kewley, R. J., Booker, G. W., Whitelaw, M. L., and Peet, D. J. (2004) Substrate requirements of the oxygen-sensing asparaginyl hydroxylase factor-inhibiting hypoxia-inducible factor, *J. Biol. Chem.* 279, 14391-14397.

78. Liu, A., Ho, R. Y. N., Que, L., Ryle, M. J., Phinney, B. S., and Hausinger, R. P. (2001) Alternative Reactivity of an alpha-Ketoglutarate-Dependent Iron(II) Oxygenase: Enzyme Self-Hydroxylation, *J. Am. Chem. Soc.* 123, 5126-5127.

79. Martell, A. E., and Smith, R. M. (1974) *Critical stability constants*, Plenum Press.

80. McCusker, K. P., and Klinman, J. P. (2009) Modular behavior of tauD provides insight into the origin of specificity in alpha-ketoglutarate-dependent nonheme iron oxygenases, *PNAS* 106, 19791-19795.

81. McCusker, K. P., and Klinman, J. P. (2010) An Active-Site Phenylalanine Directs Substrate Binding and C-H Cleavage in the alpha-Ketoglutarate-Dependent Dioxygenase TauD, *J. Am. Chem. Soc*. 132, 5114-5120.

82. McNeill, L. A., Hewitson, K. S., Claridge, T. D., Seibel, J. r. F., Horsfall, L. E., and Schofield, C. J. (2002) Hypoxia-inducible factor asparaginyl hydroxylase (FIH-1) catalyses hydroxylation at the beta-carbon of asparagine-803, *Biochem. J.* 367, 571-575.

83. Mehn, M. P., Fujisawa, K., Hegg, E. L., and Que, L. (2003) Oxygen activation by nonheme iron(II) complexes: a-Keto carboxylate versus carboxylate, *J. Am. Chem. Soc*. 125, 7828-7842.

84. Metzen, E., Berchner-Pfannschmidt, U., Stengel, P., Marxsen, J. H., Stolze, I., Klinger, M., Huang, W. Q., Wotzlaw, C., Hellwig-Burgel, T., Jelkmann, W., Acker, H., and Fandrey, J. (2003) Intracellular localisation of human HIF-1 alpha hydroxylases: implications for oxygen sensing, *J. Cell Sci.* 116, 1319-1326.

85. Miller, A.-F. (2008) Redox Tuning over Almost 1 V in a Structurally Conserved Active Site: Lessons from Fe-Containing Superoxide Dismutase, *Accounts Chem. Res.* 41, 501-510.

86. Mills, S. A., and Marletta, M. A. (2005) Metal Binding Characteristics and Role of Iron Oxidation in the Ferric Uptake Regulator from Escherichia coli, *Biochemistry* 44, 13553-13559.

87. Min, J. H., Yang, H. F., Ivan, M., Gertler, F., Kaelin, W. G., and Pavletich, N. P. (2002) Structure of an HIF-1 alpha-pVHL complex: Hydroxyproline recognition in signaling, *Science* 296, 1886-1889.

88. Mirica, L. M., and Klinman, J. P. (2008) The nature of O2 activation by the ethylene-forming enzyme 1-aminocyclopropane-1-carboxylic acid oxidase, *PNAS* 105, 1814-1819.

89. Mole, D. R., Blancher, C., Copley, R. R., Pollard, P. J., Gleadle, J. M., Ragoussis, J., and Ratcliffe, P. J. (2009) Genome-wide Association of Hypoxia-inducible Factor (HIF)-1a and HIF-2a DNA Binding with Expression Profiling of Hypoxia-inducible Transcripts, *J. Biol. Chem.* 284, 16767-16775.

90. Muller, I., Kahnert, A., Pape, T., Sheldrick, G. M., Meyer-Klaucke, W., Dierks, T., Kertesz, M., and Uson, I. (2004) Crystal Structure of the Alkylsulfatase AtsK: Insights into the Catalytic Mechanism of the Fe(II) alpha-Ketoglutarate-Dependent Dioxygenase Superfamily, *Biochemistry* 43, 3075-3088.

91. Myllyla, R., Majamaa, K., Gunzler, V., Hanauske-Abel, H. M., and Kivirikko, K. I. (1984) Ascorbate is consumed stoichiometrically in the uncoupled reactions catalyzed by prolyl 4-hydroxylase and lysyl hydroxylase, *J. Biol. Chem.* 259, 5403-5405.

92. Nagel, S., Talbot, N. P., Mecinovic, J., Smith, T. G., Buchan, A. M., and Schofield, C. J. (2010) Therapeutic manipulation of the HIF hydroxylases., *Antioxid. & Redox Sign.* 12, 481-501.

93. Neidig, M. L., Brown, C. D., Light, K. M., Fujimori, D. G., Nolan, E. M., Price, J. C., Barr, E. W., Bollinger, J. M., Krebs, C., Walsh, C. T., and Solomon, E. I. (2007) CD and MCD of CytC3 and Taurine Dioxygenase: Role of the Facial Triad in a-KG-Dependent Oxygenases, *J. Am. Chem. Soc.* 129, 14224-14231.

94. Northrop, D. B. (1981) The Expression of Isotope effects on Enzyme-Catalyzed Reactions, *Ann. Rev. Biochem.* 50, 103-131.

95. Northrop, D. B. (1991) Intrinsic isotope effects in enzyme catalyzed reactions, in *Enzyme mechanism from isotope effects* (Cook, P. F., Ed.), pp 181-202, CRC Press, Boca Raton.

96. Ohta, T., Chakrabarty, S., Lipscomb, J. D., and Solomon, E. I. (2008) Near-IR MCD of the nonheme ferrous active site in naphthalene 1,2-dioxygenase: Correlation to crystallography and structural insight into the mechanism of Rieske dioxygenases, *J. Am. Chem. Soc.* 130, 1601-1610.

97. Ozer, A., and Bruick, R. K. (2007) Non-heme dioxygenases: cellular sensors and regulators jelly rolled into one?, *Nat. Chem. Biol.* 3, 144-153.

98. Pavel, E. G., Zhou, J., Busby, R. W., Gunsior, M., Townsend, C. A., and Solomon, E. I. (1998) Circular dichroism and magnetic circular dichroism spectroscopic studies of the non-heme ferrous active site in clavaminate synthase and its interaction with alpha-ketoglutarate cosubstrate, *J. Am. Chem. Soc.* 120, 743-753.

99. Pavon, J. A., Eser, B., Huynh, M. T., and Fitzpatrick, P. F. (2010) Single Turnover Kinetics of Tryptophan Hydroxylase: Evidence for a New Intermediate in the Reaction of the Aromatic Amino Acid Hydroxylases, *Biochemistry* 49, 7563-7571.

100. Pavon, J. A., and Fitzpatrick, P. F. (2006) Insights into the catalytic mechanisms of phenylalanine and tryptophan hydroxylase from kinetic isotope effects on aromatic hydroxylation, *Biochemistry* 45, 11030-11037.

101. Peisach, J., and Blumberg, W. E. (1974) Structural implications derived from the analysis of electron paramagnetic resonance spectra of natural and artificial copper proteins, *Arch. Biochem. Biophys.* 165, 691-708.

102. Perry, D., Abraham, E. P., and Baldwin, J. E. (1988) Factors affecting the isopenicillin-N synthase reaction, *Biochem. J.* 255, 345-351.

103. Plotnikov, V. V., Brandts, J. M., Lin, L.-N., and Brandts, J. F. (1997) A New Ultrasensitive Scanning Calorimeter, *Anal. Biochem.* 250, 237-244.

104. Price, J. C., Barr, E. W., Glass, T. E., Krebs, C., and Bollinger, J. M. (2003) Evidence for Hydrogen Abstraction from C1 of Taurine by the High-Spin Fe(IV) Intermediate Detected during Oxygen Activation by Taurine:a-Ketoglutarate Dioxygenase (TauD), *J. Am. Chem. Soc.* 125, 13008-13009.

105. Price, J. C., Barr, E. W., Tirupati, B., Bollinger, J. M., and Krebs, C. (2003) The First Direct Characterization of a High-Valent Iron Intermediate in the Reaction of an a-Ketoglutarate-Dependent Dioxygenase: A High-Spin Fe(IV) Complex in Taurine/a-Ketoglutarate Dioxygenase (TauD) from Escherichia coli, *Biochemistry* 42, 7497-7508.

106. Proshlyakov, D. A., Henshaw, T. F., Monterosso, G. R., Ryle, M. J., and Hausinger, R. P. (2004) Direct Detection of Oxygen Intermediates in the Non-Heme Fe Enzyme Taurine/alpha-Ketoglutarate Dioxygenase, *J. Am. Chem. Soc.* 126, 1022-1023.

107. Pugh, C. W. (2003) Oxygen sensing in cancer, *Ann. Med.* 35, 380-390.

108. Pugh, C. W., Orourke, J. F., Nagao, M., Gleadle, J. M., and Ratcliffe, P. J. (1997) Activation of hypoxia-inducible factor-1; Definition of regulatory domains within the alpha subunit, *J. Biol. Chem.* 272, 11205-11214.

109. Pugh, C. W., and Ratcliffe, P. J. (2003) Regulation of angiogenesis by hypoxia: role of the HIF system, *Nat. Med.* 9, 677-684.

110. Que, L. (2000) One motif-many different reactions, *Nat. Struct. Biol.* 7, 182-184.

111. Rao, N. V., and Adams, E. (1978) Partial reaction of prolyl hydroxylase. (Gly-PRO-Ala)n stimulates alpha-ketoglutarate decarboxylation without prolyl hydroxylation, *J. Biol. Chem.* 253, 6327-6330.

112. Rich, P. R. (2003) The molecular machinery of Keilin's respiratory chain, *Biochem. Soc. Trans.* 31, 1095-1105.

113. Riggs-Gelasco, P. J., Price, J. C., Guyer, R. B., Brehm, J. H., Barr, E. W., Bollinger, J. M., and Krebs, C. (2004) EXAFS spectroscopic evidence for an Fe = O unit in the Fe(IV) intermediate observed during oxygen activation by taurine :alpha-ketoglutarate dioxygenase, *J. Am. Chem. Soc.* 126, 8108-8109.

114. Roach, P. L., Clifton, I. J., Hensgens, C. M. H., Shibata, N., Schofield, C. J., Hajdu, J., and Baldwin, J. E. (1997) Structure of isopenicillin N synthase complexed with substrate and the mechanism of penicillin formation, *Nature* 387, 827-830.

115. Ryle, M. J., and Hausinger, R. P. (2002) Non-heme iron oxygenases, *Curr. Op. in Chem. Biol.* 6, 193-201.

116. Ryle, M. J., Liu, A., Muthukumaran, R. B., Ho, R. Y. N., Koehntop, K. D., McCracken, J., Que, L., and Hausinger, R. P. (2003) O2- and alpha-Ketoglutarate-Dependent Tyrosyl Radical Formation in TauD, an alpha-Keto Acid-Dependent Non-Heme Iron Dioxygenase, *Biochemistry* 42, 1854-1862.

117. Ryle, M. J., Padmakumar, R., and Hausinger, R. P. (1999) Stopped-Flow Kinetic Analysis of Escherichia coli Taurine/alpha-Ketoglutarate Dioxygenase: Interactions with alpha-Ketoglutarate, Taurine, and Oxygen, *Biochemistry* 38, 15278-15286.

118. Saari, R. E., and Hausinger, R. P. (1998) Ascorbic Acid-Dependent Turnover and Reactivation of 2,4-Dichlorophenoxyacetic Acid/alpha-Ketoglutarate Dioxygenase Using Thiophenoxyacetic Acid, *Biochemistry* 37, 3035-3042.

119. Saban, E., Chen, Y.-H., A. Hangasky, J., Y. Taabazuing, C., Holmes, B. E., and Knapp, M. J. (2011) The Second Coordination Sphere of FIH Controls Hydroxylation, *Biochemistry* 50, 4733-4740.

120. Saban, E., Flagg, S. C., and Knapp, M. J. (2011) Uncoupled O2-activation in the human HIF-asparaginyl hydroxylase, FIH, does not produce reactive oxygen species, *J. Inorg. Biochem.* 105, 630-636.

121. Salowe, S. P., Marsh, E. N., and Townsend, C. A. (1990) Purification and characterization of clavaminate synthase from Streptomyces clavuligerus: an unusual oxidative enzyme in natural product biosynthesis, *Biochemistry* 29, 6499-6508.

122. Schofield, C. J., and Ratchliffe, P. J. (2004) Oxygen sensing by HIF-hydroxylases, *Nat. Rev. Mol. Cell Bio.* 5, 343-354.

123. Schofield, C. J., and Ratcliffe, P. J. (2005) Signalling hypoxia by HIF hydroxylases, *Biochem. Biophys. Res. Commun.* 338, 617-626.

124. Schofield, C. J., and Zhang, Z. (1999) Structural and mechanistic studies on 2-oxoglutarate-dependent oxygenases and related enzymes, *Curr. Opin. Struct. Biol.* 9, 722-731.

125. Schowen, K. B., and Schowen, R. L. (1982) Solvent isotope effects on enzyme systems, *Methods Enzymol.* 87, 551-606.

126. Semenza, G. L. (2001) Hypoxia-inducible factor 1: oxygen homeostasis and disease pathophysiology, *Trends Mol. Med* 7, 345-350.

127. Semenza, G. L. (2001) HIF-1 and mechanisms of hypoxia sensing, *Curr. Opin. Cell Biol.* 13, 167-171.

128. Semenza, G. L. (2003) Targeting HIF-1 for cancer therapy, *Nat. Rev. Cancer* 3, 721-732.

129. Semenza, G. L. (2004) Hydroxylation of HIF-1: Oxygen sensing at the molecular level, *Physiology* 19, 176-182.

130. Semenza, G. L. (2009) Oxygen homeostasis, Wiley Interdisciplinary Reviews: *Systems Biology and Medicine* 2, 336-361.

131. Semenza, G. L., Agani, F., Booth, G., Forsythe, J., Iyer, N., Jiang, B. H., Leung, S., Roe, R., Wiener, C., and Yu, A. (1997) Structural and functional analysis of hypoxia-inducible factor 1, *Kidney Int.* 51, 553-555.

132. Senda, T., Sugiyama, K., Narita, H., Yamamoto, T., Kimbara, K., Fukuda, M., Sato, M., Yano, K., and Mitsui, Y. (1996) Three-dimensional structures of free form and two substrate complexes of an extradiol ring-cleavage type dioxygenase, the BphC enzyme from Pseudomonas sp strain KKS102, *J. Mol. Biol.* 255, 735-752.

133. Shook, R. L., and Borovik, A. S. (2008) The effects of hydrogen bonds on metal-mediated O2 activation and related processes, *Chem. Commun.* 6095-6107.

134. Shu, L. J., Chiou, Y. M., Orville, A. M., Miller, M. A., Lipscomb, J. D., and Que, L. (1995) X-ray absorption spectroscopic studies of the Fe(II) active site of catechol 2,3-dioxygenase - Implications for the extradiol cleavage mechanism, *Biochemistry* 34, 6649-6659.

135. Solomon, E. I., Brunold, T. C., Davis, M. I., Kemsley, J. N., Lee, S. K., Lehnert, N., Neese, F., Skulan, A. J., Yang, Y. S., and Zhou, J. (2000) Geometric and electronic structure/function correlations in non-heme iron enzymes, *Chem. Rev.* 100, 235-349.

136. Soper, A. K., and Benmore, C. J. (2008) Quantum Differences between Heavy and Light Water, *Phys. Rev. Lett.* 101, 065502.

137. Takeda, K., Cowan, A., and Fong, G. H. (2007) Essential role for prolyl hydroxylase domain protein 2 in oxygen Homeostasis of the adult vascular system, *Circulation* 116, 774-781.

138. Takeda, K., and Fong, G. H. (2007) Prolyl hydroxylase domain 2 protein suppresses hypoxia-induced endothelial cell proliferation, *Hypertension* 49, 178-184.

139. Tian, H., McKnight, S. L., and Russell, D. W. (1997) Endothelial PAS domain protein 1 (EPAS1), a transcription factor selectively expressed in endothelial cells, *Genes Dev.* 11, 72-82.

140. Tomchick, D. R., Phan, P., Cymborowski, M., Minor, W., and Holman, T. R. (2001) Structural and Functional Characterization of Second-Coordination Sphere Mutants of Soybean Lipoxygenase-1, *Biochemistry* 40, 7509-7517.

141. Wackett, L. P. (2002) Mechanism and applications of Rieske non-heme iron dioxygenases, *Enzyme Microb. Technol.* 31, 577-587.

142. Walsh, C. (1979) *Enzymatic reaction mechanisms*, W. H. Freeman, San Francisco.

143. Wang, G. L., Jiang, B. H., Rue, E. A., and Semenza, G. L. (1995) Hypoxia-Inducible Factor-1 is a basic-helix-loop-helix-pas heterodimer regulated by cellular O2 tension, *PNAS* 92, 5510-5514.

144. Wax, S. D., Tsao, L., Lieb, M. E., Fallon, J. T., and Taubman, M. B. (1996) SM-20 is a novel 40-kd protein whose expression in the arterial wall is restricted to smooth muscle, *Lab. Invest.* 74, 797-808.

145. Webb, J. D., Coleman, M. L., and Pugh, C. W. (2009) Hypoxia, hypoxia-inducible factors (HIF), HIF hydroxylases and oxygen sensing, *Cell. Mol. Life Sci.* 66, 3539-3554.

146. Welford, R. W. D., Kirkpatrick, J. M., McNeill, L. A., Puri, M., Oldham, N. J., and Schofield, C. J. (2005) Incorporation of oxygen into the succinate co-product of iron(II) and 2-oxoglutarate dependent oxygenases from bacteria, plants and humans, *FEBS Letters* 579, 5170-5174.

147. Welford, R. W. D., Schlemminger, I., McNeill, L. A., Hewitson, K. S., and Schofield, C. J. (2003) The Selectivity and Inhibition of AlkB, *J. Biol. Chem.* 278, 10157-10161.

148. Wenger, R. H. (2002) Cellular adaptation to hypoxia: O2 sensing protein hydroxylases, hypoxia inducible transcription factors, O2 regulated gene expression., *FASEB J.* 16, 1151-1162.

149. Whiting, A. K., Que, L., Saari, R. E., Hausinger, R. P., Fredrick, M. A., and McCracken, J. (1997) Metal Coordination Environment of a Cu(II)-Substituted alpha-Keto Acid-Dependent Dioxygenase That Degrades the Herbicide 2,4-D, *J. Am. Chem. Soc.* 119, 3413-3414.

150. Willam, C., Maxwell, P. H., Nichols, L., Lygate, C., Tian, Y. M., Bernhardt, W., Wiesener, M., Ratcliffe, P. J., Eckardt, K. U., and Pugh, C. W. (2006) HIF prolyl hydroxylases in the rat; organ distribution and changes in expression following hypoxia and coronary artery ligation, *J. Mol. Cell. Cardiol.* 41, 68-77.

151. Wolfe, M. D., Parales, J. V., Gibson, D. T., and Lipscomb, J. D. (2001) Single turnover chemistry and regulation of O2 activation by the oxygenase component of naphthalene 1,2-dioxygenase, *J. Biol. Chem.* 276, 1945-1953.

152. Zhou, J., Gunsior, M., Bachmann, B. O., Townsend, C. A., and Solomon, E. I. (1998) Substrate Binding to the alpha-Ketoglutarate-Dependent Non-Heme Iron Enzyme Clavaminate Synthase 2: Coupling Mechanism of Oxidative Decarboxylation and Hydroxylation, *J. Am. Chem. Soc.* 120, 13539-13540.

153. Zhou, J., Kelly, W. L., Bachmann, B. O., Gunsior, M., Townsend, C. A., and Solomon, E. I. (2001) Spectroscopic studies of substrate interactions with clavaminate synthase 2, a multifunctional alpha-KG-dependent non-heme iron enzyme: Correlation with mechanisms and reactivities, *J. Am. Chem. Soc.* 123, 7388-7398.